Ref.TH.1737-CERN

# MULTIPARTICLE PRODUCTION PROCESSES AT HIGH ENERGY

Edmond L. Berger *)

CERN - Geneva

Lectures presented at :

1) International School of Subnuclear Physics, Erice, Sicily (July 1973).
2) International School of Elementary Particle Physics, Basko Polje, Yugoslavia (September 1973).
3) Ecole d'Eté de Physique des Particules, Gif-sur-Yvette, France (September 1973).

---

*) On leave from Argonne National Laboratory.

Ref.TH.1737-CERN
24 August 1973

TABLE OF CONTENTS

# MULTIPARTICLE PRODUCTION PROCESSES AT HIGH ENERGY

Edmond L. Berger
CERN - Geneva

## 1. INTRODUCTION

### 1.1. Qualitative summary

Operations of the NAL accelerator and of the CERN Intersecting Storage Rings have provided new data which extend our knowledge of many facets of hadronic production from the centre-of-mass energy of $\sqrt{s} = 8$ GeV, available previously, to $\sqrt{s} = 62$ GeV. Events of the past year have changed our outlook on high multiplicity hadronic reactions considerably. New directions have been established in theoretical and experimental research by the observation of rising proton-proton total cross-sections, of inelastic diffraction scattering of fast protons, and of reasonably strong yet short-range inclusive correlations among copious secondaries produced with relatively small momentum in the over-all collision centre-of-mass system (the "central region"). In these lectures, I attempt to examine critically these new data and corresponding theoretical developments. The focus here is restricted to recent progress. This is neither the place, nor does it seems to be the right moment, for yet another comprehensive review. For subjects not treated here, and for other points of view, the articles listed under reference 1) may be consulted profitably.

I concentrate almost entirely on the inclusive approach to multiparticle physics, because as yet too little high energy information of a more differential character is available. The desirability of greater insight into the topological structure of individual events is very apparent, however.

After a very brief survey of kinematics, notation, and sum rules, I catalogue some empirical regularities of multihadron production whose validity is confirmed and extended by measurements at NAL and the ISR. Next, a list is given of the past year's new observations which must be incorporated into an over-all phenomenological scheme. After this introduction, in Section 2, I discuss the concept of dominant short-range order as an asymptotic unifying theme. The implications of this hypothesis for single particle inclusive spectra are compared with available data, particularly with regard to energy independence of a central plateau in rapidity space.

Two more explicit phenomenological frameworks are then described in Section 3 as a basis for making further guesses. One of these is the Amati-Bertocchi-Fubini-Stanghellini-Tonin model [2] which is, in fact, the prototype of models from which the hypothesis of short-range-order is abstracted. The second is the fragmentation [3] concept, in which both short and long-range structure is found. These view-points suggest radically different topological structure of individual multiparticle events, but may be made to agree in their "predictions" of an asymptotic energy independent central plateau in the single particle inclusive rapidity distribution. From the inclusive approach, two-particle spectra can discriminate between these models, as discussed in Section 4, where data are also examined in detail. The dominant short-range order alternative is favoured by data in the central region, but more precise experimental investigations of the energy dependence of two-particle spectra is clearly called for. In contrast to one year ago, when the experimental picture was consistent with either fragmentation or dominant short-range order models, correlation data appear to favour the latter alternative. Several features of data suggest, however, that there is significant cluster formation, an aspect of hadronic phenomena emphasized in the fragmentation approach. One way to imitate data is thus to imagine a multiperipheral-like emission [4] of clusters of pions. A mean of four pions per cluster [4] is suggested by the correlation data. Cluster formation and its parametrization are described in detail in Sections 3.2 and 3.3.

Evidence for long-range correlations is present also in ISR and NAL data. A striking example is the inelastic diffractive peak observed in the inclusive proton longitudinal momentum spectrum [5]. Further experimental study is also necessary here, but present indications support a peak which is energy independent at fixed $x = 2p_L/\sqrt{s}$. Here $p_L$ is the final proton's longitudinal momentum in the centre-of-mass frame. Data and theoretical understanding are described in Section 5. As energy increases, states of ever-increasing mass are excited diffractively. Multiplicity rises accordingly. The cross-section in this inelastic diffractive peak may rise logarithmically, and thus be associated with the observed growth with $s$ of the total cross-section. This association is discussed quantitatively in terms of triple-Regge models. On the basis of this approach, predictions are made for the single and two-particle inclusive spectra in rapidity space expected for particles recoiling from the inelastic fast proton.

## 1.2. Notation, variables and sum rules

Although necessary, this section can be kept short because several treatments are published [1),6)] on the choice variables and no great advances in the subject are evident. I specialize to proton-proton collisions, since much of the NAL and all the ISR data are of this type.

In an inclusive single particle process,

$$pp \rightarrow hX$$

one is interested in the differential cross-section for production of particle h, with four-momentum $(E,\vec{p})$, regardless of whatever else ("X") accompanies h. An implicit or, even, explicit sum is made over states with various quantum numbers which comprise X. The Lorentz-invariant inclusive cross-section, denoted

$$f(s,\vec{p}) = E\frac{d\sigma}{d^3p} \tag{1.1}$$

is a function of the total energy $s = (p_a+p_b)^2$ and of the momentum $\vec{p}$ of produced hadron h. Here $p_a$ and $p_b$ are four-momenta of the incident protons in the collision. The factor E appears in (1.1) in order to (partially) remove inessential kinematical effects.

In a two-particle inclusive process, $pp \rightarrow h_1h_2X$, one studies

$$\frac{E_1E_2\,d^2\sigma}{d^3p_1\,d^3p_2} = G(s,\vec{p}_1,\vec{p}_2)\,. \tag{1.2}$$

According to the definition of $f(s,\vec{p})$, one count is registered in a counter subtending element $d^3p/E$ of phase space for each time a hadron of type h falls into the counter. It is then clear that the integral of f over all phase space gives the <u>mean</u> multiplicity of hadrons of type h, times the cross-section.

$$\int f(s,\vec{p})\,\frac{d^3p}{E} = \int \frac{d\sigma}{d^3p}\,d^3p = \langle n_h\rangle\,\sigma \tag{1.3}$$

In (1.3), termed the "multiplicity sum rule", we may employ either the total, the inelastic, or some other cross-section $\sigma$ ; the meanings of $< n_h >$ change accordingly. Obviously, an alternative expression for $< n_h >$ is

$$\sigma \langle n_h \rangle = \sum n \sigma_n \tag{1.4}$$

where $\sigma_n$ denotes the partial cross-section for production of $n$ and only $n$ hadrons of type $h$.

Another useful sum rule is that expressing energy conservation. Since $\sigma^{-1} f(s,\vec{p})$ can be thought of as a number density, the product $\sigma^{-1} E_h f_h(s,\vec{p})$ $(d^3p/E)$ is the fraction of energy deposited in phase-space element $(d^3p/E)$ by hadrons of type $h$. Upon summing over hadrons of all types and integrating over all phase space, we obtain

$$\sum_h \int E_h f_h(s,\vec{p}) \left(d^3p/E\right) = \sqrt{s}\,\sigma \tag{1.5}$$

Expression (1.5) is especially relevant in attempts to assess the implications of a rising cross-section for the $s$ dependence of inclusive cross-sections. This is treated in Sections 2.4 and 5.

The reader can easily supply other sum rules expressing conservation of charge, baryon number, and random other quantities.

For a single particle process, with spin ignored, there are three independent kinematic variables necessary for a specification of $pp \to hX$. Three popular choices, dictated by differing physics considerations, are :

1) $s$ , $|\vec{p}_T|$ , $p_L$

2) $s$ , $|\vec{p}_T|$ , $y$

3) $s$ , $t$ , $M_X^2$

In all three sets, $s = (p_a+p_b)^2$. In sets 1 and 2, an attempt is made to exploit the observed fact that the distribution in transverse *) momentum $\vec{p}_T$ is a rapidly decreasing and roughly energy-independent function. Thus, in some sense, all the physics goes on in the single longitudinal dimension. In set 1, $p_L$ is the longitudinal momentum in some chosen rest-frame (e.g., centre-of-mass, stationary target frame, beam frame, etc.).

The Feynman scaling variable is defined as

$$x = 2p_L/\sqrt{s} \quad , \tag{1.6}$$

where here $p_L$ is the centre-of-mass value.

In set 2, rapidity **)

$$y = \frac{1}{2} \log \left[ \frac{E+p_L}{E-p_L} \right] = \log \left[ \frac{E+p_L}{m_T} \right] \tag{1.7}$$

with

$$m_T^2 = p_T^2 + m_h^2 \tag{1.8}$$

One advantage of rapidity as the choice of longitudinal variable is well known. Under a longitudinal Lorentz transformation from one rest frame to another,

$$y \longrightarrow y' + \text{constant}$$

Thus, distributions in $y$ are easily shifted from one frame to another.

Inverting (1.7), we write

$$E = m_T \cosh y \; ; \tag{1.9}$$

---

*) Transverse is defined with respect to the longitudinal axis given by the incident particle direction in the over-all centre-of-mass frame.

**) Throughout this paper, log means natural logarithm, i.e., to the base e.

$$p_L = m_T \sinh y . \tag{1.10}$$

The full kinematic range of x is obviously

$$-1 < x < 1$$

independent of s, whereas

$$-\tfrac{1}{2} Y < y < \tfrac{1}{2} Y \; ; \; Y = \log\left(\frac{s}{m_p^2}\right) \tag{1.11}$$

For future reference, a table is given here of various momenta, energies, and the corresponding full interval Y in rapidity.

| Momentum on a stationary target in GeV/c | Momenta of ISR colliding beams in GeV/c | s $(\text{GeV})^2$ | $\sqrt{s}$ GeV | Y/2 |
|---|---|---|---|---|
| 30 | | 58.2 | | 2.1 |
| 70 | | 133.4 | | 2.5 |
| 100 | | 189.8 | | 2.7 |
| 200 | | 377.8 | | 3.1 |
| 300 | | 565.8 | | 3.3 |
| | 11 | | 23.2 | 3.2 |
| | 15.4 | | 30.4 | 3.5 |
| | 22 | | 44.4 | 3.9 |
| | 26.7 | | 52.7 | 4.0 |

The third set $(s,t,M_x^2)$ will be used primarly in Section 5.

Expressed in terms of the three variable sets, the inclusive cross-section is

$$E\frac{d\sigma}{d^3p} = \frac{\bar{x}\, d\sigma}{\pi\, dx\, dp_T^2} = \frac{d\sigma}{\pi\, dy\, dp_T^2} = \frac{d\sigma}{\pi\, dt\, d(M^2/s)} \tag{1.12}$$

$(\bar{x} = 2E/\sqrt{s})$

Because it expands the region of phase space in which $p_L^{(cm)} \approx 0$, $y$ is a good variable for displaying pion inclusive spectra, whose cross-section is largest at small $y^{(cm)}$ (or small $x$). By contrast, the physics of proton inclusive spectra is such that $< x_p > \approx 0.5$ ; and $Ed\sigma/d^3p$ peaks near $x_p \simeq 1$, as will be discussed in Section 5. Thus plots in terms of $x$ seem to be better when final proton spectra are displayed.

## 1.3. Ancient history

Having disposed of kinematics, we turn to revered old facts whose range of validity is extended by observations at NAL and ISR.

1.3.1. As discussed eloquently elsewhere [7], measurements of the total [8] and elastic [9] pp cross-sections at ISR have produced their surprises. However, it remains true that inelastic production accounts for the bulk of the total cross-section, with a roughly energy independent fraction of 80% :

$$\sigma_{inel} \simeq 0.8\, \sigma_{tot}$$

1.3.2. Although larger at large $p_T$ than perhaps expected, the distribution in transverse momentum $d\sigma/dp_T^2$ is largest at small $p_T$, and falls precipitously as $p_T$ increases. A very crude parametrization [10] over the range $0.1 < p_T < 1$ $(GeV/c)^2$ is

$$E\, d\sigma/d^3p \sim \exp(-6\, p_T) \qquad (1.13)$$

Surely this form is not appropriate all the way to $p_T = 0$ [28]. Moreover, the parameter 6 is subject to some variation with $x$, and with the type of hadron observed.

For $p_T > 2$, the scaling form

$$E\, d\sigma/d^3p \sim p_T^{-8}\, g(p_T/\sqrt{s}) \qquad (1.14)$$

is suggested by some theories [11] and appears to fit data [12], with

$$g_{\pi^0}(p_T/\sqrt{s}) \sim \exp\left[26\, p_T/\sqrt{s}\right] \qquad (1.15)$$

Nevertheless, the integrated cross-section for $p_T > 1$ (GeV/c) is on the order of tenths-of-millibarns. Thus, to a good approximation throughout the ISR range, the mean $< p_T >$ has the "small" value $\approx$ 350 MeV and is independent of energy. Transverse momenta are "limited" for the great bulk of $\sigma_{inel}$.

Some recent data are shown in Fig. 1.

1.3.3. An interesting compilation of mean multiplicities from pp collisions has been published [13] by the CERN-Bologna group ; it is reproduced here as Fig. 2. Representative fits made to the mean number of charged hadrons per collision give [13),14]

$$\langle n_{ch} \rangle \approx 1.4 \log s - 1. \qquad (1.16)$$

$$\approx 1.5\, s^{0.3} \qquad (1.17)$$

$$\approx 1.9 \log s - 3.8 + \frac{6.4}{s^{1/2}} \qquad (1.18)$$

Although these functional forms differ, they show that $< n_{ch} >$ grows much less rapidly than the maximum possible rate of growth ($< n_{ch} >_{max} \simeq \simeq \frac{2}{3}\sqrt{s}$). With "minor corrections" for differing leading particle energy fractions, multiplicity data from $\pi p$, Kp, and $\bar{p}p$ reactions fall on roughly the same curve as the pp data [15].

1.3.4. Inasmuch as the energy available does not go into transverse motion (point 1.3.2.) nor fully into particle production (point 1.3.3.), its influence is most obvious in altering the longitudinal momentum dimension. To first approximation, the mean centre-of-mass longitudinal momentum grows in proportion to $\sqrt{s}$ :

$$\langle p_L \rangle = k_h \sqrt{s} \,. \qquad (1.19)$$

The constant of proportionality $k_n$ differs for different hadrons h. Statement (1.19) is related, of course, to the hypothesis of Feynman scaling. If

$$f(x, p_T^2, \sqrt{s}) \longrightarrow f(x, p_T^2) \tag{1.20}$$

then, obviously,

$$\langle x_h \rangle = k_h \tag{1.21}$$

For final protons, $k \simeq \frac{1}{2}$. This relatively large value of $k_p$ emphasizes a result known for years from cosmic ray data that the final baryons carry away on the average a substantial fraction of the collision energy.

1.3.5. Scaling in the fragmentation regions. For the sake of definiteness, I limit the fragmentation region to the kinematic region $|x| > 0.1$. Because

$$x \simeq \exp\left[-(y_{end} - y)\right] , \tag{1.22}$$

fragmentation covers roughly two units of rapidity from the kinematic edges of the y plot.

In this fragmentation region, as discussed at length in earlier reviews [1], inclusive distributions of $\pi^{\pm}$ in pp collisions show a remarkable independence of s from $p_{lab}$ = 10 to 30 GeV/c, when plotted versus the scaling variable x. Thus, for $pp \to \pi^{\pm}X$, whereas $Ed\sigma/d^3p = f(s,x,p_T^2)$ is in general a function of three independent variables, the dependence on s seems to drop out. ISR data extend the region of experimental validity of this statement to $\sqrt{s} \simeq 53$ GeV. I defer further discussion of new data to Section 2.2.

Not all single particle inclusive spectra scale in the 10-30 GeV/c interval, to be sure. Some (e.g., $pp \to KX$) rise and others fall with s. A systematic experimental study of the question of approach to scaling through the Serpukhov and NAL energy ranges would be very valuable.

## 1.4. New developments

As a result of data accummulated during the past year, new items to be included in the grand design are : (1) the rise with $s$ of the total cross-section [8] ; (2) the behaviour of the elastic differential cross-section [9] $d\sigma/dt$ as a function of $s$ and of momentum transfer $t$ ; (3) scaling and non-scaling behaviour of single particle inclusive spectra $(a+b \rightarrow h+X)$ ; (4) the dependence of these spectra on momentum of the observed hadron, including the emergence of a plateau in rapidity [16] ; (5) correlations [17]-[19] seen between hadrons in two-particle inclusive processes $(a+b \rightarrow h_1+h_2+X)$ ; (6) the behaviour of the cross-section [20] $\sigma_n$ for $n$ charged particles (prongs) as a function of $n$ and $s$ ; (7) the remarkably large hadronic inclusive cross-section at large transverse momentum [12] $p_T$ ; and, last but far from least important, (8) salient features gleaned from more differential, exclusive analyses of events.

This itemization is arbitrary to a certain extent. Category (7) could well be included in (4). It is separated off just to point out that there may be different physics dominating the low and high $p_T$ parts of data. Next, the nebulous subject of "diffraction dissociation" could well be listed by itself, but I include it in (3) and (4) ; in later pages I will treat it separately. The listing is also by experimental topics, rather than according to such theoretical concepts as short-range order, long-range order, cluster formation, diffraction, factorization, particle exchange, fragmentation and so forth. However, some of these concepts emerge as simplifying themes and are emphasized throughout the text.

Elastic and total $pp$ cross-sections are discussed in detail by others [7], so I can dispense with my categories (1) and (2), and concentrate on inelastic multibody phenomena. The growth with $s$ of $\sigma_{tot}$ will of course still affect our discussion.

Because it is still unclear how to integrate large $p_T$ phenomena into the whole picture, and because of lack of time, I do not treat this topic here. Multiplicity distributions have generated a vast literature of their own during the past year [21]. I will avoid increasing this volume. There is little to add. It seems necessary now to develop a view-point in which an explanation of both the inclusive spectra and $\sigma_n(s)$ emerge together.

## 2. SHORT-RANGE ORDER AND SINGLE-PARTICLE SPECTRA

### 2.1. Statement of the hypothesis of short-range order

Although I risk biasing the presentation, I think it is useful to introduce the hypothesis of short-range order [22] at this point, because it serves well as a putative asymptotic unifying theme. It is a principle which can be abstracted from a broad class, but by no means from all reasonable models. Furthermore, as will be discussed, it is consistent with much experimental data from ISR, in particular data on the behaviour of pions which are relatively slow in the over-all centre-of-mass frame. On the other hand, there is at least one class of events which does not seem to satisfy the hypothesis ; this is the inelastic diffraction class which is treated in Section 5. It is important to keep in mind from the start that the approximate domain of applicability of the hypothesis must be specified carefully.

Beginning on a purely intuitive level, it is perhaps easy to swallow the casual remark that if particles are far enough apart in phase-space, then they behave in an uncorrelated manner. Such a remark is true enough of gas molecules in a room. Can it also be true of hadrons, where for them rapidity difference is the measure of separation ? It is surely not true of fairly low multiplicity events, where momentum conservation, if nothing else, provides strong correlation. Nevertheless, various models, the prototype of which is the multiperipheral ansatz [2] and, more recently, inclusive Regge (Mueller) analysis [23], suggest the validity of a short-range order (SRO) hypothesis for inclusive spectra at asymptotic energies, as defined below.

We begin with an $n$ particle inclusive rapidity distribution

$$\frac{d^n \sigma_{ab}}{dy_1 \cdots dy_n} \equiv f_{ab}^{(n)}(y_1, y_2, \cdots, y_n ; y_a, y_b) \qquad (2.1)$$

As usual, $y_a$ and $y_b$ are centre-of-mass rapidities of the incident (beam) particles : $|y_a| = |y_b| = Y/2$. By Lorentz invariance, $f^{(n)}$ is actually function of rapidity differences [e.g., $(y_i - y_j)$] not individual rapidity variables. The number $n$ may be $1,2,\ldots$, etc.

Suppose we group rapidity variables into two sets

$$(y_a ; y_1, \cdots y_k)$$

and

$$(y_{k+1}, \cdots y_m ; y_b) ,$$

where $y_k$ is the largest rapidity of the first set, and $y_{k+1}$ the smallest of the second set.

The hypothesis of SRO states that if the rapidity difference $|y_{k+1} - y_k|$ is large enough, then $f^n(y_j)$ does not depend on this difference and factorizes into a product of terms :

$$f^{(n)}(y_j) \longrightarrow g_a^{(k)}(y_a ; y_1, \cdots, y_k)\, g_b^{(\ )}(y_{k+1}, \cdots, y_m ; y_b) \qquad (2.2)$$

The functions $g_a$ and $g_b$ are not specified generally, but in strong versions of SRO, each factor is itself a separately measurable inclusive cross-section.

$$\sigma_{ab} f_{ab}^{(n)} \longrightarrow$$

$$f_{ab}^{(k)}(y_a ; y_1, \cdots, y_k ; y_b)\, f_{ab}^{(n-k)}(y_a ; y_{k+1}, \cdots, y_m ; y_b) \qquad (2.3)$$

The strong version carries an additional postulate about the functional form and normalization of the factors. The strong version may not agree with data, whereas the weaker form has experimental support.

To have a measure of distance in $y$ space, we introduce an energy independent correlation length $\lambda$. We can then rephrase the hypothesis : if $|y_k - y_{k+1}| \gg \lambda$, then (2.2) follows.

The hypothesis itself does not provide a scale of distance but models agree that $\lambda \approx 2$. This value is found from inclusive Regge analysis [23], since $\lambda \equiv (\alpha_P(0) - \alpha_R(0))^{-1} \simeq 2$. In models in which behaviour at small rapidity differences is dominated by resonance-like behaviour (fragmentation models, cluster formation models, etc.), $\lambda \simeq 2$ is dictated essentially by kinematics, and by the mean transverse momentum (or $Q$ value) of the decay (cf. Section 3.3). Data from ISR are consistent with the value $\lambda \simeq 2$ (Section 4).

The SRO hypothesis suggests a division of the inclusive rapidity axis into three regions :

1) target fragmentation, length $\lambda$ about $y_b$ ;

2) projectile fragmentation, length $\lambda$ about $y_a$ ;

3) central region of length $Y - 2\lambda$.

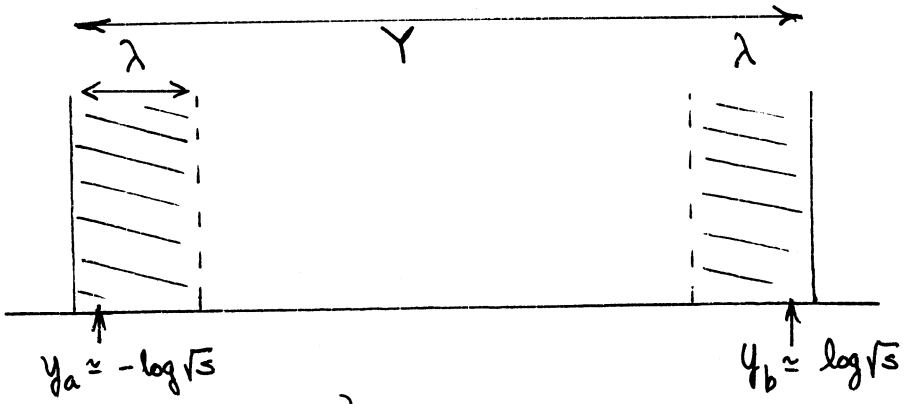


Particles within a distance $\lambda$ from $y_a$ (or $y_b$) are possibly highly correlated among themselves. Central region particles should be uncorrelated from those near $y_a$ and/or $y_b$.

Existence of a central region requires $Y = y_b - y_a > 4$, if $\lambda \simeq 2$. Thus, it is meaningful to discuss the possibility of a physically distinct central region only if $p_{lab} > 30$ GeV/c (cf. the Table in Section 1.2).

The hypothesis of SRO is primarily a statement about (the absence of) correlations. As such, its predictions are most useful at the level of two and more particle inclusive processes. However, the hypothesis makes testable assertions also about single-particle inclusive spectra in various regions of phase space. It is well to examine how well these agree with data before proceeding to more complex situations.

## 2.2. Implications of SRO for single-particle spectra in the fragmentation regions

The single-particle inclusive distribution $Ed\sigma/d^3p = \pi^{-1}d^2\sigma/dydp_T^2$ is a function of three variables $y$, $p_T^2$ and $s$. The dependence on $s$ can be reexpressed as a dependence on $Y = \log(s/m_p^2) = y_b - y_a$. Thus, in terms of $p_T^2$ and rapidity differences, the three free variables are $p_T^2$, $(y - y_a)$, and $(y - y_b)$.

If $y$ is in the fragmentation region of $b$, then $|y - y_b|$ is small and the difference $|y - y_a| \approx |y - Y|$ is large, provided that $s$ is high enough. According to the SRO hypothesis, dependence on $|y - y_a|$ drops out, and

$$f(y, s, p_T^2) \longrightarrow f(p_T^2, |y - y_b|) \tag{2.4}$$

Because $x \simeq \exp[-(y_b - y)]$, a function of $(y - y_b)$, only, is a function of $x$ only. Thus, SRO gives

$$f(x, s, p_T^2) \longrightarrow f(x, p_T^2) \tag{2.5}$$

Expressions (2.4) and (2.5) are alternative statements of the famous <u>scaling</u> law of ABFST [2] and Wilson [22], rediscovered by Feynman [24], Yang [3] and Mueller [23].

The hypothesis also predicts an energy independent flat central plateau in $y$ for single-particle spectra, as discussed in the next subsection. Observation of scaling in the fragmentation regions and/or an $s$ independent central plateau does not prove SRO, of course. There are models, without dominant SRO in which both predictions emerge naturally. The observation is a first consistency check. Note, furthermore, that no energy scale is provided. For different produced hadrons $h$, we are not told a priori the energy value at which non-asymptotic terms should be negligible. For the latter, we need more detailed models.

For comparison of scaling predictions with data, I will confine myself to spectra with $p_T < 1$ (GeV/c)$^2$. At larger $p_T$, an increase of $f$ with $s$ is observed in the ISR range.

Beginning with the fragmentation regions, and restricting attention to $0.2 < x < 0.8$ for the moment, we observe in Figs. 3.a-c that for all practical purposes $\bar{p}$, $\pi^-$, and $K^-$ inclusive distributions are all energy independent (scale) within the ISR range [25]. Data on $\pi^+$, $K^+$ and $p$ spectra show similar behaviour [26]. Energy independence for pions ($\pi^\pm$) seems to extend down to much lower energy [27], beginning somewhere in the 10-30 GeV/c PS range. The PS/ISR comparison demonstrates that $K^+$ spectra rise somewhat as energy is increased, $K^-$ and $\bar{p}$ spectra grow even more dramatically, and the $p$ rate falls. As remarked above, these statements apply to the region $0 < p_T < 1$ GeV/c and $0.2 < x < 0.8$.

For $x > 0.8$, where only protons (and, perhaps neutrons) are observed, we encounter the intriguing question of whether the leading proton peak scales. ISR data [5], confined to a few $p_T$ values, are shown in Fig. 4. This topic will be treated again in Section 5.

## 2.3. Single-particle spectra in the central region

When both $|y_a - y| \gg \lambda$ and $|y_b - y| \gg \lambda$, the SRO hypothesis assures us that $f(y - y_a, y - y_b, p_T^2)$ can depend only on $p_T^2$. Thus, an energy independent, flat rapidity distribution is predicted in the central region.

$$\frac{d\sigma}{dy\, dp_T^2} \longrightarrow f(p_T^2) \tag{2.6}$$

One immediate implication is that of an asymptotic log growth of $< n >$ inasmuch as

$$\langle n \rangle \sigma = \int \frac{d\sigma}{dy\, dp_T^2}\, dy\, dp_T^2 \longrightarrow \log s \int f(p_T^2)\, dp_T^2 + A \tag{2.7}$$

Constant A arises from the s independent contribution of the fragmentation regions to the integral.

The coefficient of log s is given by the plateau height divided by cross-section $\sigma$. This log s growth is characteristic of an effectively one-dimensional phase space, the single-dimension arising because $p_T$ is sharply limited. An incremental increase of energy goes into expanding the longitudinal dimension in the uniform manner specified by SRO. Note that the log prediction is not necessarily expected to hold below $p_{lab} \approx 50$ GeV/c, i.e., until there is reason to have a plateau in y.

Experimental tests of (2.6) and, more generally, the question of the existence of an energy independent plateau in y, are beset with unnecessary confusion. Three types of data exist. By far the best are data on particles of well defined type (e.g., $\pi$, p, K, $\bar{p}$, etc.) whose y and $p_T$ values are both specified. The two-dimensional distribution $d^2\sigma/dydp_T^2$ is given as a function of s. Second, some data on particles of a specific type are given only in the integrated form $d\sigma/dy$ versus s. Finally, the most difficult data to interpret are those in which the distribution $d\sigma/d\eta$, for all

charged particles combined, is given as a function of $s$. Variable $\eta = \log \tan(\theta/2)$ is an approximation to $y$, and involves a necessary average over $p_T$. Angle $\theta$ is the ISR frame or centre-of-mass frame scattering angle of the charged particle.

Bubble chamber data on $d\sigma/d\eta$ for $\pi^-$ production at 200 GeV/c at NAL [28] are compared with 28.5 GeV/c data [29] in Fig. 5. An approximate plateau covering $|\eta| < 1$ is seen in the NAL data, whereas no such plateau is visible for $p_{lab} < 30$ GeV/c. At least a 30% increase of $d\sigma/d\eta$ at $\eta = 0$ is seen from 28.5 to 200 GeV/c.

A summary of some ISR data on the $s$ and $y$ dependences of $d^2\sigma/dp_T^2 dy$ for $pp \to \pi^+ X$ is given in Fig. 6. Qualitatively similar results are true for $pp \to \pi^- X$. The British-Scandinavian [30] (BS) and Saclay-Strasbourg [31] (SS) data at $y = 0$ are consistent. The BS data at $\sqrt{s} = 30.6$ and 52.8 GeV show that the invariant cross-section at fixed $p_T$ and fixed $s$ increases by $\approx 15\%$ as $y$ changes from 1 to 0. Thus, even at $\sqrt{s} = 52.8$ GeV, there is not a flat plateau, but, rather, a bulge in $d\sigma/dy$ near $y = 0$. The magnitudes of the slopes in $y$ decrease, however, from $0.18 \pm 0.01$ for $\pi^-$ and $0.15 \pm 0.01$ for $\pi^+$ at $\sqrt{s} = 30.6$ GeV to $0.13 \pm 0.01$ and $0.12 \pm 0.01$ at $\sqrt{s} = 52.8$ GeV, consistent with a gradual approach to a flat plateau in the central region at infinite energies, for small $p_T$ ($< 1.0$ GeV/c). This aspect of the SRO prediction is therefore supported for pions.

Turning next to $s$ dependence, two observations may be made. For fixed $p_T$, it appears from Fig. 6 that data at different $y$ and $Y = \log s$ are consistent with lying on a universal curve which is a function of the difference $y_{proj} = (y_{cm} + \frac{1}{2}Y)$. If this were true, then knowledge of the $y$ dependence at fixed $s$ would give us directly the $s$ dependence at fixed $y_{cm}$. The 15% increase of $d\sigma/dy$ from $y = |1|$ to $y = 0$ then translates into an 8% rise of the "plateau height" $d\sigma/dy|_{y=0}$ from $\sqrt{s} = 30.6$ to $\sqrt{s} = 52.8$ GeV. However, experimental uncertainties in energy calibration of flux monitors are unfortunately sufficiently large that this rise cannot be asserted strongly. The BS group [30] cautions therefore that the $\pi$ production cross-section, integrated over the measured range of $p_T$ and over the centre-of-mass system rapidity range 0 to 0.5, shows an increase between the two energies of $8 \pm 7\%$. Saclay-Strasbourg data [31] on $\pi^\pm$ production show perhaps a 10% rise of $Ed\sigma/d^3p$ at $x = 0$ and $0.3 < p_T < 0.9$ GeV/c as $\sqrt{s}$ changes from 22 to 30 GeV. Over the range

$\sqrt{s} = 30$ to $\sqrt{s} = 53$, no further increase is observed within the 5% systematic error set by limitations on luminosity measurements.

Thus, the picture which emerges from measurements of s dependence of $d\sigma/dy$ for $\pi^{\pm}$ near $y = 0$ and $0.1 < p_T < 1$ GeV/c is one of a factor of 2 or so rise from the 20-30 GeV/c BNL-PS energy range to the ISR. Within the ISR range of $\sqrt{s} = 30$ to $\sqrt{s} = 53$ GeV, the data are consistent with an energy independent inclusive cross-section $d\sigma/dydp_T^2$ at $y = 0$ and $0.1 < p_T < 1$ GeV/c, as would be predicted by the hypothesis of short-range order.

Data on <u>antiproton</u> production are given in Fig. 7. The cross-section integrated over $0 < y_{cms} < 0.5$ for fixed $p_T$ shows an average increase from $\sqrt{s} = 30.6$ to 52.8 GeV of 25 ± 7% for $\bar{p}$. At fixed s and fixed $p_T$, $d\sigma/dydp_T^2$ increases by 42 ± 8% as $y_{cms}$ changes from $|1|$ to 0. Thus, neither a plateau nor s independence is apparent for $\bar{p}$ production even in the ISR energy range. Validity of an SRO hypothesis for $\bar{p}$ inclusive production would require energies perhaps an order of magnitude higher than available at ISR. A comparison of $Ed\sigma/d^3p$ for $\bar{p}$ and $\pi^-$ production at $y = 0$ and $p_T = 04.$ GeV/c gives $(\bar{p}/\pi) \simeq 1/15$.

For proton production, $pp \rightarrow pX$, the BS group [30] reports an energy independent flat inclusive distribution in y from $1 > |y_{cm}| > 0$, and $0.3 < p_T < 1.0$ GeV/c.

The final figure on the plateau situation is Fig. 8. These data from the Pisa-Stony Brook ISR collaboration [32] are plots at different energies of the distribution $\sigma_{inel}^{-1} d\sigma/d\eta$ summed over all $p_T$ and over all types of charged particles (including background). As suggested by the P-SB authors [32], the $\eta$ and energy dependences shown by these data cannot be taken entirely at face value because of the background problem and neglect of certain experimental corrections. However, in Section 4, I discuss correlation data at different energies published by the same group. The s dependence of these correlation data is given experimentally in terms of the s dependence of the single particle spectra. Because s dependence of the correlation data is a much more crucial test of SRO than single particle spectra, it is important to see what s dependence is present, for whatever reason, in the P-SB single particle spectra.

Figure 8 shows good scaling of the distribution $\sigma^{-1} d\sigma/d\eta$ in the fragmentation regions. However, the very rough plateau in the central interval $|\eta| < 1$ rises with $\sqrt{s}$ by 20% or so over the ISR energy range. Combining this with the 10% rise of $\sigma_{inel}$, we see a net increase of $\approx 30\%$ for $d\sigma/d\eta\,|_{y\approx 0}$, which is a far greater increase than is seen by BS or SS.

The P-SB data are, of course, of a very different type from those of the BS and SS groups. The P-SB results include production at both larger $p_T$ and at smaller $p_T$. Directly produced charged particles as well as converted neutrals are accepted. It is unlikely that energy dependent large $p_T$ data, with small cross-section, can account for the discrepancy in $s$ dependence. Curious $s$ dependent, background-related phenomena at low $p_T$, where cross-sections are large, could be the problem.

To summarize, the BS and SS collaborations present what seems to be compelling evidence for the existence of a central, energy independent plateau in $y$, for pions, extending over at least $-1 < y < +1$ at ISR energies. The rise with $s$ of other inclusive spectra in the central region (e.g., $pp \to \bar{p}X$) suggests that there are still important threshold effects in the ISR range for production of heavy secondaries. The strong energy dependence of $d\sigma/d\eta$ seen by the P-SB group is of concern for conclusions about inclusive correlations, discussed in Section 4.

## 2.4. Implications of a rising total cross-section

The total cross-section is a function of $s$, or, equivalently, of $(y_a - y_b)$ : $\sigma_{tot}(y_a - y_b)$. Applying the SRO hypothesis naively to this function, we expect that

$$\sigma_{tot} \longrightarrow \text{constant} \tag{2.8}$$

inasmuch as $|y_a - y_b| \gg \lambda$. Thus, the rise of $\sigma_{tot}$ over the ISR range shows a violation of SRO or, at least, that there are important non-asymptotic effects in this energy region.

It may be argued that the SRO statement should really be made for the ratio

$$\sigma_{tot}^{-1}\, d^m\sigma/dy_1 \cdots dy_m \;,$$

which is, after all, a density. Such a procedure would be suggested by some proponents of gas/liquid analogies [33]. On the other hand, it is not clear that dynamical models from which the SRO hypothesis is abstracted support the suggestion that the ratio is the appropriate quantity. For example, we may take the inclusive Regge (Mueller) approach [23], and introduce cuts or other singularities to reproduce the rise in $\sigma_{tot}$. Then such effects will presumably be present also in inclusive spectra. However, these dependences on s generally need not cancel out in the ratios $\sigma^{-1} d^{(n)}\sigma/dy_1 dy_2,\ldots,dy_n$.

I will consistently apply the SRO hypothesis to inclusive cross-sections and not to ratios. Purely empirically, the 10% rise of $\sigma_{tot}$ over the ISR range can then be used to estimate the extent to which we should expect the constant plateau and the scaling predictions of SRO to be valid in this energy range.

Sum rules give us further insight, but they do not solve the problem. As we will see below, it is possible for most inclusive spectra to scale perfectly, simultaneously with a rising $\sigma_{inel}$. It is a very intriguing <u>experimental</u> question to ascertain precisely where the rise of $\sigma_{inel}$ really comes from. Theoretical models suggest different possibilities.

Rewritten in terms of other variables, the energy-conservation sum rule (1.5) takes the forms

$$2\sigma_{inel} = \pi \sum_h \int dx \int dp_T^2 \, f_h(s, x, p_T^2) \tag{2.9}$$

and

$$\sqrt{s}\,\sigma_{inel} = \sum_h \int dy \int dp_T^2 \, m_T \cosh y \, \frac{d\sigma_h}{dy\, dp_T^2} \tag{2.10}$$

We note that if all hadronic spectra scale perfectly [$f_h = f_h(x, p_T^2)$ in the integrand of (2.9)], and if none has singular behaviour near the end points of integration ($|x| \to 1$), then Eq. (2.9) requires $\sigma_{inel}$ = constant. Thus, the rise of $\sigma_{inel}$ over the ISR range demands that at least for some h, $f_h$ has residual non-scaling dependence on s, and/or that some $f_h$ behave in singular fashion as $|x| \to 1$. As an example of the latter possibility, the triple-Pomeron Regge formalism discussed in Section 5 gives

$$f_p(x) \propto (1-x)^{-1} \tag{2.11}$$

as $x \to 1$, with an upper cut-off $x_c = 1-M_c^2/s$. With this form

$$\int^{x_c} f_p(x)\, dx \propto \log s \tag{2.12}$$

which is then the basis for a theoretical suggestion [34] that the rise of $\sigma_{inel}$ comes from inelastic diffraction. The experimental credibility of this idea is examined in Section 5.

The sum rule clearly allows that some spectra (e.g., $\pi$ spectra in the fragmentation region) may scale perfectly. As discussed above (Section 2.2), $\pi^-$ and K data in the region $|x| \gtrsim 0.1$ do seem to satisfy this possibility. On the other hand, the pion spectra may rise with s for $|y| < 1$. It is worth while to see how much of the rise of $\sigma_{inel}$ can be associated directly with a rise of the central plateau height for pions and other hadrons.

Beginning with Eq. (2.10), let us make the simplifying assumption (criticized later) that there is a full pion plateau, for $-Y/2 < y < Y/2$. Thus,

$$\frac{d\sigma}{dy\, dp_T^2} = h(p_T^2) \tag{2.13}$$

$$\sqrt{s}\ \sigma_{inel} = \frac{\langle m_T \rangle}{m_p} \sqrt{s} \int dp_T^2\, h(p_T^2) \equiv \frac{\langle m_T \rangle}{m_p} \sqrt{s}\ H \tag{2.14}$$

and

$$\frac{\Delta \sigma_{inel}}{\sigma_{inel}} = \frac{\langle m_T \rangle}{m_p} \frac{\Delta H}{H} \left( \frac{H}{\sigma_{inel}} \right) \tag{2.15}$$

Experimentally, $H\sigma_{inel}^{-1} \simeq 0.8$ to $1.0$ for $\pi^-$, and $\langle m_T \rangle = \langle \sqrt{m^2 + p_T^2} \rangle \simeq 350$ MeV. Taking equal contributions from $\pi^+$, $\pi^-$ and $\pi^0$, I multiply (2.15) by 3, and find

$$\left(\frac{\Delta\sigma_{inel}}{\sigma_{inel}}\right)_{\pi} \simeq \frac{\Delta H}{H} \tag{2.16}$$

Thus, an 8% rise of the pion plateau height $H$ implies directly an 8% rise of $\sigma_{inel}$. A more careful analysis should be done, of course, in which actual data are integrated over $y$, not the full plateau form I used. This will reduce the right-hand side of (2.16) by a correction factor which I estimate to be $\gtrsim 0.5$. A net rise is left for $\sigma_{inel}$ due to central pion production perhaps as large as 8%, based on the British-Scandinavian numbers, of 8±7%, (and perhaps zero, also !, such are the experimental errors).

For the rise of $\sigma_{inel}$ attributable to antibaryon production in the central region, a similar exercise gives

$$\left(\frac{\Delta\sigma_{inel}}{\sigma_{inel}}\right)_{\bar{B}} \lesssim \left(\frac{\Delta H}{H}\right)_{\bar{p}} \left(\frac{H}{\sigma_{inel}}\right)_{\bar{p}} \tag{2.17}$$

On the right-hand side I have included a factor of 2 to take into account unseen $\bar{n}$ production. This is cancelled by other numerical factors in the computation. As described above, experiment gives $(\Delta H/H)_{\bar{p}} \simeq 25\pm7\%$ from $\sqrt{s} = 30$ to 53 GeV, and $H_{\bar{p}} \simeq H_{\pi^-}/15$. Thus, from antibaryon production, I obtain

$$\left(\frac{\Delta\sigma_{inel}}{\sigma_{inel}}\right)_{\bar{B}} \lesssim \left(\frac{\Delta H}{H}\right)_{\bar{p}} \left(\frac{H_{\bar{p}}}{H_{\pi^-}}\right) \left(\frac{H_{\pi^-}}{\sigma_{inel}}\right) \lesssim 2\% \tag{2.18}$$

from $\sqrt{s} = 30$ to 53 GeV. This is a 1 mb, or so, increase - and so may account for about 1/3 of the observed rise of $\sigma_{inel}$. It would not be correct to multiply this number by 2 on the grounds that $\bar{p}$'s are produced as baryon/antibaryon pairs. Data show no increase of the proton flux at $y = 0$, meaning, in this context, that an increase with $s$ of the proton's $d\sigma/dy$ due to production of $p$ from $(\bar{p}p)$ pair formation is offset by a decrease coming from some other source.

It is not easy to sum over all produced hadrons in the central region to obtain the net increase of $\sigma_{inel}$ due to central production. For example, one must decide how to treat $K^o$, $\Lambda$, and $\eta$ production. Are they effectively included already inasmuch as we have looked at inclusive spectra of $\pi$'s, p's, $\bar{p}$'s, etc., into which these other particles decay ? Such questions aside, the sum rule argument certainly supports an increase of $\sigma_{inel}$ over the ISR range. All observed inclusive spectra in the central region, except p, are consistent with an increase with s over the ISR range (the p spectra are constant). In the fragmentation regions, all spectra are essentially s independent over the ISR range. The sum rule (2.9), (2.10) will then show a net increase of $\sigma_{inel}$ over this same range. From central production alone, I estimate an increase $1mb < \sigma_{inel} < 3mb$.

## 3. TWO EXPLICIT MODELS

Crucial predictions of the SRO hypothesis appear only at the level of two-particle inclusive spectra and inclusive correlations. Indeed, the implications of SRO for single-particle spectra are not unique to models with only short-range order. Correlations are treated in Section 4, but first, to provide a more concrete idea of the short-range order concept it is useful to introduce a specific, if idealized, model embodying short-range order and, further, to contrast such a model with the fragmentation view-point [3], which has both long-range and short-range structure.

### 3.1. ABFST reviewed

We begin with the traditional Amati-Bertocchi-Fubini-Stanghellini-Tonin multiperipheral model [2], in which the amplitude for $pp \to (n+2)$ hadron final state is sketched below. The inclusive spectra are obtained from this model after an appropriate integration and sum is made over unobserved particles.

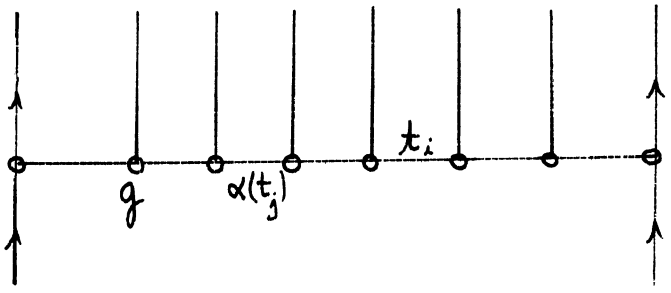

The amplitude is large only when all momentum transfers $t_i$ along the multiperipheral chain are small. For our present purposes it does not matter very much what specific particles or Reggeons $\alpha(t_i)$ are exchanged.

Analytically, the amplitude is represented as

$$A(2 \to n+2) = g^n \prod_{i=0}^{n} s_{ij}^{\alpha(t_i)} f_i(t_i) \tag{3.1}$$

Here $f(t_i)$ falls off rapidly as $|t_i|$ grows.

Detailed analyses may be found elsewhere [35] but here I will simply catalogue some predictions of the approach.

(a) $$\langle n \rangle = g^2 \log s \tag{3.2}$$

(b) $$\sigma_n = \sigma_0 e^{-\langle n \rangle} \langle n \rangle^n / n! \quad \text{(Poisson form)} \tag{3.3}$$

(c) $\dfrac{d\sigma}{dy}$ is s independent and flat. (3.4)

(d) $\dfrac{d\sigma_n}{dy}$ The single-particle spectrum from an n particle final state is s independent and flat for each n. (3.5)

The sum $\sum \sigma_n = \sigma_{inel}$ is an energy independent constant. What emerges is a picture in which particles are expected to be produced with a roughly uniform spacing in y. Each event has the plateau structure of the inclusive sum, except, of course, for statistical fluctuations. The density of particles along the rapidity axis, $\langle n \rangle / Y$, is given by $g^2$.

## 3.2. Cluster formation

In the summary above, I imagined that individual hadrons are emitted along the multiperipheral chain. This need not be the case. Indeed, if all exchanges are pions, then obviously G parity forbids emission of single pions. That the objects emitted should be resonances or, at least, clusters of several hadrons is theoretically possible and, moreover, seems phenomenologically required.

Three facts argue against independent emission of single hadrons along the chain.

(a) Important resonances are known to exist. There is no reason to suppose that they are not formed in multiparticle events. Duality arguments, in which resonance formation is presumed to be represented by a sum of exchange terms, are not quantitatively reliable at small invariant mass. Resonance-like effects should be present explicitly in a production model.

(b) The parametrizations of $< n_{ch} >$ given in Section 1.3 suggest that for the total number of hadrons

$$\langle n \rangle \sim b \log s$$

with $b \sim 2$ to 3. Thus the mean spacing $\Delta y$ of particles along the rapidity axis is only $\Delta y \sim 0.3$ to 0.5. Because

$$\langle M_{ij} \rangle \simeq \langle m_T \rangle \exp\left(\tfrac{1}{2} \Delta y\right) \tag{3.6}$$

the mean invariant mass of two produced hadrons is of order 500 MeV, well within the resonance region. Thus, strong correlations should be expected among produced hadrons, not independent emission.

(c) A direct measure of correlation is the parameter

$$f_2 = \langle n(n-1) \rangle - \langle n \rangle^2 \tag{3.7}$$

Shown in Fig. 9 is a compilation of data for negative tracks (i.e., $n = n_-$). Note that $f_2$ grows increasingly positive for $p_{lab} \gtrsim 50$ GeV/c. The independent emission Poisson distribution, Eq. (3.3), gives $f_2 \equiv 0$, for all $s$. Moreover, energy-momentum related effects in an independent emission model would depress $f_2$ to negative values [42]. Thus, the positive $f_2$ suggests clustering, as discussed more explicitly below.

We imagine, therefore, that a possible <u>imitation</u> of nature is one in which clusters of hadrons are emitted along a multiperipheral chain [4]. The mean number of clusters $< N >$ grows as

$$\langle N \rangle = g^2 \log s \tag{3.8}$$

In an (over) idealized model, the number of clusters produced may follow a Poisson law

$$\sigma_N = \sigma_0 \left[\exp(-\langle N\rangle)\right] \langle N\rangle^N / N! \qquad (3.9)$$

Thus, if there is an average of $\langle K \rangle$ hadrons per cluster, the net mean number $\langle n \rangle$ of produced hadrons in the final state is

$$\langle n\rangle = \langle K\rangle\langle N\rangle = \langle K\rangle g^2 \log s \qquad (3.10)$$

and

$$f_2 = \langle n(n-1)\rangle - \langle n\rangle^2 = \frac{\langle K(K-1)\rangle}{\langle K\rangle}\langle n\rangle \qquad (3.11)$$

Parameter $f_2$ will be naturally positive if $\langle K(K-1)\rangle >> 0$.

According to our multiperipheral ansatz, the distribution of clusters in y space $\rho(y_c) = 1/\sigma\,(d\sigma/dy_c)$ will be asymptotically uniform and s independent. To pass from this remark to one about the final distribution of hadrons requires a study of the distribution in rapidity of hadrons from cluster decay.

## 3.3. Cluster decay

Resonance behaviour implies many things - Breit-Wigner line shape, phases, spin-related decay characteristics and so forth. What I shall most like to emphasize, however, is the idea that decay particles from resonances occupy neighbouring regions of rapidity. Since the parent resonance invariant mass is relatively low, decay particles have small $\Delta y$ [cf. Eq. (3.6)]. For my purposes, then, the idea of resonance is solely that cross-section is enhanced at small invariant mass, and therefore that small $\Delta y$ is also enhanced. Clearly this effect is strongest where quantum numbers allow resonance formation.

Although some clustering very likely results physically from resonance formation, in order to stress the proximity of particles in rapidity, and to avoid other connotations of the term resonance, I use the word cluster to label the phenomenon of closer than average spacing of particles in rapidity space. The search of cluster formation in individual multiparticle events at NAL and ISR energies is only now beginning [36),37)]. Efforts in this direction deserve the strongest encouragement.

The parametrization of clusters and of their expected contribution to inclusive processes is straightforward. Begin by defining an average decay distribution in the cluster rest frame $D(\vec{q})$. Next, a transformation of variables is made to a set including rest-frame rapidity, namely the set $(q,y,\phi)$ where $q$ is the magnitude of three momentum in the cluster rest frame. We easily obtain exactly

$$\frac{dy}{\cosh^2 y} = \frac{q\, d\cos\theta}{2\omega} \tag{3.12}$$

and thus

$$\frac{d^3q}{\omega} = \frac{dq^2\, d\phi\, dy}{\cosh^2 y} \tag{3.13}$$

with $\omega^2 = \mu^2 + q^2$ ; $\mu$ is the decay particle's mass. If one is interested only in the final decay rapidity distribution, he may integrate so as to derive [36)]

$$\frac{dD}{dy} = (\cosh y)^{-2} \int dq^2\, d\phi\, D(\vec{q}) . \tag{3.14}$$

In general, $D$ in Eq. (3.14) may depend on $\cos\theta$ (i.e., on $y$). However, let us make an assumption that the cluster decay distribution is isotropic in the cluster rest frame : $D(\vec{q}) \to D(q)$. Then setting $r = q/\langle q \rangle$, we get [36)]

$$\frac{dD}{dy} = \frac{2\pi \langle q \rangle^2}{\cosh^2 y} \int_L^\infty dr\, D(r) , \tag{3.15}$$

with lower limit

$$L = \left( \frac{\mu \sinh y}{\langle q \rangle} \right)^2 . \tag{3.16}$$

In (3.16), $< q >$ is determined by the energy available (Q value) of the cluster decay. Empirically, the observed $< p_T >$ determines this scale, and for pions, $\mu/< q >$ is small. For small y, then $L \to 0$, and the decay spectrum

$$\frac{dD}{dy} \propto (\cosh y)^{-2} \tag{3.17}$$

The function $\cos h^{-2} y$ is in turn well approximated numerically by a Gaussian $\exp(-y^2/2\delta^2)$ whose dispersion $\delta \approx 0.9$. Corrections owing to $L \neq 0$ in general reduce $\delta$ by a small amount, but are relevant only for larger y where the Gaussian has fallen substantially from its peak. Dispersion $\delta$ is independent of both cluster mass and multiplicity.

Properly normalized to (integrate to) unity, the isotropic decay distribution in rapidity of a single cluster may then be given as

$$g(y) \simeq \frac{1}{\delta\sqrt{2\pi}} \exp\left(-y^2/2\delta^2\right), \tag{3.18}$$

or as

$$g(y) \simeq 0.5 \cosh^{-2} y \,. \tag{3.19}$$

(Note that the two approximations differ by $\approx 10\%$ at $y = 0$.)

Suppose, next, we have some production model which specifies the dynamical distribution of clusters in y space. Call this distribution $\rho(y_c) = 1/\sigma\,(d\sigma/dy_c)$. Obviously, the inclusive rapidity distribution for decay particles is then

$$\frac{1}{\sigma}\frac{d\sigma_h}{dy} = \int dy_c\, \rho(y_c)\, n_h(y_c)\, g(y - y_c) \tag{3.20}$$

Function $n(y_c)$ is just the average multiplicity of decay particles of the type h which come from a cluster located at $y_c$. Note that

$$\langle n_h \rangle \equiv \sigma^{-1} \int \frac{d\sigma_h}{dy}\, dy = \int dy_c\, \rho(y_c)\, N_h(y_c) \,. \tag{3.21}$$

In very similar fashion, we write the two-particle inclusive $y$ distribution for identical hadrons $h$ as

$$\frac{1}{\sigma}\frac{d^2\sigma}{dy_1 dy_2} = \int dy_c\, \rho(y_c) \langle n_h(n_h-1)\rangle_{y_c} g(y_1-y_c)\, g(y_2-y_c) \tag{3.22}$$

$$+ \int dy_{c1}\, dy_{c2}\, \rho(y_{c1})\, \rho(y_{c2})\, g(y_1-y_{c1})\, g(y_2-y_{c2}) \times n_h(y_{c1})\, n_h(y_{c2}) .$$

There are two terms, corresponding to situations in which both particles decay from the same cluster and in which they arise from different clusters. In the integrand of the first term as the right-hand side of (3.22), $\langle n_h(n_h-1)\rangle_{y_c}$ stands for twice the mean number of pairs of hadrons of type $h$ in the decay cluster of a cluster located at $y_c$. In this integrand, the simplifying approximation is made that two decays from a given cluster are independent, i.e.,

$$g_2(y_1, y_2 ; y_c) = g(y_1, y_c)\, g(y_2, y_c) .$$

Surely this guess must be corrected at least for energy momentum and charge conservation effects in a more serious treatment [4]. In the two cluster term, the second integral on the right of (3.22), I have explicitly made the assumption that the distribution for two cluster formation $\rho_2(y_{c1}, y_{c2})$ factors to give

$$\rho_2 = \rho(y_{c1})\, \rho(y_{c2}) ,$$

as would be the case for independent production of clusters. Again, this guess would be modified in more careful treatment of the effects of energy momentum conservation in, say, a Monte Carlo computation [4]. The second integral therefore gives $\sigma^{-2}(d\sigma_h/dy_1)(d\sigma_h/dy_2)$.

Defining a "correlation function"

$$C(y_1, y_2) = \sigma^{-1}\frac{d^2\sigma}{dy_1 dy_2} - \sigma^{-2}\frac{d\sigma}{dy_1}\frac{d\sigma}{dy_2} , \tag{3.23}$$

we see that $C(y_1,y_2)$ is given by the first integral on the right-hand side of Eq. (3.22)

$$C(y_1,y_2) = \int dy_c\, \rho(y_c) \langle n_h(n_h-1)\rangle_{y_c}\, g(y_1-y_c)\, g(y_2-y_c) \qquad (3.24)$$

The integral

$$f_2 \equiv \iint C(y_1,y_2)\, dy_1\, dy_2 = \int dy_c\, \rho(y_c) \langle n_h(n_h-1)\rangle_{y_c} \qquad (3.25)$$
$$\equiv \langle n_h(n_h-1)\rangle^2 - \langle n_h\rangle^2 \,.$$

The above arguments are reasonably general, independent of the forms chosen for $\rho(y_c)$, $n_h(y_c)$ and $< n_h(n_h-1) >_{y_c}$. The only (and serious) approximations involve cavalier treatment of kinematic correlations connected with energy momentum and charge conservation, as I indicated above. I now turn to specific models for the rapidity distribution and multiplicity content of clusters, to see what these imply for $\sigma^{-1} d\sigma/dy$, $C(y_1,y_2)$, $f_2$ and so forth.

## 3.4. Multiperipheral emission of clusters *)

For exercise, we can take both $n(y_c)$ and $\rho(y_c)$ as (both s and $y_c$ independent) constants : $< K >$ and B respectively, whereupon

$$\frac{d\nu_h}{dy} = \nu \langle K\rangle B \int_{-kY/2}^{kY/2} g(y-y')\, dy' \qquad (3.26)$$

$$= \frac{\nu\langle K\rangle B}{2} \left\{ \tanh\left(y+\frac{kY}{2}\right) - \tanh\left(y-\frac{kY}{2}\right)\right\}$$

---

*) Much of the work I discuss in this section and in Sections 5.6-5.7 was done in a long-range collaboration with G.C. Fox during the past year. See also Ref. 4).

As can readily be seen, when $y \ll Y$, $d\sigma_h/dy \to \sigma \langle K \rangle B$, which is just the energy independent flat distribution in rapidity, indicated by data and to which so many models aspire.

$$\langle n_h \rangle \sigma \simeq \sigma \langle K \rangle B \log s \tag{3.27}$$

With this same multiperipheral-like model, $\langle n_h(n_h-1) \rangle = \langle K(K-1) \rangle$ is independent of $y_c$ and $s$. We obtain from (3.24)

$$C(y_1, y_2) = \frac{B\langle K(K-1)\rangle}{2\delta\sqrt{\pi}} \exp\left[\frac{-(y_1-y_2)^2}{4\delta^2}\right] \tag{3.28}$$

An alternative form is

$$C(y_1, y_2) = \frac{\langle K(K-1)\rangle}{2\delta\sqrt{\pi}\,\langle K\rangle\sigma} \left.\frac{d\sigma}{dy}\right|_{y=0} \exp\left[\frac{-(y_1-y_2)^2}{4\delta^2}\right] \tag{3.29}$$

The correlation function falls off in a Gaussian fashion as a function of $|(y_1-y_2)|$. It is independent of energy $s$, if the single particle plateau height is itself energy independent. The distance $\lambda$ over which $C(y_1-y_2)$ falls to $e^{-1}$ of its peak value may be defined to be a "correlation length"

$$\lambda = 2\delta \simeq 1.8 \tag{3.30}$$

This correlation length is essentially identical to that given in inclusive Regge (Mueller) analysis [23),38)]. In this latter approach, $\lambda = (\alpha_P - \alpha_R(0))^{-1} \simeq 2$ if $\alpha_R(0) \simeq \frac{1}{2}$. The two approaches may differ, however, if the quantum numbers of the two-particle system in question are exotic. In this case, it is not altogether clear whether inclusive Regge analysis is applicable ; if it is, then $\alpha_R(0) < 0$ and $\lambda < 1$. It will be noted that the Gaussian form in (3.29) is valid only for small $|y_1-y_2|$, where neglect of the pion mass implicit in (3.17) is justified. On the other hand, the exponential form for $C$ predicted by Mueller analysis [38)] is correct only at large $|y_1-y_2|$. The two approaches are in a sense complementary. The relevant data are all at small $|\Delta y|$.

The integral of $C(y_1,y_2)$ [Eq. (3.29)] over all phase space gives

$$f_2^{(h)} = B\langle K(K-1)\rangle Y \quad \left(\cong \frac{\langle K(K-1)\rangle}{\langle K\rangle}\langle n_h\rangle\right) \tag{3.31}$$

where $Y = \log s$. The coefficient of $\log s$ is positive as long as the number of particles per cluster $N \geq 2$.

Taking $f_2^{(-)} \simeq (0.7\pm0.1)\langle n_-\rangle$ as a crude parametrization of data [20] on negative particle production for $p_{lab} > 50$ GeV/c, I find that hadronic clusters produced in the multiperipheral chain contain roughly 1.7 negative hadrons on the average. More detailed analysis (Section 4.3) shows this is a slight overestimate.

Before leaving the multiperipheral approach and turning to an alternative explanation of the scaling plateau, I should call attention to the fact that, as I have developed it here, the multiperipheral cluster emission model cannot describe a possible diffractive component in the data. Thus, in the model all $\sigma_n(s) \to 0$ as $s \to \infty$. This is equivalent to the statement that there are no Pomeron exchanges in our multiperipheral chain. Data on the $s$ dependence on $\sigma_n$ are consistent with this possibility, but it may also turn out that $\sigma_n(s) \to C_n$, with all least some $C_n > 0$ as $s \to \infty$. A stronger indication of the presence of a diffractive component is the observation of an inelastic diffractive peak in the proton $x$ spectrum near $x = 1$ (cf. Section 5). By introducing an additional set of graphs in which one Pomeron is present in the chain of exchanges, we can reproduce both the inelastic peak and obtain $\sigma_n(s) \to C_n > 0$. This point is developed in Section 5. For the present, we can regard the model discussed in the present subsection as a model for the non-diffractive component of multiparticle data. For discussion of more theoretical points associated with the multiperipheral cluster emission approach, the papers of Hamer and Peierls may be consulted [39].

## 3.5. Fragmentation models

The constant assumptions $\rho(y_c) \to B$ and $n(y_c) \to \langle K\rangle$ made in Section 3.4 are not the only way to generate a plateau in $y$ for the single particle rapidity spectrum. As a second example, I may cite the nova fragmentation approach [3),40)] in which production of a cluster of mass $M$ is postulated to have production cross-section $d\sigma/dM \sim \sigma_0/M^2$, and decay multiplicity $n(M) \sim K_0 M$. Only one or at most two clusters are produced per event.

For simplicity I will use these formulas over the full interval $1.0 < M < \sqrt{s}$. Thus

$$\sigma_{inel} = \int (d\sigma/dM)\, dM = \sigma_0 \qquad (3.32)$$

$$\langle n \rangle = \tfrac{1}{2} K_0 \log s$$

The kinematic relationship between $y_c$ and $M$ is $|y_c| = \log(\sqrt{s}/M)$. Therefore,

$$\rho(y_c) = \frac{1}{\sigma} \frac{d\sigma}{dM} \frac{dM}{dy_c} = \frac{1}{M} \qquad (3.33)$$

and

$$n(y_c) = K_0 M = K_0 \sqrt{s}\, \exp(-|y_c|). \qquad (3.34)$$

The important result is that the product

$$n(y_c)\, \rho(y_c) = \text{Constant} = K_0 \qquad (3.35)$$

This guarantees the single particle inclusive plateau, as in Eq. (3.26).

Although both models can be made to agree on the existence of an asymptotic $s$ independent central plateau, the fragmentation and multi-peripheral cluster models are seen to differ in a spectacular way when one looks at their very different expectations for the evolution of dynamics with energy. The differences are seen most clearly upon examination of idealized individual event structure.

Below $p_{lab} = 30$ GeV/c, the two models are in essential agreement. Both expect one or two clusters to be produced per event. Indeed, low multiplicity, low mass clusters seem clearly present in data [41], but it is possible that these effects are explained as a reflection of leading particle effects. At these low energies, presence of clustering may also be inferred indirectly from successful fits with cluster-dominated models to two particle inclusive spectra [40], in contrast to the failure of independent emission models [42].

As energy grows, and phase space opens, the fragmentation approach restricts the number of clusters to 2. In the multiperipheral approach, more clusters pop out of the vacuum. Their number grows in proportion to log s, $< N > \simeq B \log s$. Based on fits [4] to data,

$$B \simeq 0.5 \text{ to } 0.75 \qquad (3,36)$$

Thus, the mean distance between clusters in the multiperiphal approach is

$$|\Delta Y_c| \simeq 1.3 \text{ to } 2$$

This interval is comparable to the intrinsic typical spread of $\Delta y = 2$ for decay particles from a single cluster.

To fulfil the requirement that $< n > \sim \log s$, the typical multiplicity (mass) in a cluster of the fragmentation type must grow with s. In our multiperipheral approach, the mean number of hadrons per cluster ($\simeq 4$) is energy independent. For $p_{lab} \gtrsim 100$ GeV/c, typical events in the two models are sketched below in rapidity y space.

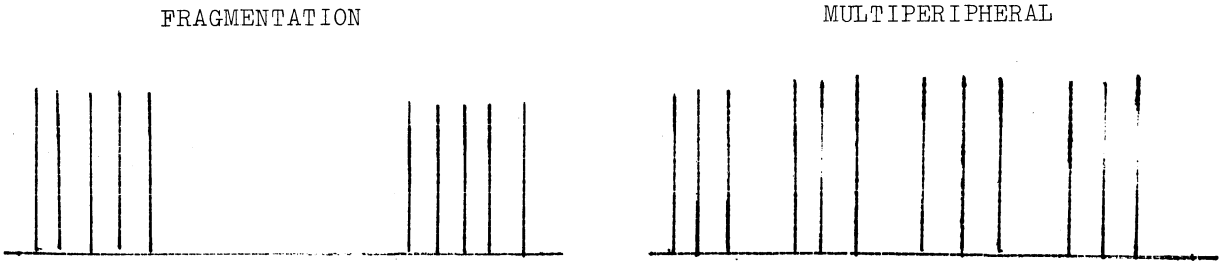


Each vertical bar marks the position in y of a charged track.

New techniques of data analysis must be developed to help in identifying patterns of these types in individual events. One possibility is the measurement of the dispersion $\delta^1$ of tracks in y space [36]. In Monte Carlo simulations, this parameter shows good promise in distinguishing between the two broad classes discussed above [4),36),37)]. Moreover, within the multiperipheral class of models, one finds

$$\langle \delta^1 \rangle = c \log s + d \qquad (3.37)$$

The value c is sensitive to the number of particles per cluster [4),37)].

At the conventional inclusive level, discrimination between the (two-cluster) fragmentation and (multicluster) multiperipheral view-points is possible by studying certain features of the two-particle rapidity distribution [40),43)]. The magnitude of predicted cross-sections at $y_1 \approx y_2 \approx 0$ as well as s dependence are very different in the two cases, with data seeming to favour the first example.

In the fragmentation case, with $n(M) = K_0 M$, as stated above, we have $n(M)(n(M)-1) \sim K_0^2 M^2$. Thus, the product

$$\rho(y_c) \langle n_h (n_h - 1) \rangle_{y_c} \sim K_0^2 M = K_0^2 \sqrt{s} \exp(-y_c) \qquad (3.38)$$

For the single fragmentation component, with one cluster per event, the correlation function is

$$C_1(y_1, y_2) = \frac{K_0^2}{4} + \frac{K_0^2 \sqrt{s}}{4\pi\delta^2} \left\{ \int_0^{\log\sqrt{s}} dy' \exp(-y') I(y_1, y_2, y') + \int_{-\log\sqrt{s}}^{0} dy' \exp(y') I(y_1, y_2, y') \right\}$$

$$I(y_1, y_2, y') = \exp\left[ \frac{-(y_1 - y')^2 - (y_2 - y')^2}{2\delta_0^2} \right]$$

After some algebraic manipulation, we can re-express this as

$$C_1(y_1, y_2) = \frac{K_0^2}{4} + \sqrt{s} \exp\left[ \frac{-(y_1 - y_2)^2}{4\delta^2} \right] F\left( (y_1 + y_2), \log s \right) \qquad (3.39)$$

The function $F(0, \log s)$ is approximately constant. A second contribution $C_2(y_1, y_2)$ with similar structure arises from the double fragmentation component, having two clusters per event.

We observe several features of this expression.

(A) For $(y_1+y_2)$ fixed, it has the same Gaussian fall-off in $(y_1-y_2)$ as does the multiperipheral example (3.29).

(B) However, it displays explicit dependence on $(y_1+y_2)$ which the multiperipheral-like example did not. It is not a function just of the difference $(y_1-y_2)$.

(C) It shows a growth with s proportional to $\sqrt{s}$ at $y_1 = y_2 = 0$, when $K_2$, the height of the single-particle inclusive spectrum in the model is constant. Again, this is in contrast with (3.29) which shows no s dependence.

Data [17)-19)] seem to favour (3.29), although there is some doubt (cf. Section 4). In fact, the hint from data that correlations are s independent in the central region and a function only of the difference $(y_1-y_2)$ is confirmation of much deeper ideas than those which are apparent in either of the crude examples treated here. We return now to the short-range order hypothesis which gives these effects in a model independent manner.

## 4. INCLUSIVE CORRELATIONS

### 4.1. Apology

The measurement of correlation is after all a major part of what physics is all about. Short of an article on the subject by itself, I could not attempt a complete treatment even of all the two-body correlation measurements presently made or desirable for theoretical reasons. I will therefore only mention in passing data on neutral-charged particle correlations in multiplicity distributions [44)]. Likewise, owing to scanty data, I will not treat the intriguing question of inclusive correlations between hadrons as a function of angle $\phi$ between their respective transverse momentum vectors. Experimental hints [17)] that such correlations are positive and of long-range in y deserve detailed investigation. Since I have set aside any treatment of large $p_T$ phenomena, neither will I speculate here on the character of events which give hadrons with large $p_T$ [11)]. Collective phenomena, such as clustering, require new methods for statistical analysis of data [36),37),41)].

My focus will be restricted essentially to inclusive correlations in rapidity between two hadrons. There are important theoretical expectations and relevant data on this interesting subject [45].

## 4.2. Two-particle rapidity correlations

The two-particle inclusive cross-section is a priori a function of five independent variables : $s$, $y_1$, $y_2$, $|p_{T1}|$, $|p_{T2}|$ and $\phi$, where $\phi$ is the angle between the two transverse vectors $\vec{p}_{T1}$ and $\vec{p}_{T2}$. I will henceforth neglect the $\phi$ and $p_T$ dependences, concentrating only on $y$ dependences. Therefore,

$$\frac{d^2\sigma}{dy_1\, dy_2} = G(y_1, y_2, s) \qquad (4.1)$$

In this section, I will discuss in detail only correlations observed between hadrons which are both in the central region. Correlations found when one or the other hadron may be outside this central region are summarized well by Sens [1]. Obvious long-range correlations present when one or both protons have $|x| > 0.8$ are treated in Section 5.

If both observed hadrons are in the central region, then $|y_i - y_a| > \lambda$ and $|y_i - y_b| > \lambda$. As before, $y_a$ and $y_b$ are the rapidities of the incident protons. According to the SRO hypothesis, in this central region, $G$ cannot depend on $|y_i - y_a|$ or $|y_i - y_b|$. The only remaining rapidity variable is $|y_1 - y_2|$. The hypothesis predicts therefore that

$$\frac{d^2\sigma}{dy_1\, dy_2} \longrightarrow g(y_1 - y_2) \qquad (4.2)$$

In other words, the two-particle distribution should tend to an energy independent function of $\Delta y$. [If, further, it were kinematically possible to have $(\Delta y) > \lambda$, with both $y_i$ still in the central region, then $g \to$ const. This latter prediction seems to have little practical significance even at ISR energies.] The hypothesis does not predict the magnitude of $g(y_1 - y_2)$ nor its functional form. For this, we need explicit SRO model, such as that discussed in Section 3.4.

An alternative to the simple prediction (4.2) is provided by fragmentation models, in which one finds both long-range and short-range structure. Explicit fragmentation predictions were developed in Section 3.5, where, we saw that a $\sqrt{s}$ growth of $G(y_1,y_2,s)$ was expected, in contrast to (4.2). Furthermore, in fragmentation models, dependence on the variables $|y_i-y_a|$ and $|y_i-y_b|$ does not drop out.

I now turn to an examination of available correlation data from NAL [19], and from the Pisa-Stony Brook [18] and CERN-Hamburg-Vienna [17] ISR collaborations. All these data are expressed in terms of

$$R(y_1,y_2) = \frac{C(y_1,y_2)}{\left(\frac{1}{\sigma_{inel}}\right)^2 \frac{d\sigma}{dy_1}\frac{d\sigma}{dy_2}} \,. \qquad (4.3)$$

This ratio is simpler to determine experimentally than $C(y_1,y_2)$. To the extent that $\sigma^{-1}d\sigma/dy$ is independent of $s$ and $y$, the denominator is a constant, and conclusions about $R(s,y_1,y_2)$ bear directly on $C(s,y_1,y_2)$.

The existence of a scaling plateau is best established for pion production at fixed small $p_T$ : $0.1 < p_T < 1.0$ GeV/c. Thus, inclusive correlations between pions ($\pi^+\pi^-$, $\pi^+\pi^+$, $\pi^-\pi^-$, $\pi^\pm\pi^0$) in the central region, with $0.1 < p_{Ti} < 1.0$ GeV/c for both pions would offer the greatest opportunity for a clean investigation of new phenomena. Unfortunately, all present central region correlation data are averaged over all $p_T$. Moreover, in the Pisa-Stony Brook experiment [18], correlations are observed between any pair of charged particles, without regard to sign ($\pm$) and particle type ($\pi$,K,$\bar{p}$, etc.). In the CHV study [17], correlations between a $\gamma$ ray and a charged track are studied. Finally, in the NAL and ISR experiments, the approximate rapidity variable $\eta = \log(\tan\theta/2)$ rather than $y$ is used for charged particles. For these reasons, results are not as precise as one might like.

In Fig. 10 results of the CHV collaboration [17] are shown for $\sqrt{s}$ = 22, 30, 45 and 53 GeV. Presented is

$$R(y_\gamma,y_{ch}) = \frac{\sigma_{inel}\, d^2\sigma/dy_\gamma dy_{ch}}{(d\sigma/dy_\gamma)(d\sigma/dy_{ch})} - 1 \qquad (4.4)$$

versus $y_\gamma$ for $y_{ch} \approx 0$ (open circles) and $y_{ch} \approx -2.5$ (dark circles). The point $y_{ch} \approx -2.5$ falls outside the central region. Thus those predictions of SRO developed above do not apply to the data shown in dark circles.

Concentrating on the data for which $y_{ch} \approx 0$, we see that $R(0,0)$ is positive ($\approx 0.65$). R is essentially independent of s from $\sqrt{s} = 23$ to 53, for all $|y_\gamma| < 3$. The function $R(y_\gamma, 0)$ is well fitted by a Gaussian [cf. Eq. (3.28)] with correlation length $\lambda \approx 2$.

A compendium of Pisa-Stony Brook charged-charged correlation data [18] appears in Fig. 11 for $\sqrt{s} = 23$ and 63 GeV. The function $R(\eta_1, \eta_2)$ is plotted versus $\eta_2$ for several fixed values of $\eta_1$. For small $|\eta_i|$ it is clear that $R(\eta_1, \eta_2)$ is largest at $\eta_1 \approx \eta_2$, and that the maximum value $R(\eta_1 \approx \eta_2) \approx 0.65$ is s independent. An energy independent function of $(\eta_1 - \eta_2)$ is certainly in accord with <u>dominant</u> features of these data, but some deviations are notable even at $|\eta_i| < 2$. In particular, while the average correlation length $\lambda$ is $\approx 2$, the plot with $\eta_1 \approx 0$ shows that this length is effectively larger at $\sqrt{s} = 63$ than it is at $\sqrt{s} = 23$. Some dependence on $|\eta_i - \eta_{a,b}|$ (i.e., on $|\eta - \frac{1}{2}\log s|$) may also be discerned in the plots.

Data on charged-charged correlations from an NAL bubble chamber experiment [19] at 200 GeV/c are portrayed in Fig. 12. These results are plotted versus $|\eta_1 - \eta_2|$ for two fixed values of $\eta_1$. The maximum occurs at $\eta_1 \cong \eta_2$, where $R = 0.6 \pm 0.1$. A correlation length of 2 is also appropriate here. Similar results for $\pi^- \pi^-$ correlations show $R(0,0) \simeq 0.3$ with large errors.

It would be heartening to be able to conclude from these data that the principle of short range order is in perfect accord with data on two-particle inclusive spectra, and that the fragmentation alternative in the central region is dead. However, the crucial issue of energy dependence is still unresolved. As will be recalled, the CHV and P-SB groups observe a healthy 20-30% rise of their $\sigma^{-1} d\sigma/dy$ over the ISR energy range. Therefore, their true correlation functions

$$C = R\left(\sigma^{-1} d\sigma/dy_1\right)\left(\sigma^{-1} d\sigma/dy_2\right)$$

rise by 50% or more. In a sense, this rise splits the difference between the zero growth and $\sqrt{s}$ growth predictions of pure SRO and pure fragmentation, respectively [Eqs. (3.29) and (3.39)].

Partisans of either view can have their way. One may speculate that whatever causes the rise of $\sigma^{-1} d\sigma/dy$ and $\sigma^{-1} d\sigma^2/dy_1 dy_2$ in the CHV and PSB experiments properly cancels out in the ratio $R(\eta_1, \eta_2)$, and therefore, that R rather than C represents unbiased reality. This will remain a speculation until clean data on pion-pion central region rapidity correlations become available, with $p_T$ of both pions in the range $0.1 < p_T < 1.0$ GeV/c (where the pion scaling plateau is established).

A summary of rapidity correlation data in the central region follows.

(a) Strong positive correlations are observed ; $R(0,0) = 0.6$ to $0.7$ for the charged-charged configuration.

(b) The correlation length $\lambda$ is roughly energy independent ; $\lambda \simeq 2$.

(c) The magnitude and shape of $R(\eta_1, \eta_2)$ is roughly the same for $\gamma$ charged and charged-charged correlations.

(d) For $|\eta_1 - \eta_2| < 2$ and $|\eta_i| < 2$ $R(\eta_1, \eta_2)$ shows dominant dependence on the difference $|\eta_1 - \eta_2|$, in accord with expectations of pure SRO.

(e) $R(0,0)$ is energy independent. With uncomfortable reservations, this suggests that $C(0,0)$ may be approaching the s independent limit predicted by pure SRO.

## 4.3. Implications for models

The issue of s dependence of $C(0,0)$ is crucial for two-fireball models [46]. The particular fragmentation example discussed in Section 3.5 provides a $\sqrt{s}$ growth of $C(0,0)$. While somewhat weaker [e.g., $(\log s)^2$ or $s^{1/4}$] behaviour might be obtained in other versions of the two fireball approach, growth with s seems inescapable. Qualitatively, the reason is simple. Since a fireball by definition occupies a finite spread in rapidity, its centre $y_F$ must be located reasonably near $y = 0$, in order that we observe its decay particles in the region near $y = 0$. In a one or two fireball event, the kinematic relationship $y_F \simeq \log(\sqrt{s}/M_F)$ holds, where $M_F$ is the fireball mass. Therefore, the fireball mass $M_F \propto \sqrt{s}$. Inasmuch as multiplicity grows with mass ($n \gtrsim \log M$), the fireball providing particles near $y \simeq 0$ will have multiplicity of order $(\log s)^p$ or $s^q$, where powers p and q depend upon assumptions made about fireball decay. Given a hadron near $y = 0$, the chance of finding another is proportional to the multiplicity of the fireball from which the particles come. Thus

$$C(0,0) \simeq f(s), \qquad (4.5)$$

where function $f(s)$ grows with $s$.

Observation of a scaling $C(0,0)$ would seem therefore to eliminate the entire two fireball class, not just the specific realization discussed in Section 3.5.

There is, of course, other circumstantial evidence against two fireball models. For example, it has been argued that with two fireball models it is impossible to obtain a simultaneous numerical fit to both the plateau $d\sigma/dy$ for pions and the NAL prong cross-section data [47]. A successful fit to $\sigma_n$ vs. $n$ at large $n$ forces a dip in $d\sigma/dy$ near $y = 0$. A judgement here depends, however, on the cleverness of the person fitting data. I know I can overcome this particular objection, and several others, but the resulting model is not what everyone would consider most natural [48]. In particular, the use of non-asymptotic terms and of elongated (multiperipheral-like) decay distributions in the nova or two fireball approach begins to beg the issue of what a fireball or nova is meant to be.

In the minds of many people, a multiperipheral or short-range order dominated model is emerging as the most natural explanation at hand for describing phenomena in the central region. The approach easily provides an energy independent plateau for single particle spectra, energy independent short-range correlations, and prong cross-sections $\sigma_n$ which fall off as $(n!)^{-1}$ for $n > < n >$, all in <u>qualitative</u> agreement with data. If the objects emitted along the chain are hadronic clusters (cf. Sections 3.2 and 3.4), then many quantitative aspects of data are also reproducible. Diffractive effects, discussed in Section 5, are easily accommodated by inclusion of graphs in which a Pomeron link is present in the multiperipheral chain. Geoffrey Fox and I have performed a specific calculation along these lines [4]. For details of the parametrization, consult Ref. 4). Spectra were evaluated with a Monte-Carlo program in which all energy-momentum and other constraints are fully respected. A sample of results is presented in Figs. 13, 14, 15 and 16.

Charged particle multiplicity data [20] from 50 to 300 GeV/c are well reproduced (Fig. 13). Rapidity distributions at several energies [49] are shown in Fig. 14. Scaling in the fragmentation regions and the eventual appearance of a plateau at ISR energies are apparent. The general shape and energy dependence (including the rise at $y = 0$ versus energy) are in accord with data [28),29),49),30),31)]. Our results for $R(y_1,y_2)$ are given in Fig. 15 (a,b). We see that $R$ is energy independent over the ISR range for $y_1 \approx 0$. For a value of $y_1$ which is outside the plateau, $R$ rises with energy to its limiting form as a function of $(y_1-y_2)$ only. These features all agree with data discussed earlier in this section, as does the rough shape and, in particular the zero in $R$ seen at $y_1 \approx 0$, $|y_2| \approx 3$.

Although diffractive effects can in principle and do affect correlations in the central region (cf. Section 5.7), our analytic calculations and Monte-Carlo results both indicate that essentially all correlation in the central region is of a short-range character. Thus,

$$R(0,0) \simeq 0.1 + R_{SR}(0,0) \tag{4.6}$$

Here,

$$R_{SR}(0,0) \simeq C_{SR}(0,0) \Big/ \left(\frac{1}{\sigma_{SR}} \frac{d\sigma_{SR}}{dy}\right)^2_{y=0} \tag{4,7}$$

with $C_{SR}$ given by Eq. (3.29). The constant term (0,1) in Eq. (4.6) is the net long-range contribution. It is associated with diffractive effects, as discussed in Section 5.7. [Its magnitude is controlled, of course, by the net cross-section $\sigma_D$ associated with single inelastic diffraction, Our results for $\sigma_D$ agree well with information available from NAL and ISR on the magnitude and shape of $Ed\sigma/d^3p$ for $pp \to pX$ at large $x_p$ ; cf. Section 5.]

From Eqs. (4.6) and (3.29) we deduce that

$$\frac{\langle K(K-1)\rangle}{2\sqrt{\pi}\,\delta\langle K\rangle} \simeq 0.55 \left(\frac{1}{\sigma_{SR}} \frac{d\sigma_{SR}}{dy}\right)_{y\simeq 0} \tag{4.8}$$

An average $< K > = 4$ pions (of all charges) per cluster decay fits both the correlation data and correlation moment $f_2$. Other more complicated correlation data [50] from ISR have also been examined, and so far, we find good agreement. (In our approach, $< K >$ is s independent.)

The dispersion of tracks in rapidity provides a good model independent measure of the extent of cluster formation in individual events [36]. Its measurement would provide an independent check on the approximate validity of the idea of multiperipheral emission of clusters.

For each event, we define

$$\bar{y} = \sum_{i=1}^{\ell} y_i/\ell$$

$$\delta_{ch}^{1}(y) = \left\{ \frac{1}{\ell-1} \sum_{i=1}^{\ell} (y_i - \bar{y})^2 \right\}^{1/2} \qquad (4.9)$$

where the sum runs over the $\ell$ particles obtained by removing the leading particle (farthest away in rapidity) from an $(\ell+1)$ charged particle final state. Our model, as in all multiperipheral models, predicts a logarithmic rise in $\delta_{ch}^{1}(y)$. The prediction is shown for two multiplicities in Fig. 16 as a function of $p_{lab}$. At 300 GeV/c, we calculated $\delta$ from this cluster model, from a simple multiperipheral model with production of single $\pi$'s (not in clusters), and from the nova model. Both the nova model and the cluster model agree qualitatively with the experimental dispersions at this energy [37]. [The Monte Carlo program indicates that these models would be distinguishable at 300 GeV/c if true rapidity and not the approximation $-\log(\tan\theta_{proj}/2)$ were used.] Data on $\delta^1$ at ISR energies should be forthcoming soon from the Pisa-Stony Brook group. It will be instructive to see how the experimental results compare with predictions of Fig. 16.

Data on $\delta_n^1$ vs. n will provide an independent estimate of the mean number of particles per cluster, which can be compared with the value $< K > = 4$ we obtained from inclusive rapidity correlation data. It is not obvious a priori that the two estimates should agree, because $\delta_n^1$ measures clustering seen in individual events, of fixed multiplicity n, whereas the magnitude and shape of $C(y_1,y_2)$ are influenced in part by the over-all multiplicity distribution $\sigma_n$ vs. n. [This last point is evident from the relationship

$$f_2 = \langle n(n-1) \rangle - \langle n \rangle^2 = \iint C(y_1, y_2)\, dy_1\, dy_2 \,.]$$

Although I am admittedly too close to the effort to be entirely objective, this is one of the few analyses I know of which attempts a description of all known aspects of inclusive data. For $p_{lab} \geq 50$ GeV/c, we tried to accommodate knowledge of the x, y, $p_T$ and s dependences of single particle spectra, the prong distributions [20] $\sigma_n(s)$, the systematic change with multiplicity [28),51)] n of $d\sigma_n/dy$, and the two-particle inclusive correlation data. Thus, our successful description of the inclusive correlation data was not tailored to this purpose alone.

To be sure, obvious improvements are needed on several fronts, but the reasonable agreement between our model and experiment for most important attributes of multiparticle data at small $p_T$ provides support for the input clustering and multiperipheral-like matrix element. Having in hand a simple framework which successfully imitates the more striking features of NAL and ISR results allows us to estimate the dynamical significance of other observations, in particular those not interpretable directly by fully inclusive (Mueller) analysis [23].

At $p_{lab} \leq 30$ GeV/c, where the nova model is particularly successful [40], our model and the nova model are very similar. At these energies, we produce only one or two clusters, just as in the nova model. As s increases, the number of clusters grows in our model, rather than remaining fixed at one or two.

The evolution of dynamics with increasing energy may be portrayed as in the following crude sketch.

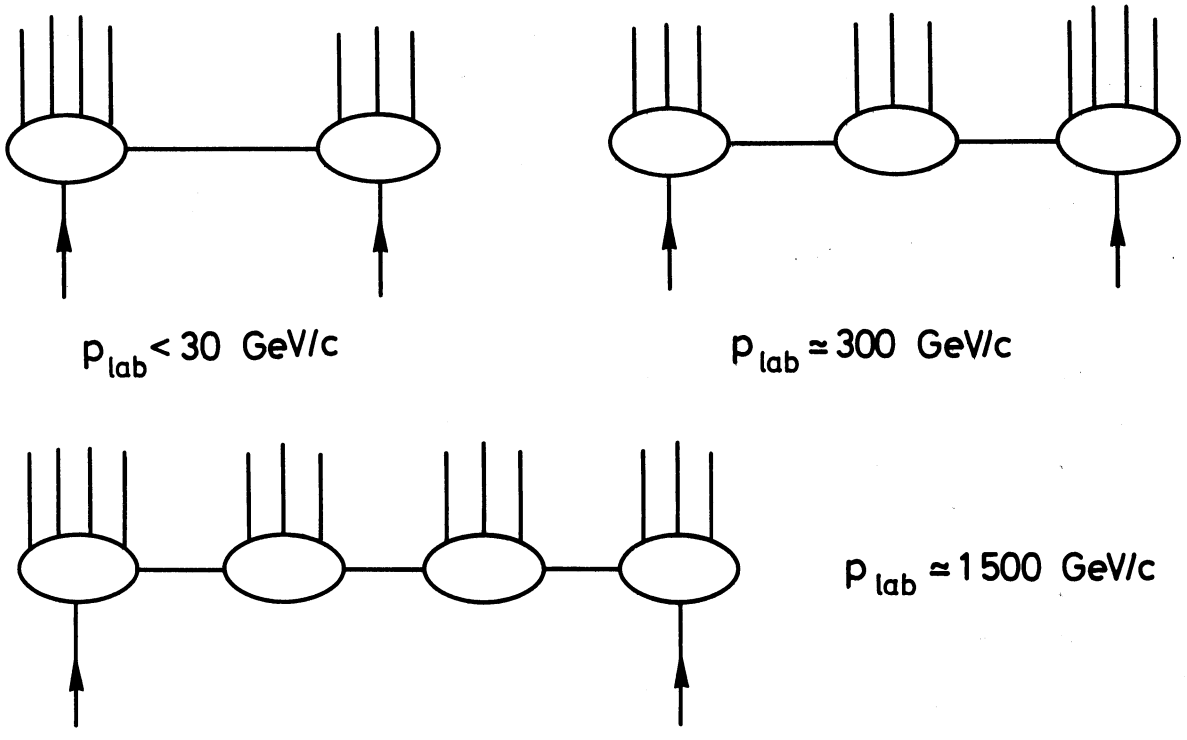

As I have drawn them, clusters always decay into 3-4 particles. However, a broader distribution about the mean of 4 is certainly to be expected. The end clusters, in fact, are sometimes to be replaced by a single diffractively scattered proton. The ratio of diffractive to non-diffractive scattering is an important parameter, which may be determined by careful fits to the inclusive proton spectrum $Ed\sigma/d^3p$ (cf. Section 5). Data in the fragmentation regions are observed to reach their asymptotic form at relatively low $p_{lab}$. In the model, this would mean that the clusters at the end of the chain attain their asymptotic limiting character at low $s$. Further increases in energy allow these two end-clusters to separate in $y$ space. New clusters are generated in the intervening space.

## 5. INELASTIC DIFFRACTION SCATTERING

### 5.1. Qualitative remarks ; long-range correlations

In the last sections, I emphasized the rôle and magnitude of short-range correlations among hadrons in the central region of rapidity. There appears to be evidence in ISR data also for important long-range effects. These can manifest themselves in several ways. Obvious long-range correlation would be present if the inclusive correlation function is enhanced when the distance $\Delta y$ between two hadrons is large. This is an inclusive long-range correlation between two hadrons. A second and more general type of long-range correlation is one in which global information about an entire event is gained simply from an observation (e.g., momentum measurement) made on one particle in the final state [52]. [By contrast, recall that if only short-range correlations are present, a measurement gives us information about inclusive spectra only in the immediate neighbourhood ($\Delta y \leq 2$) of the first observation.]

Both types of long-range correlation seem to be present in the ISR data associated with single inelastic diffraction scattering of one of the initial protons [5]. The process may be sketched below, where, for the moment, I intend absolutely nothing of dynamical content in drawing the wiggly exchange line. By the line I mean only that after entering a collision, a proton departs essentially alone in the final state with a small loss of energy. The energy loss is converted into mass $M$ of the recoil system. Kinematically,

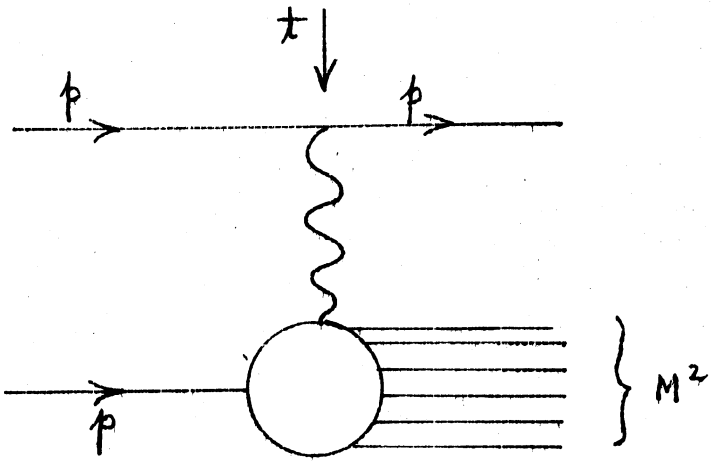


$$M^2 \simeq s\,(1 - x_p)\,. \qquad (5.1)$$

The recoil system is the result of "dissociation" or fragmentation of the other proton.

Use of the word "diffraction" is in some ways unfortunate, since it has had many imprecise meanings to many people over the past 10-20 years, However, in the NAL and ISR ranges, it does seem finally possible to discuss a component of inelastic data which shows an energy (in)dependence similar to that of elastic scattering data. Thus, an attempt at more precise definition can now be justified, perhaps.

Along with single inelastic diffraction, it may be kept in mind that a process such as sketched below probably also contributes at some level. As

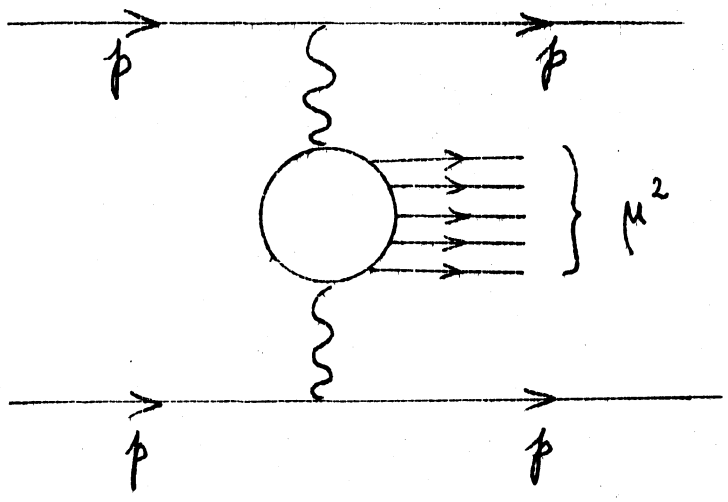

double-arm spectrometer experiments are developed at NAL and ISR, it will be extremely interesting to study correlations in the $(x_{p_1}, x_{p_2})$ plane, as a function of multiplicity of the system of mass $\mu$ indicated above.

$$\mu^2 \simeq s(1-|x_{p1}|)(1-|x_{p2}|) \qquad (5.2)$$

Obviously very large correlation $(x_{p_1} = -x_{p_2})$ is present at low multiplicity, owing to momentum conservation. However, as multiplicity rises, one may or may not see a residual dynamical long-range effect [53].

Finally, a third process is double dissociation, in which two clusters are formed, in some appropriate diffractive sense.

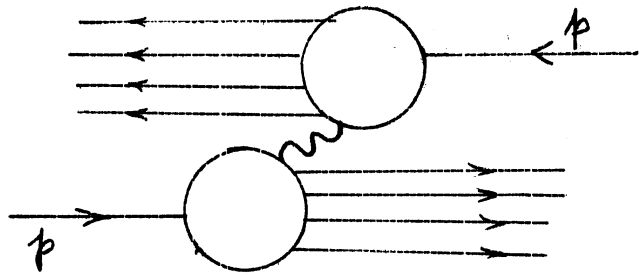


Whether this process can be defined precisely and kinematically isolated is not yet clear.

I will confine my remarks here to <u>single</u> inelastic diffraction, or single "diffraction dissociation", as defined above.

In the following pages, I first summarize present data on single inelastic diffraction and then discuss theoretical interpretations. The variables I use are mass-squared $M^2$ of the recoil system and invariant momentum transfer $t$ from the incident to the fast outgoing proton, as well as $x$, defined in Eq. (5.1).

## 5.2. <u>Summary of data</u>

It is useful to begin with some crude idea of what region of phase space is populated by protons which are directly scattered inelastically, without having "decayed" from some cluster or resonance. To this end, suppose a resonance-like object, with mass $M^*$ is produced at $x_{M^*}$ and with momentum transfer $t$. As a result of the decay $M^* \to p\pi$, for example,

$$x_p \simeq x_{M^*}(m_p/M^*) < 0.8\, x_{M^*} . \qquad (5.3)$$

Thus, the chance of seeing direct scattering is enhanced if one looks at $x_p > 0.8$, and small $t$. The notion of "diffractive" scattering adds the requirements that the differential cross-section $d^2\sigma/dx\,dt$ should fall off reasonably sharply in $t$, and have a dependence on energy which is more or less as independent of $s$ as that of $d\sigma_{el}/dt$.

Relevant data have been obtained by the Rutgers [54] and Columbia-Stony Brook [55] groups at NAL, the NAL pp bubble chamber collaborations [56),57),58)] at 100, 200 and 300 GeV/c, and by the CERN-Holland-Lancaster-Manchester [5] and Aachen-CERN-Harvard-Genova-Torino [53] groups at the ISR. The reaction $\pi^- p \to pX$ at 205 GeV/c has also been studied by the NAL-LBL collaboration [59]. The picture is far from complete, but nevertheless very intriguing. Several points can be made.

5.2.1. x dependence

At fixed $s$, there is a sharp forward peak for $x > 0.9$ in the invariant $Ed\sigma/d^3p$ plotted versus $x$. This peak is present for a broad range of $p_T$ values. At the larger $p_T$ values a valley appears between the peak near $x \approx 1$ and a broad secondary maximum in the range $x < 0.8$. These points are illustrated in Fig. 17.

5.2.2. Scaling in x

At some fixed values of $p_T$ it has been possible to obtain data at several values of $\sqrt{s}$. Because of a non-zero lower bound on the scattering angle, fixed by the apparatus, the $p_T$ values accessible at all $\sqrt{s}$ are unfortunately rather large, where cross-section and physical interest are not at their greatest. However, present measurements at ISR are consistent with an $s$ independent $Ed\sigma/d^3p$ at (all) fixed $x$ and fixed $p_T$. These data are illustrated in Fig. 4. At lower energies [54] both scaling and non-scaling components can be identified.

The scaling properties of $Ed\sigma/d^3p$ for $x > 0.8$ are of great interest, as will be discussed below. More precise data over the widest possible $s$ and $p_T$ range are awaited anxiously.

5.2.3. Mass dependence

Mass dependence mixes $s$ and $x$ dependences. Because

$$d\sigma/dt\, d(M^2/s) = d\sigma/dt\, dx \qquad (5.4)$$

s independence of $Ed\sigma/d^3p$ at fixed x, implies that

$$s\, d\sigma/dM^2$$

is s independent at fixed $(M^2/s)$. That is, $d\sigma/dM^2 = s^{-1}g(M^2/s)$.

The traditional view of fixed mass diffraction holds that a particular mass region or resonance [e.g., N*(1688)] is produced with an energy independent cross-section

$$\frac{d\sigma}{dM^*} = \text{constant}$$

Note that perfect scaling in x all the way to the kinematic limit

$$x_{max} = 1 - m_p^2/s$$

may be incompatible with this tradition. Experiments with excellent mass resolution are needed to examine carefully the s and $M^2$ dependences of cross-section in the region $M^2 \lesssim 5$ GeV$^2$. Spectra from NAL and ISR are shown in Figs. 18 and 19, respectively.

5.2.4. t dependence

Data on the t dependence of inelastic diffraction are available at several energies. Bubble chamber data [57] from 200 GeV/c pp collisions are shown in Fig. 20. The slope $\beta$ in a parametrization of the form

$$\frac{d^2\sigma}{dM^2\,dt} \sim \exp(\beta t) \qquad (5.5)$$

varies smoothly with $M^2$, as shown in the Table below [57]

| $M^2$ | $\beta$ |
|---|---|
| <5 | 9.1 ± 0.7 |
| 5 - 10 | 8.0 ± 1.1 |
| 10 - 25 | 6.1 ± 0.7 |
| 25 - 50 | 5.8 ± 0.7 |

These data show no evidence of any turn-over, dip, or vanishing of $d\sigma/dt$ near $t = 0$. Thus, these bubble chamber results, which should be reliable at small $|t|$, contradict some NAL counter data [55] at 200 GeV/c, in which

a dip in $d\sigma/dt\,dM^2$ is seen at small $|t|$, for $M^2 < 20$ GeV$^2$. Because the t dependence at small $|t|$ is very interesting theoretically (see below), more experimental work seems in order. Owing to the minimum scattering angle limitation mentioned above, ISR data are confined to a range of t values with $|t| \gtrsim 0{,}1$ (GeV/c)$^2$.

For pp scattering, the slope $B_{el}$ of $d\sigma_{el}/dt$ is about $B_{el} \simeq 12$ (GeV/c)$^{-2}$. Combining this with $d\sigma_D/dt \simeq \exp(-6|t|)$, and using factorization, we see that there appears to be no t suppression associated with the coupling :

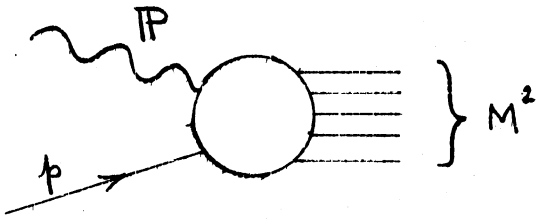


The double dissociation process would appear to suffer from no strong t dependence, therefore, and may grow very rapidly in importance as s increases [60].

5.2.5. Cross-section

The cross-section for single inelastic diffraction is easy to estimate, but it is hard to define precisely. In analyses of NAL bubble chamber results, different groups make different assumptions about the "background" to substract from the observed missing-mass distributions $d\sigma/dM^2$, in order to reduce these to proper cross-sections $d\sigma/dM^2$, differential in mass-squared of a cluster recoiling from a free proton. Next, there is the question of how high up in $M^2$ one should integrate. These ambiguities result in different answers [56),57),58),61)]. Nevertheless, most groups agree on a cross-section somewhere in the interval 5 to 8 mb, for energies in the NAL and ISR range. At $\sqrt{s} = 23.2$ and $\sqrt{s} = 30.4$ GeV, estimates by the CHLM collaboration [61)] give $\sigma_D = 5.4 \pm 1.0$ and $5.0 \pm 1.0$ mb, respectively. These numbers result from summing cross-section for $|x| > 0.94$, after an extrapolation is made in t with the help of NAL data.

5.2.6. Multiplicity

The structure of the recoil cluster and the manner in which its decay particles populate phase space are two areas well worth investigation. The mean charged multiplicity $n(M_x)$ has been obtained from NAL data on $pp \to pX$ as a function of missing mass [56),57),58)]. A compilation is given in Fig. 21. It would be valuable to investigate the t dependence also : $n(M_x,t)$.

Observe that $n(M_x^2)$ appears not to depend on energy s. It grows slowly with $M_x^2$. Two curves are drawn on Fig. 21 to provide a basis for comparison. Neither curve is in any sense a best fit. I took the coefficient b = 1.4 in the parametrization

$$\langle n(M^2) \rangle = a_M + b \log M^2 \qquad (5.6)$$

directly from my fit to the s dependence of over-all pp charged multiplicity [14]

$$\langle n(s) \rangle = a_s + b \log s$$

No attempt is made to reproduce threshold effects for $M^2 < 10$ GeV$^2$. As will be seen, the rate of growth of $\langle n(M^2) \rangle$ with $\log M^2$ is consistent with being the same as the rate of growth of $\langle n(s) \rangle$ versus $\log s$ [62].

The linear curve [58]

$$\langle n(M^2) \rangle = 0.6\, M + 2 \qquad (5.7)$$

is not an unreasonable parametrization at low M, but begins to fail for $M^2 > 50$ GeV$^2$.

Theoretical interpretation of these multiplicity data is not altogether direct. The nova approach [40] is predicated on a linear increase of multiplicity with mass of a properly defined recoil cluster. In fits to low energy data [$p_{lab} \leq 30$ (GeV/c)] with this model, the form

$$\langle n_{ch}(M) \rangle \simeq 1.4 (M - m_p) \qquad (5.8)$$

was found appropriate (for charge multiplicity) [40]. The rather small coefficient (0.6) of the linear term found in NAL data would appear to contradict nova model parametrizations, even at low M. This objection is not as strong as it might be, however, because the missing mass in NAL experiments is not identical to recoil cluster mass of the model. Likewise, direct interpretation of the logarithmic fit [Eq. (5.6)] in terms of multiperipheral-like models is ambiguous inasmuch as a unique or clean exchange situation is not obtained in the data unless appropriate selections are made on $M^2$ and t.

On a purely qualitative level, the fact that the same coefficient $b \simeq 1.4$ is found in fits $< n(s) > \sim b \log s$ and $< n(M^2) > \sim b \log M^2$ suggests that what is important for determining asymptotic multiplicity is the energy available $Q$ in whatever system or subsystem one is dealing with [63]. One might hazard the guess that this remark is both model independent, and invariant to changes of parametrizations of $n_{ch}$ vs. $Q$.

5.2.7. Correlations

The actual distribution in phase space of particles which decay from the single dissociation cluster is intriguing to contemplate. There are, of course, some limitations imposed purely by kinematics. If the fast proton has a given $x_p$, then the mass of the cluster is $M^2 = s(1-x_p)$. The position in rapidity of the centre of the cluster is

$$|y_c| = \log(\sqrt{s}/M) = \frac{1}{2}\log(1-|x_p|). \qquad (5.9)$$

Thus, if $x_p \simeq 0.95$, then the recoil cluster is centred at $y_c \simeq 3/2$.

The manner in which decay particles distribute themselves about $y_c$ is a question of dynamics. Two (extreme) alternatives are provided by the isotropic cluster assumption, on the one hand, and an elongated bremsstrahlung picture on the other. If the decay is isotropic, then the distribution in $y$ has dispersion of about one unit [cf. Eq. (3.18)]. A bremsstrahlung picture allows a roughly uniform spread of pions extending from $y = -\log M + y_c$ to $y = +\log M - y_c$.

Taking $s = 2000$ GeV$^2$ and $x = 0.95$, again, $\log M = 2.3$. The two extreme pictures would predict very different behaviour at this value of $s$, for $x_p \simeq 0.95$.

With $x_p \geq 0.99$, and $s = 2000$ GeV$^2$, $M^2 = 20$ GeV$^2$ and $\log M \tilde{=} 1.5$. Thus, for $x_p \tilde{>} 0.99$, the two view points lead to pretty much the same (largely kinematic) conclusion at ISR energies : a tight cluster moving directly opposite the fast proton.

A sample of available data is shown in Fig. 22. The CHLM group has a series of counters placed in various locations about an ISR intersection region enabling them to record a charged particle signal in coincidence with the fast proton in their small angle spectrometer [50]. The auxiliary

charged particle counters record only a rough angle measurement, not momentum, charge, or mass. As shown in Fig. 22, detection of a charged particle in or near the central region (counters at angles $90\pm14^{\circ}$ and $117{,}5\pm12.5^{\circ}$) has a considerable effect on the shape of $f_p(x)$. The inclusive cross-section shows a dip rather than a peak as $x \to 1$.

These data therefore give direct evidence for negative long-range two-particle inclusive correlations. They suggest also that events providing a proton with large $x$ ($|x| > 0.95$) are events in which the remaining produced hadrons are to be found primarily in the opposite hemisphere. This result, partly of kinematic origin, is evidence for the second type of collective long-range correlation mentioned in the opening paragraphs of this section.

More correlation data obtained by the CHLM group are published [50], and other groups are also undertaking analyses of correlations associated with diffractive events [53),64]. As data become more detailed, their full understanding will undoubtedly require development of phenomenological models realistic enough to accommodate most gross features of data. These correlation data will then probe further features of models and help in identification of new dynamical aspects heretofore buried.

## 5.3. Theoretical games

Perhaps the most obvious theoretical guess to make is that the system of mass $M$ recoiling from the fast proton is produced with an $s$ independent cross-section $d\sigma/dM^2 = f(M^2)$. Attempting a power-behaved structure for $f(M^2)$, we write

$$\frac{d\sigma}{dM^2} = (M^2)^{-\lambda} \qquad (5.10)$$

The total cross-section associated with this phenomenon, which I label $\sigma_D$, is then

$$\sigma_D = \int_{M_0^2}^{M_c^2} M^{-2\lambda}\, dM^2 \qquad (5.11)$$

where $M_o$ and $M_c$ are the lower and upper limits some dynamical model would assign for the region of validity of (5.10).

Taking $M_c = \alpha s$, we find the following choices for the $s$ dependence of $\sigma_D$ :

$$\begin{aligned} &\text{constant} - s^{1-\lambda} && \lambda > 1 \\ &\log(s/\text{constant}) && \lambda = 1 \\ &s^{1-\lambda} && \lambda < 1 \end{aligned}$$

The possibility $\lambda < 1$ is ruled out <u>asymptotically</u> inasmuch as it implies a violation of the Froissart bound.

Because of the kinematic relationship

$$\frac{d\sigma}{dt\, d(M^2/s)} = \frac{d\sigma}{dt\, dx}$$

(5.10) implies

$$\frac{d\sigma}{dx} \propto \beta M^{-2\lambda} = s^{1-\lambda} (1-x)^{-\lambda} \qquad (5.12)$$

Perfect scaling in $x$ of the proton inclusive spectrum then requires $\lambda = 1$. The choice $\lambda = \frac{3}{2}$ made in diffractive excitation models [3], produces a non-scaling form

$$\frac{d\sigma}{dx} \propto \frac{1}{\sqrt{s}} \frac{1}{(1-x)^{3/2}} \qquad (5.13)$$

whose falling $s$ dependence seems in disagreement with ISR data, unless resolution problems are playing curious tricks. (For similar reasons, any $\lambda > 1$ is inappropriate.) Thus, the ISR results are most simply interpreted as requiring $\lambda = 1$. This latter choice is, in fact, that suggested by the triple-Pomeron Regge formalism, as I shall now describe. However, it is perhaps useful to remark that the expressions $d\sigma/dM^2 \propto M^{-2}$, $d\sigma/dx \propto (1-x)^{-1}$, and $\sigma_D \propto \log s$ could well turn out to be in good agreement with data, while the simple triple-Regge formalism may have to be abandoned.

5.4. Triple-Regge limit

Specific Regge based predictions can be made for single-particle inclusive spectra near the "phase-space boundary", where $|x| \to 1$. Inasmuch as only protons have substantial cross-section in this region, I limit my remarks to them : $pp \to pX$.

Consider the diagram drawn in Fig. 23a in the limit $s \to \infty$, small fixed $t = (p_c - p_b)^2$, and, for the moment, fixed $M_x^2 = (p_a + p_b - p_c)^2$. An ordinary Regge limit is appropriate here as indicated in 23b. The cross-section is

$$\frac{d^2\sigma}{dt\,dM^2} = \sum_j \frac{1}{\pi^2}\,\beta_j(t, M^2)\,\left(\frac{s}{M^2}\right)^{2\alpha_j(t)}, \qquad (5.14)$$

where a sum is made over the different trajectories $\alpha_j(t)$ which can be exchanged.

We now sum and integrate over the various contributions in missing mass $M_x$. The procedure is equivalent to standing Fig. 23b on its head, and then sewing together the unobserved missing mass channels, as illustrated in Fig. 23c. Summation in the X channel at fixed $M_x^2$ is accomplished in the usual fashion of unitarity sums. We obtain the Reggeon particle ($\alpha_j a$) total cross-section

$$\beta_j(t, M^2) \sim \sigma_{aj}(M^2). \qquad (5.15)$$

If $M^2$ is large, with $(s/M^2)$ kept large, a Regge expansion in the X channel gives

$$\beta_j(t, M^2) \propto \gamma_P(t)\, M^{2\alpha_P(0)} + \gamma_R\, M^{2\alpha_R(0)} \qquad (5.16)$$

where $\alpha_P(0)$ is the $t = 0$ intercept of the Pomeron trajectory, and $\alpha_R(0)$ the intercept of secondary trajectories ($\rho$, $\omega$, $A_2$, f). This is illustrated in Fig. 23d. The end result is Fig. 23e. For the moment I assume that poles are the only singularities we need to consider. Intercept $\alpha_P(0)$ is $\leq 1$ ; with $\alpha_P(0) \equiv 1$, we obtain constant total cross-sections for all processes. The complications and requirements of rising $\sigma_{tot}$ will be addressed subsequently.

Imagine that $M_x^2$ and $(s/M^2)$ are both large enough to justify our keeping only the leading Pomeron contributions. Assembling pieces, we obtain

$$\frac{d\sigma}{dt\, d(M^2/s)} = \gamma_P(t)\,(s/M^2)^{2\alpha_P(t) - \alpha_P(0)} . \qquad (5.17)$$

Here $\gamma_P(t)$ is proportional to the function which describes the coupling of three Pomerons (!). Transforming variables to the proton's scaled longitudinal momentum $x = 2p_L/\sqrt{s} \simeq 1 - M^2/s$, we rewrite (5.17) as

$$E\frac{d\sigma}{d^3p} = \frac{d^2\sigma}{\pi\, dt\, d(M^2/s)} = \gamma_P(t)\,(1-x)^{-1-2\alpha' t} \qquad (5.18)$$

Because of the requirement $s \gg M^2 \gg M_{th}^2$, this formula is meant to be valid in a small region bounded by $(1-x) \ll 1$ or $x > x_0$ and $x \ll (1-M_c^2/s)$.

Before proceeding to a comparison of (5.18) with data, let us catalogue other important triple Regge contributions ; taking $\alpha_R(0) = \frac{1}{2}$ in (5.16)

| Graph | f(x) at t = 0 | |
|---|---|---|
| 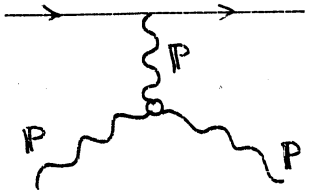  | $\frac{1}{1-x}$ | |
| 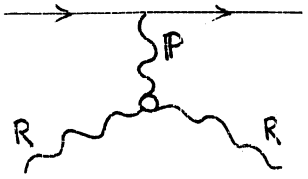  | $(1-x)^{1-2\alpha_R(t)} \longrightarrow$ constant | (5.19) |
| 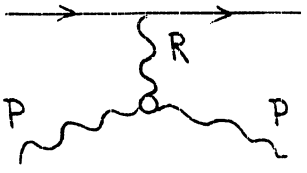  | $\frac{1}{\sqrt{s}}\,(1-x)^{-3/2}$ | (5.20) |
| 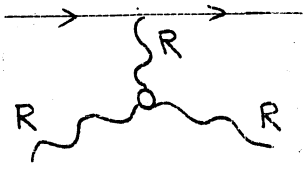  | $\frac{1}{\sqrt{s}}\,(1-x)^{-1/2}$ | (5.21) |

Only the first two contributions survive for all $x$ as $s \to \infty$.

It will be particularly instructive to compare expressions (5.18) with detailed data from NAL and ISR. Fits will require keeping some of the non-Pomeron contributions (5.19)-(5.21) to be sure. Expression (5.17) is particularly interesting in that it specifies both the $s$ dependence at fixed $M^2$ and the $M^2$ dependence at fixed $s$, in terms of the same ratio $(s/M^2)^{2\alpha(t)-\alpha(0)}$.

At fixed ISR energy, for $x > 0.9$, analyses of experimental $M^2$ dependence by members of the CERN-Holland-Lancaster-Manchester group [65] give reasonable fits to (5.17) with $\alpha_P(t) \approx 1 + 0.2\,t$. To be sure, experimental errors allow some variation of intercept $\alpha_P(0)$ about 1 and of slope in the vicinity of 0.2. The value $\alpha(0) \approx 1$ for $x > 0.9$ should be contrasted with $\alpha(0) \simeq 0.5$ which is obtained for $0.3 < x < 0.8$ ; this latter region is evidently dominated by the RRP term.

## 5.5. Implications of the triple-Pomeron term

Since the formula with $\alpha_P(0) = 1$ is at least consistent with the $M^2$ dependence of data, let us take it seriously and contemplate some of its implications. Expression (5.18) shows directly the prediction of a scaling ($s$ independent) peak in the proton $x$ spectrum near $x_p = 1$, in qualitative agreement with data. The apparent infinity as $x \to 1$ is really not present. The formula ceases to be valid there.

Other consequences of a finite coupling of the triple-Pomeron amplitude are also interesting. We consider first its contribution to the total inelastic cross-section, and then proceed to a possible description of the structure of inelastic events associated with the fast diffractively-scattered proton.

The cross-section $\sigma_D$ is given by

$$\sigma_D = \int \frac{d^2\sigma}{dt\,dM^2}\,dt\,dM^2 \qquad (5.22)$$

where the integral extends over the region in $t$ and $M_0^2 < M^2 < M_c^2 \propto s$ in which the PPP is dominant. In principle, $[\leq n_p > ]_D$ and not just $\sigma_D$ should appear on the left-hand side of (5.22). However, I take $< n_p > = 1$, consistent with our interpretation of expression (5.17) in the intended range of integration. Converted to $x$, and with the PPP term displayed explicitly, (5.22) becomes

$$\sigma_D = \int dt \int_{x_0}^{x_c} \gamma_P(t)\,(1-x)^{-1-2\alpha' t}\,dx \qquad (5.23)$$

As before, $x_0$ = constant, and $x_c = 1-(M_c^2/s)$.

If $\gamma_P(0)$ is finite and $\alpha'_P = 0$, we find

$$\sigma_D \propto \log\left(\frac{1-x_0}{1-x_c}\right) = \log\left(\frac{s(1-x_0)}{M_c^2}\right). \qquad (5.24)$$

This form of the PPP coupling therefore provides a log s increase of the single inelastic diffractive cross-section $\sigma_D$.

Before proceeding further, I should like to illustrate how this log s increase comes about. In the top half of Fig. 24, I show the region of integration in x from fixed $x_0$ to $x_1$, at $s = s_1$ ; and from $x_0$ to $x_2$, at $s = s_2 > s_1$. Here $x_i = 1 - M_c^2/s_i$, with $M_c^2$ fixed to be independent of s. The increase $\Delta\sigma_D$ as s is changed from $s_1$ to $s_2$ arises because at higher s, we integrate up closer to $x = 1$ along the scaling curve $f_p(x)$. However, it is important to keep in mind that this extra cross-section really comes from high values of excitation mass $M^2$. As shown in the lower part of Fig. 24, the equivalent region of integration in $M^2$ is from the fixed lower limit $M_c^2$ to a variable upper limit. The correspondence between the x and $M^2$ plots is simple. As energy is increased, more and more of the $M^2$ plot is squeezed up in x above our fixed lower cut-off $x = x_0$.

Unless compensating terms are hidden, the log s increase of $\sigma_D$ will result in a component of $\sigma_{inel}$ which rises as log s. Such a growth is not, in itself, theoretically inadmissible [34] nor experimentally contradicted, as discussed in more detail below. However, once the PPP coupling is admitted, then graphs are also allowed in which an arbitrarily large number of Pomerons are exchanged. As shown some years ago [66] with an exchange of n Pomerons, we derive a cross-section

$$\sigma_n \sim (\log s)^{n-1}.$$

For $n > 3$, an asymptotic violation of the Froissart bound results.

Because the Froissart bound is by no means saturated in the ISR range, a local growth of $\sigma_D$ faster than $(\log s)^2$ is presumably acceptable. However, the problem of principle arises sooner or later. Considerable theoretical effort has gone into the general question of Pomeron couplings [67].

The choices $\alpha' \neq 0$ and/or $\gamma_P(0) = 0$ in Eq. (5.23) modify the argument. Taking $\gamma_P(t) = \exp(bt)$ and $\alpha' \neq 0$, we find

$$\sigma_D \propto \log\left[b + 2\alpha' \log(s/M_c^2)\right] . \tag{5.25}$$

This expression gives a slow $\log(\log s)$ increase asymptotically, but, to the extent that $(2\alpha'/b)\log s \ll 1$, we obtain here also a direct logarithmic increase

$$\sigma_D \propto \frac{2\alpha'}{b} \log s \tag{5.26}$$

over some range of $s$. With $\alpha' \simeq 0.3$ and $b \simeq 6$, the appropriate range is $\log(s/M_c^2) \ll 10$. With $M_c^2 \simeq 10\ \mathrm{GeV}^2$, $s \lesssim 100\ \mathrm{GeV}^2$ is acceptable. The theoretical problem of asymptotic violation of the Froissart bound is still present.

If $\alpha' \neq 0$ and $\gamma_P(0) = 0$, the cross-section $\sigma_D$ also rises, but now to a constant asymptotic limit. Taking $\gamma_P(t) = t \exp(bt)$, we find easily that

$$\sigma_D \propto -\int_{x_0}^{x_c} \frac{d\log(1-x)}{\left[b - 2\alpha' \log(1-x)\right]^2} \tag{5.27}$$

$$= K_1 - \frac{K_2}{1 + \frac{2\alpha'}{b}\log(s/M_c^2)}$$

Vanishing of the triple-Pomeron coupling $\gamma_P(0) = 0$, thus prevents an unbounded increase of $\sigma_D$ and avoids eventual violation of the Froissart bound.

Data, however, seem to show no evidence for a zero at $t = 0$, at least at 200 GeV/c (Fig. 20). It seems, therefore, that $\gamma_{PPP}(t=0) \neq 0$, and one must look to some other method to achieve a consistent theoretical picture in which the asymptotic bound $\sigma_D \lesssim (\log s)^2$ is satisfied. Much effort in this direction is expected during the coming months.

The logarithmic rise shown in (5.24) suggests that we may attempt to "blame the rise" of $\sigma_{tot}$ observed in the ISR range on $\sigma_D$. As pointed out by various people [34], the numbers do in fact seem to work out, in the following sense.

A fit by Capella and collaborators [34] to CHLM ISR data at $\sqrt{s} = 23$ and 30 GeV, where the covered $x$ and $t$ ranges are reasonably large, gives

$$E\frac{d\sigma}{d^3p} = \frac{2\exp(4.65t)}{(1-x)} \tag{5.28}$$

under the assumption that $\alpha'_P = 0$. Using the form

$$E\frac{d\sigma}{d^3p} = \frac{A_D \exp(B_D t)}{(1-x)} \tag{5.29}$$

my eyeball fit to these data (Figs. 4 and 17) gives $A_D = 1.6$ to 2.0, $B_D = 4.5$ to 6, consistent with Capella's numbers. Thus, the predicted change $\Delta\sigma_D$ in inelastic diffractive cross-section from $s = s_1$ to $s = s_2$ is easily seen to be

$$\Delta\sigma_D = 2\pi \frac{A_D}{B_D} \log\left(\frac{s_2}{s_1}\right) . \tag{5.30}$$

The factor 2 in (5.30) arises from the fact that either proton may be diffractively scattered. There are two graphs. I ignore diffractive scattering of both protons simultaneously. With $\sqrt{s_1} = 23$, $\sqrt{s_2} = 53$, I find

$$\Delta\sigma_D = (3 \pm 0.7)\ \text{mb} . \tag{5.31}$$

Adding to this the experimental increase $\sigma_{el} \simeq 1$ mb, from the elastic channel, we see that diffractive inelastic events may indeed fully account for the observed experimental rise of $\sigma_{inel}$. However interesting, this conjecture is of course by no means proved. First, it may be stressed that, purely experimentally, it has not yet been possible to ascertain whether $\Delta\sigma_D > 0$. The experimental numbers [61] $\sigma_D = 5.4 \pm 1$ and $5.0 \pm 1$ mb at $\sqrt{s} = 23.2$ and 33.4 show no trend because of the large quoted errors. From $\sqrt{s} = 23.2$ GeV to $\sqrt{s} = 30.4$ GeV, the predicted rise of $\sigma_D$ based on (5.30) is $\Delta\sigma_D = (1.0 \pm 0.3)$ mb, which is consistent with the data, in view of the large experimental error. Direct experimental observation of a rise of $\sigma_D$ would be much more convincing. Second, our previous discussion (Section 2.4) showed that the rise of $\sigma_{inel}$ is at least partially accounted for by the increase of inclusive spectra in the central region. In this sense, (5.31) is too large.

Obviously, data which should be forthcoming during the coming months from NAL and ISR on the $t$ and $x$ structure of inelastic diffraction will allow a much more careful separation and determination of the various triple-Regge terms, including PPP. How much of $\Delta\sigma_{inel}$ is due to $\Delta\sigma_D$ will then be much better known.

## 5.6. Multiperipheral model for diffractive events *)

The suggestion that the exchanged Pomeron couples as a simple pole, consistent with data on $Ed\sigma/d^3p$, leads to the possibility of constructing a model for the full diffractive event [69]. Indeed, because of the simple exchange assumption, the amplitude $\mathbb{P}\, p \to$ anything in a multiperipheral-like approach

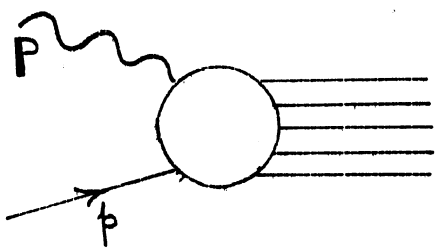


*) The work discussed in this and the next section was done in collaboration with G.C. Fox during the past year, Ref. 4). Similar work was done by E. Rabinovici (private communication from H. Harari).

should bear much similarity to that for $pp \to$ anything. For example, in $\mathbb{P} p \to M^2$, the produced hadrons should populate a rough plateau in rapidity space of width $\log M^2$ and centred at

$$|y_c| = \log(\sqrt{s}/M) \ .$$

Therefore, at $s = 1000$ GeV$^2$ an inelastic diffractive event - in which $x_p = 0.95$ (i.e., $M^2 = 50$ GeV$^2$) should appear in $y$ space as shown below.

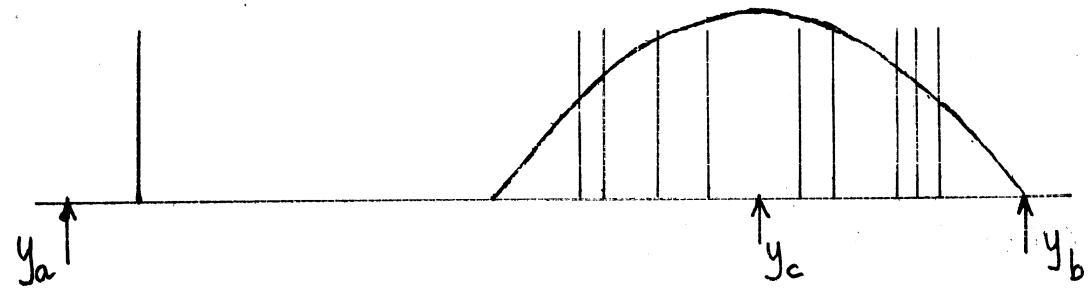


Given are both vertical bars, suggesting a single event, and a smooth curve simulating the distribution of tracks in $y$ which might arise after a sum is taken over many events with $x_p \tilde{=} 0.95$. At energy $s$, it would be of great interest to measure the experimental quantity [68]

$$\left(\frac{d\sigma}{dx_p\, dt_p}\right)^{-1} \left(\frac{d^2\sigma}{dx_p\, dt_p\, dy}\right) \qquad (5.32)$$

where, here, $x_p$ and $t_p$ are variables connected with the fast proton, and $y$ is the rapidity of a pion from the system which has recoiled from the fast proton. In the model we are discussing, (5.32) should look similar to $d\sigma/dy$ for pions from $pp \to \pi X$, measured at the lower energy $s_L = M^2 = s(1-x_p)$.

Lacking experimental data to the contrary, we continue to speculate. The multiplicity $n(M^2)$ in the model should be given by the same functional form which fits the total multiplicity $n(s)$. In particular, if

$$n(s) = a + b \log s \qquad (5.33)$$

we expect

$$n(M^2) = a' + b \log M^2 \qquad (5.34)$$

Here coefficient b is the same in both (5.33) and (5.34), but the constant term may be different. Such a conjecture is at least consistent with NAL data, Fig. 21, discussed above.

It is now a simple matter to integrate over $M^2$ (equivalently, over $x_p$) to obtain the full distribution in rapidity space for pions from inelastic diffractive events. By this I mean that we no longer single out the proton, but ask rather just about the $\pi$ spectrum which our Pomeron exchange model predicts.

The required analysis is formally similar to that done in Section 3. Here, we begin with a cluster of mass M centred at $y_c$ whose decay distribution $D(y,y_c)$ is a plateau in $y$ from $y_c - \log M < y < y_c + \log M$,

$$\langle n(M^2)\rangle = \int D(y,y_c)\,dy = b \log M^2 .$$

The kinematic relationship between M and $y_c$ is

$$|y_c| = \log(\sqrt{s}/M) \tag{5.35}$$

or

$$M^2 = s \exp(-2|y_c|) . \tag{5.36}$$

According to our PPP formalism, the cluster is produced with a density distribution

$$\rho(y_c) = \frac{1}{\nabla_D^{(1)}} \frac{d\nabla_D^{(1)}}{dy_c} = \frac{M^2}{\nabla_D^{(1)}} \frac{d\nabla_D^{(1)}}{dM^2} = \frac{2K}{\nabla_D^{(1)}} . \tag{5.37}$$

Constant K is fixed by

$$\nabla_D^{(1)} = K \int_{M_0^2}^{M_c^2} M^{-2}\, dM^2 \tag{5.38}$$

Setting $M_c^2 = s$ and $M_o^2 = 1$ we find $\sigma_D^{(1)} = K \log s$. The inclusive y distribution for pions in conjunction with a proton which is inelastically diffractively scattered (into the hemisphere $x_p < 0$) is then

$$\frac{d\sigma^{(1)}}{dy} = \sigma_D^{(1)} \int \rho(y_c)\, dy_c\; D(y, y_c) = 2\sigma_D^{(1)} b \int I(y_c)\, dy_c \tag{5.39}$$

where $I(y_c) = 1$ if $\log\sqrt{s} > y > 2y_c - \log\sqrt{s}$ and is zero otherwise. Thus,

$$\frac{d\sigma^{(1)}}{dy} = K b \left(y + \log\sqrt{s}\right) \tag{5.40}$$

This triangle shaped distribution is shown by the shaded area in the sketch below.

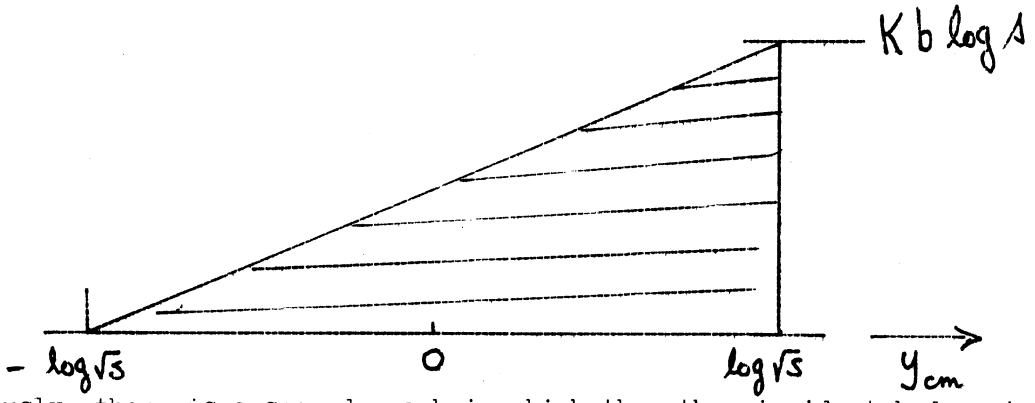


Obviously, there is a second graph in which the other incident hadron is diffractively scattered (into the forward hemisphere). Pions produced by the latter process provide a distribution

$$\frac{d\sigma^{(2)}}{dy} = K b \left(\log\sqrt{s} - y\right) \tag{5.41}$$

which peaks at $y = -\log\sqrt{s}$. The sum of both contributions is a plateau in y, extending (ideally !) from $y = -\log\sqrt{s}$ to $y = +\log\sqrt{s}$ and whose height rises in proportion to log s :

$$\frac{d\sigma_D}{dy} = K b \log s = \tfrac{1}{2}\sigma_D b \tag{5.42}$$

The net diffractive pion multiplicity $< n_D >$ is given by

$$\langle n_D \rangle = \sigma_D^{-1} \int K b \log s \, dy = \sigma_D^{-1} K b (\log s)^2$$

where

$$\sigma_D = \sigma_D^{(1)} + \sigma_D^{(2)} = 2\sigma_D^{(1)} .$$

Thus,

$$\langle n_D \rangle = \tfrac{1}{2} b \log s \tag{5.43}$$

Three features of this last expression are notable. First, the multiplicity of the diffractive component is not constant, but grows with s. Second, the coefficient of log s, here $(\frac{1}{2}b)$, is $\frac{1}{2}$ that of the coefficient of $\log M^2$ in the expression $< n(M^2) > = b \log M^2$, which was input to our calculation [69]. Therefore, <u>owing to the singular nature of the PPP coupling</u> as $x \to 1$, the coefficient of log s in the expression $< n_D >$ is one-half the coefficient of log s for the multiplicity provided by non-diffracting graphs. [If P' with $\alpha(0) \simeq \frac{1}{2}$ were exchanged, rather than P, there would be no singularity as $x \to 1$, and $d\sigma/dM^2 \propto 1/s$. With this assumption for $\rho(y_c)$, it is easy to show that $n(M^2) \propto b \log M^2$ results in $n(s) \propto b \log s$.]

Third, and last, the net multiplicity arising from both diffractive and non-diffractive graphs has the form

$$\langle n \rangle = \langle n_{ND} \rangle \frac{\sigma_{ND}}{\sigma} + \langle n_D \rangle \frac{\sigma_D}{\sigma} \tag{5.44}$$

Here $\sigma = \sigma_{ND} + \sigma_D$. If we were to take our model seriously as $s \to \infty$, we would find

$$\langle n \rangle_\infty \propto \langle n_D \rangle \sim \tfrac{1}{2} b \log s \tag{5.45}$$

whereas, at low energy, where $\sigma_{ND} \gg \sigma_D$

$$\langle n \rangle \sim \langle n_{ND} \rangle \sim b \log s \tag{5.46}$$

This would imply that the measured coefficient $b_{exp}$ of log s in fits of the form

$$\langle n \rangle \sim b_{exp} \log s$$

should decrease as s increases. This is clearly in disagreement with data, which if anything show an increase of $b_{exp}$ as s increases [13),14)]. However, it was at least implicit from the start that the model should be invoked only in a limited region [34),69)] (ISR range ?) where $\sigma_D \ll \sigma_{ND}$. At energies at which $\sigma_D \approx \sigma_{ND}$, we would have to take seriously into account the prospect of non-negligible multi-Pomeron exchange. Thus I intend all my remarks here about a simple multiperipheral model with factorized Pomeron exchange to be restricted in validity to a region of energy encompassing NAL and ISR. The really asymptotic properties of the model have not been worked out satisfactorily *). (In this sense, and owing directly to the rising nature of $\sigma_{tot}$ with s, the ISR is not an asymptotic machine !).

Besides s dependence, several other aspects of our treatment are obviously overly naïve. First, the pure plateau assumption for the cluster decay distribution needs to be modified with rounded-off fragmentation edges. Second, use of the PPP term for the full range $s \geq M^2 \geq 1$ GeV$^2$ is outrageous. Corrections to both, however, do not change the essential lessons of the discussion :

(a) that pions from the diffractively produced cluster may well reach the middle **) of the rapidity plot, and

(b) their multiplicity grows with s, perhaps logarithmically.

These results suggest that clean kinematic separation of a full "diffractive component" is virtually impossible. Of course, an enriched part of the component may be had by selecting events with one $|x_p| > 0.95$ (say), but this a biased sample which may not be trustworthy for reaching general conclusions.

---

*) For discussions of a multiperipheral "perturbative" approach to hadron production, see Refs. 34).

**) Note that the centre is reached whenever $(y_c - \log M) < 0$ ; that is, whenever $M > s^{1/4}$. At $s = 1000$ GeV$^2$, and $x_p = 0.9$, $M = 10$ GeV, which is greater than $s^{1/4} = 5.6$.

Our argument showed that diffractive events lead to a log s increase of the height of the central plateau for $pp \to \pi X$ : $d\sigma_D/dy = \frac{1}{2}\sigma_D b$. It is worth evaluating numerically how great this increase is over the ISR range. We start from $d\sigma/dy = d\sigma_{ND}/dy + d\sigma_D/dy$. Taking differences, we find

$$\Delta\left(\frac{d\sigma}{dy}\right) = \frac{1}{2}(\Delta\sigma_D)\, b \qquad (5.47)$$

because $d\sigma_{ND}/dy$ is, by hypothesis, energy independent. For pions of fixed charge (i.e.) $\pi^-$, $b \simeq 0.7$ to $1.0$. Thus, using Eq. (5.47),

$$\Delta\left(\frac{d\sigma}{dy}\right)\Big|_{y=0} \simeq 1.2 \text{ mb}$$

is the expected increase from $\sqrt{s} = 22$ to $\sqrt{s} = 53$ GeV. Data from NAL at 200 GeV/c give [28]

$$\frac{d\sigma}{dy}\Big|_{y=0} \simeq 26 \text{ mb}$$

Thus, our diffractive contribution provides a rise of ≈4.5% in the plateau height (integrated over $p_T^2$). This number is to be compared with the increase of (8±7)% quoted by the British-Scandinavian group [16], and so may fully account perhaps for any experimental rise. Insofar as s dependence is concerned, the remaining distribution $d\sigma_{ND}/dy$ would be in "perfect" agreement with the predictions of the short-range order hypothesis.

The British-Scandinavian data [16] showed also that the y distribution was not flat at fixed $\sqrt{s} = 53$ GeV. Whether pions from the diffractive cluster could cause the observed bulge at $y_{cm} \approx 0$ is not obvious, but, in any case, requires a less approximate treatment than can be given purely analytically [4]. [It is very unlikely that the diffractive component could explain the rise of the $\bar{p}$ inclusive rate at $y = 0$.]

## 5.7. Correlations in the diffractive component

That pions from the diffractive component may reach $y = 0$, and the idea that long-range correlations are intimately associated with diffraction make it imperative that we examine the structure of rapidity correlations among pions produced in a diffractive exchange situation. I turn to this

subject now and derive the form of $d^2\sigma_D/dy_1 dy_2$, where $y_1$ and $y_2$ denote rapidities of pions which have come from a system which recoils from a fast inelastic proton scattered diffractively.

As we discussed above, if $x_p$ is fixed, the recoil system of mass $M = [s(1-x_p)]^{\frac{1}{2}}$ behaves in our model just as would a final state of $\sqrt{s} = M$ in an over-all pp collision. Thus, <u>if we fix $x_p$</u>, and we look only at pions from the recoil system, we expect to see only short-range rapidity correlations, whose correlation function $C_{x_p}(y_1,y_2)$ has exactly the same form as that in (3.29) [so long, of course, as both $y_i$ are in the allowed kinematic range $y_c - \log M < y < y_c + \log M$ ; $y_c = \log(\sqrt{s}/M)$]. Explicitly,

$$\frac{1}{\sigma_x}\frac{d^2\sigma_x}{dy_1 dy_2} = \frac{1}{\sigma_x^2}\frac{d\sigma_x}{dy}\frac{d\sigma_x}{dy_2} + C_x(y_1,y_2)\,, \tag{5.48}$$

where $C_x(y_1,y_2)$ is given by Eq. (3.28). Here, cross-section $\sigma_x$ is just the inclusive cross-section given by the triple-Pomeron formula

$$\sigma_x = f_p(x,t)$$

$1/\sigma_x(d\sigma_x/dy_1)$ = plateau of height $b$ extending over the interval $y_c - \log M < y_1 < y_c + \log M$. Expression (5.48) applies for fixed $(M^2(x),t)$ of the fast proton.

We ask next for the full form of correlations among pions in the diffractive component, after we integrate over $x_p$. As will be derived below, this function has both short-range and long-range pieces.

Formally, it is clear that

$$\frac{1}{\sigma_D^{(1)}}\frac{d^2\sigma_D^{(1)}}{dy_1 dy_2} = \int dy_c\, \rho(y_c)\, D_2(y_1,y_2;y_c) \tag{5.49}$$

where $\rho(y_c)$ is given by (5.37) and $D_2(y_1,y_2,y_c)$ is provided by (5.48). Inserting the first term of (5.48) into (5.49), we obtain the contribution

$$\frac{1}{\sigma_D^{(1)}}\, 2K b^2 \int dy_c\, I_2(y_1,y_2;y_c)$$

where $I_2 = 1$ if both $2y_c < y_1 + \log\sqrt{s}$ and $2y_c < y_2 + \log\sqrt{s}$, but $I_2 = 0$ otherwise. The result is

$$\frac{K b^2}{\sigma_D^{(1)}} \left( \log\sqrt{s} + y_L \right) \tag{5.50}$$

where $y_L$ is the lesser of $(y_1, y_2)$. Similarly, the integral over $C_x(y_1, y_2)$, [when (5.48) is inserted in (5.49)] gives

$$\frac{K}{\sigma_D^{(1)}} C(y_1, y_2) \left[ \log\sqrt{s} + y_L \right] . \tag{5.51}$$

Recall that $\sigma_D^{(1)} = K \log s$ defines K. Thus,

$$\frac{1}{\sigma_D^{(1)}} \frac{d^2\sigma_D^{(1)}}{dy_1\, dy_2} = \frac{1}{2}\left[ 1 + \frac{y_L}{\log\sqrt{s}} \right]\left[ b^2 + C(y_1, y_2) \right] \tag{5.52}$$

The second diffractive graph, whose fast proton heads towards $x > 0$, gives

$$\frac{1}{\sigma_D^{(2)}} \frac{d^2\sigma^{(2)}}{dy_1\, dy_2} = \frac{1}{2}\left[ 1 - \frac{y_G}{\log\sqrt{s}} \right]\left[ b^2 + C(y_1, y_2) \right] \tag{5.53}$$

where $y_G$ is the greater of $(y_1, y_2)$.

The total two-pion inclusive spectrum from the diffractive component is therefore

$$\frac{1}{\sigma_D} \frac{d^2\sigma_D}{dy_1\, dy_2} = \frac{1}{2}\left[ 1 - \frac{|y_1 - y_2|}{\log s} \right]\left( b^2 + C(y_1, y_2) \right) \tag{5.54}$$

Setting $C = 0$, just for the moment, I sketch below $d^2\sigma_D/dy_1 dy_2$ versus $y_1$ for $y_2 = 0$

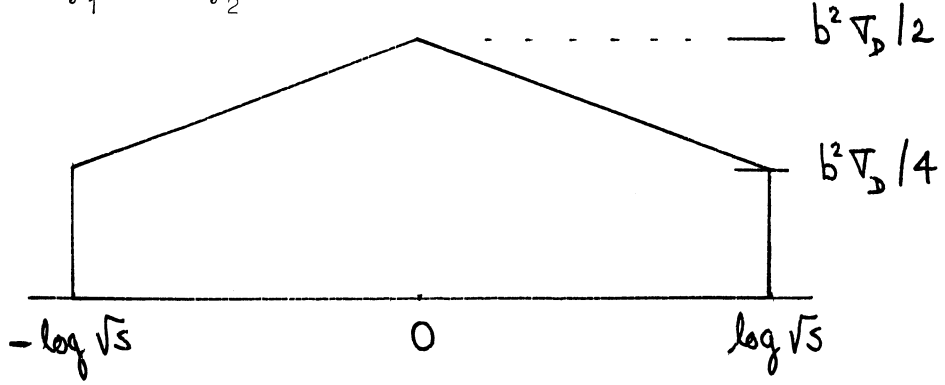

Defining a diffractive component correlation function $C_D(y_1,y_2)$ by

$$C_D(y_1,y_2) = \frac{1}{\sigma_D}\frac{d^2\sigma_D}{dy_1\,dy_2} - \frac{1}{\sigma_D^2}\frac{d\sigma_D}{dy_1}\frac{d\sigma_D}{dy_2}$$

I find

$$C_D(y_1,y_2) = \frac{1}{2}\left[\frac{1}{2} - \frac{|y_1-y_2|}{\log s}\right] b^2 + \frac{1}{2}\left[1 - \frac{|y_1-y_2|}{\log s}\right] C_{ND}(y_1,y_2) \tag{5.55}$$

The term $C_{ND}$ appearing in (5.55) is exactly the function $C$ of Eq. (3.29). I have now added the subscript ND (for non-diffractive) to distinguish it from $C_D$. The constant $b$ appearing in (5.55) is the coefficient of $\log s$ in the expansion

$$\langle n_{ND}\rangle = a + b\log s$$

Equivalently, it is the full height of the central plateau in the single-particle inclusive spectrum

$$b = \frac{1}{\sigma_{ND}}\frac{d\sigma_{ND}}{dy}$$

It will be noted that $C_D$ has both a long-range part, given by the first term in (5.55), and a short-range piece. At $y_1 = y_2 = 0$, the long-range part is $1/4\ b^2$ ($\approx 0.5$ to 1 for charged-charged correlations). The short-range piece at $y_1 = y_2 = 0$ is $0.5\ C_{ND}(0,0)$. To evaluate this latter term, we note that

$$C_{ND}(0,0) \cong b^2 R_{ND}(0,0)$$

where

$$R(y_1,y_2) = C(y_1,y_2)\Big/\left[\frac{1}{\sigma^2}\frac{d\sigma}{dy_1}\frac{d\sigma}{dy_2}\right]$$

Experimentally, $R(0,0) \simeq 0.6$ (which I interpret as largely due to non-diffractive effects). Thus, the long-range and short-range parts of $C_D(0,0)$ are roughly equal in numerical value.

It is interesting to evaluate the integral $f_2^D$ defined as

$$f_2^D = \iint C_D(y_1, y_2)\, dy_1\, dy_2 \qquad (5.56)$$

Simple arithmetic gives

$$f_2^D = \frac{b^2}{12}(\log s)^2 = \frac{1}{3}\langle n_D\rangle^2 = \frac{1}{12}\langle n_{ND}\rangle^2 \qquad (5.57)$$

Note that the correlation moment $f_2^D$ grows as $(\log s)^2$, not as $(\log s)$. Therefore, our diffractive component shows long-range correlations both in the intuitive sense, discussed in the opening paragraphs of Section 5.1, and in the formal sense [70] as well.

It may seem somewhat surprising that we obtain long-range correlations from a pure multiperipheral model. After all the cluster recoiling from the fast proton has pure short-range correlation structure, internally, and the exchanged Pomeron is a pure factorized pole in our model. Thus, at a superficial glance, one might expect the pure short-range answer $f_2^D \sim O(\log s)$. However, on closer inspection, one sees that the $f_2^D \sim (\log s)^2$ result is related directly to the $f_p(x) \sim (1-x)^{-1}$ singularity structure of the exchange. A typical non-diffractive multiperipheral situation would arise if we were to replace the exchanged Pomeron by an $f^o$ or $\rho$ trajectory. In this case, the proton $x$ distribution is non-singular as $x \to 1$, and we calculate $f_2^{ND} \sim O(\log s)$. The long-range effect does not arise simply from our having integrated over a spectrum of masses, but over a quite particular spectrum [which has behaviour $d\sigma/dM^2 \sim (M^2)^{-1}$].

It is intriguing that the multiperipheral approach can reproduce both long-range and short-range correlation effects in data. Only detailed analyses will verify whether the approach is successful quantitatively ; present steps in this direction are promising [4].

The full correlation function observed experimentally receives contributions from both diffractive and non-diffractive graphs. Ignoring interference effects between these two types of processes *), we may write formally

---

*) Clearly this would need justification, in a more complete treatment, inasmuch as diffractive and non-diffractive graphs populate overlapping regions of phase space.

$$C(y_1,y_2) = \alpha_D C_D + \alpha_{ND} C_{ND}$$

$$+ \alpha_D \alpha_{ND} \left[ \frac{1}{\sigma_{ND}} \frac{d\sigma_{ND}}{dy_1} - \frac{1}{\sigma_D} \frac{d\sigma_D}{dy_1} \right] \times (1 \to 2) \qquad (5.58)$$

Here $\sigma_D = \sigma_D / \sigma_{inel}$ ; $\sigma_{ND} = \sigma_{ND} / \sigma_{inel}$ ; $\sigma_D + \sigma_{ND} = 1$. The last term in (5.58) produces an apparent long-range correlation effect in the central region $(y_1 \simeq y_2 \simeq 0)$, as long as

$$\left[ \frac{1}{\sigma_{ND}} \frac{d\sigma_{ND}}{dy_i} - \frac{1}{\sigma_D} \frac{d\sigma_D}{dy_i} \right] \neq 0$$

In a sense, this apparent long-range effect is fictitious, since it does not come directly from dynamics, but rather from the existence of two contributing different dynamical mechanisms [71]. That the presence of two mechanisms (each of which may be purely of short-range character) can result in a term in $C(y_1,y_2)$ which has apparent long-range structure, points up the danger of expressing data always in terms of $C(y_1,y_2)$ [or $R(y_1,y_2)$]. Interpretations based on $C(y_1,y_2)$ may be less reliable than those based directly on $\sigma^{-1} d^2\sigma/dy_1 dy_2$.

The maximum size of the "fictitious" long-range term in the central region is controlled by

$$\alpha_D \alpha_{ND} \left| \frac{1}{\sigma_{ND}} \frac{d\sigma_{ND}}{dy} - \frac{1}{\sigma_D} \frac{d\sigma_D}{dy} \right|_{y \simeq 0} \qquad (5.59)$$

Models in which $d\sigma_D/dy|_{y\simeq 0} \simeq 0$ produce very large apparent long-range effects. For example, using their concept of diffraction, Pirilä and Pokorski [72] have estimated that the fictitious long-range term accounts for one-half of the experimentally observed correlation at $y_1 = y_2 = 0$. This estimate is directly tied to their assumption that their entire diffractive component of $\approx 7$ mb gives no pions at $y = 0$ (i.e., $d\sigma_D/dy = 0$).

In the multiperipheral-like model I have been discussing here,

$$\frac{1}{\sigma_D}\frac{d\sigma_D}{dy} \simeq \frac{1}{2}\frac{1}{\sigma_{ND}}\frac{d\sigma_{ND}}{dy} \qquad (5.60)$$

Thus, the difference in (5.59) is only 1/4 the value it has in models such as Pokorski and Pirilä's. Combining (5.56), (5.58) and (5.55) with subsequent discussion, I find that our multiperipheral model gives

$$C(0,0) = \left(1-\frac{\alpha_D}{2}\right)C_{ND}(0,0) + \frac{\alpha_D b^2}{4}\left(1+\alpha_{ND}\right) \qquad (5.61)$$

Upon forming

$$R(0,0) \simeq C(0,0)/b^2$$

I obtain

$$R(0,0) = \left(1-\frac{\alpha_D}{2}\right)R_{ND}(0,0) + \frac{\alpha_D}{4}\left(1+\alpha_{ND}\right) \qquad (5.62)$$

The diffraction associated long-range correction term $\alpha_D(1+\alpha_{ND})/4 \simeq 0.09$ thus provides a very small net long-range effect at $y_1 \simeq y_2 \simeq 0$. Most of the observed charged-charged correlation $[R(0,0) \simeq 0.6]$ is therefore interpreted as a pure short-range effect in the multiperipheral approach I have developed here [73].

The same term $0.25\alpha_D(1+\alpha_{ND})$ which appears in (5.62) will be present in all two-pion correlations, independent of charges. Thus, this term, whose magnitude ($\approx 0.1$) is insignificant for charged-charged correlations, is relatively more important, for example, for $(\pi^-\pi^-)$ correlations. This points up again that experimental study of $(\pi^-\pi^-)$ and $(\pi^+\pi^-)$ correlations in $y$, at fixed $p_T$, will greatly improve our present picture, which unfortunately must be based solely on data for charged-charged correlations in $\log\tan(\theta/2)$, averaged over $p_T$.

REFERENCES

1) G. Giacomelli - Rapporteur's talk, Chicago-NAL International Conference (1972) ;

D.R.O. Morrison - Review given at the Royal Society Discussion Meeting on Proton-Proton Scattering (March, 1973) ;

A.N. Diddens - Lectures given at IV Seminar on Theoretical Physics, GIFT, Barcelona (1973) ;

M. Jacob - Rapporteur's talk, Chicago-NAL International Conference (1972) ;

J.C. Sens - Invited Review, Conference on Recent Advances in Particle Physics, New York Academy of Sciences (1973) ;

D. Horn - Physics Reports 4C, 1 (1972) ;

W.R. Frazer et al. - Revs.Modern.Phys. 44, 284 (1972) ;

K. Gottfried - CERN Academic Training Lectures, CERN Preprint TH. 1615 (1973) ;

M. Jacob - 1973 CERN School of Physics, Ebeltoft, and 1973 Louvain Summer Institute Lectures, CERN Preprint TH. 1683 (1973) ;

H.M. Chan - Lectures given at IV Seminar on Theoretical Physics, GIFT Barcelona (1973) ;

J.D. Jackson - Summary talk, International Conference on High Energy Collisions, Vanderbilt (1973) ;

A. Mueller - Parallel Session Summary, Chicago-NAL International Conference (1972) ;

L. Foà - Invited review, Italian Physical Society Meeting, Cagliari (1972).

2) D. Amati, S. Fubini and A. Stanghellini - Nuovo Cimento 26, 896 (1962) ;

L. Bertocchi, S. Fubini and M. Tonin - Nuovo Cimento 25, 626 (1962).

3) J. Benecke, T. Chou, C.N. Yang and E. Yen - Phys.Rev. 188, 2159 (1969) ;

R. Hwa - Phys.Rev.Letters 26, 1143 (1971) ;

M. Jacob and R. Slansky - Phys.Rev. D5, 1847 (1972) ;

R. Adair - Phys.Rev. 172, 1370 (1968) ; D5, 1105 (1972).

4) E.L. Berger and G.C. Fox - CERN Preprint TH. 1700 (1973), to be published in Physics Letters.

5) CERN-Holland-Lancaster-Manchester ISR Collaboration, M.G. Albrow et al. - Nuclear Phys. B51, 388 (1972) ; Nuclear Phys. B54, 6 (1973) ; Phys. Letters 42B, 279 (1972).

6) L. Van Hove - Physics Reports 1C, 347 (1971).

7) U. Amaldi - 1973 Erice School Lectures ;

M. Jacob - CERN Preprint TH. 1683 (1973).

8) CERN-Rome ISR Collaboration, U. Amaldi et al. - Phys.Letters 44B, 112 (1973) ;

Pisa-Stony Brook ISR Collaboration, S.R. Amendolia et al. - Phys.Letters 44B, 119 (1973).

9) Aachen-CERN-Harvard-Genova-Torino ISR Collaboration, M. Holder et al. - Phys.Letters 35B, 355 (1971) ; 36B, 400 (1971) ;

G. Barbiellini et al. - Phys.Letters 39B, 663 (1972) ;

CERN-Rome ISR Collaboration, U. Amaldi et al. - Phys.Letters 36B, 504 (1971).

10) CERN-Bologna ISR Collaboration, A. Bertin et al. - Phys.Letters 42B, 493 (1972) ;

CERN-Holland-Lancaster-Manchester ISR Collaboration, M.G. Albrow et al. - Phys.Letters 42B, 279 (1972) ;

Saclay-Strasbourg ISR Collaboration - Phys.Letters 41B, 547 (1972).

11) S.M. Berman, J.D. Bjorken and J.B. Kogut - Phys.Rev. D4, 3388 (1971) ;

R. Blankenbecler, S.J. Brodsky and J.F. Gunion - Phys.Letters 42B, 461 (1972) ;

P.V. Landshoff and J.C. Polkinghorne - Phys.Letters 45B, 361 (1973) ;

D. Amati, L. Caneschi and M. Testa - Phys.Letters 43B, 186 (1973) ;

E.L. Berger and D. Branson - Phys.Letters 45B, 57 (1973).

12) CERN-Columbia-Rockefeller ISR Collaboration, F.W. Büsser et al. - CERN Report (1973), submitted to Phys.Letters.

Other large $p_T$ ISR data :

Saclay-Strasbourg ISR Collaboration, M. Banner et al. - Phys.Letters 44B, 537 (1973) ;

British-Scandinavian ISR Collaboration, B. Alper et al. - Phys.Letters 44B, 521 (1973).

13) CERN-Bologna ISR Collaboration, M. Antinucci et al. - Nuovo Cimento Letters 6, 121 (1973).

14) E.L. Berger - Phys.Rev.Letters 29, 887 (1972).

15) France-Soviet Union and CERN-Soviet Union Serpukhov Collaborations, V.V. Ammosov et al. - Nuclear Phys. B58, 77 (1973).

16) British-Scandinavian ISR Collaboration - CERN Reports (1973), submitted to Phys.Letters.

17) CERN-Hamburg-Vienna ISR Collaboration, H. Dibon et al. - Phys.Letters 44B, 313 (1973).

18) Pisa-Stony Brook ISR Collaboration, S.R. Amendolia - CERN Report (1973), submitted to Phys.Letters.

19) Argonne-NAL-Iowa-Maryland-Michigan State 205 GeV/c Collaboration, as reported by J. Whitmore - International Conference on High Energy Particle Collisions, Vanderbilt (1973).

20) Multiplicity data in pp collisions :

13-28.5 GeV/c : E.L. Berger, B.Y. Oh, Z.-M. Ma and G.A. Smith, to be published ;

50 and 69 GeV/c : France-Soviet Union Mirabelle Collaboration - paper submitted to XVI International Conference on High Energy Physics Chicago-NAL (1972) ;

100 GeV/c : J.W. Chapman et al. - Phys.Rev.Letters 29, 1686 (1972) ;
200 GeV/c : G. Charlton et al. - Phys.Rev.Letters 29, 515 (1972) ;
300 GeV/c : F.T. Dao et al. - Phys.Rev.Letters 29, 1627 (1972).

21) Recent discussions include :
A. Wroblewski - Lectures given at XIII Cracow School, Zakopane (1973) ;

Z. Koba - 1973 CERN School of Physics, Ebeltoft ;
W.R. Frazer - Conference on Recent Advances in Particle Physics, New York Academy of Sciences (1973).

22) K. Wilson - Acta Phys.Austriaca 17, 37 (1963) ;
A. Krzywicki - Nuclear Phys. B58, 633 (1973).

23) A.H. Mueller - Phys.Rev. D2, 2963 (1972).

24) R.P. Feynman - Phys.Rev.Letters 23, 1415 (1969).

25) CERN-Holland-Lancaster-Manchester ISR Collaboration, M.G. Albrow et al. - Nuclear Phys. B56, 333 (1973).

26) For additional references to the scaling behaviour of single-particle spectra, see the articles by Diddens, Foà, Giacomelli and Jacob, Ref. 1), as well as the proceedings of the IV International Conference on High Energy Collisions, Oxford (1972).

27) J.V. Allaby et al. - Contribution to IVth International Conference on High Energy Collisions, Oxford (1972).

28) Argonne-NAL 205 GeV/c Collaboration, Y. Cho et al. - NAL-Pub-73/26-EXP ; ANL/HEP 7316 (1973), submitted to Phys.Rev.Letters.

29) W.H. Sims et al. - Nuclear Phys. B41, 317 (1972).

30) British-Scandinavian ISR Collaboration - Ref. 16).

31) Saclay-Strasbourg ISR Collaboration, M. Banner et al. - Phys.Letters 41B, 547 (1972).

32) Pisa-Stony Brook ISR Collaboration, G. Bellettini et al. - Phys.Letters 45B, 69 (1973).

33) J.D. Bjorken - in "Particles and Fields" (1971), Ed. by A.C. Mellissinos and P. Slattery (AIP, New York) ;
R. Arnold - Argonne Lectures ANL/HEP 7317 (1973).

34) A. Capella and M.-S. Chen - Stanford Report SLAC-PUB-1252 ;
W.R. Frazer, D.R. Snider and C.-I. Tan - San Diego Preprint UCSD-10P10-127 (1973).
G.F. Chew - Berkeley Preprints LBL-1556 and LBL-1701 (1973).
D. Amati, L. Caneschi and M. Ciafaloni - CERN Preprint TH. 1676 (1973) ;
M. Bishari and J. Koplic - Berkeley Preprints (1973), and Phys.Letters 44B, 175 (1973).

35) C. De Tar - Phys.Rev. D3, 128 (1971) ;
S. Fubini - in "Strong Interactions and High Energy Physics", Ed. by R.G. Moorhouse (Oliver and Boyd, Edinburgh, 1964) ;
W. Frazer et al. - Ref. 1).

36) E.L. Berger, G.C. Fox and A. Krzywicki - Phys.Letters 43B, 132 (1973) ;
E.L. Berger and A. Krzywicki - Phys.Letters 36B, 380 (1971).

37) F.T. Dao et al. - Phys.Letters 45B, 73 (1973).
Data on $\delta$ should also be forthcoming soon from the Pisa-Stony Brook ISR Collaboration.

38) C. Quigg - in Proceedings of the Vanderbilt Conference on High Energy Collisions (1973).

39) C.J. Hamer and R. Peierls - Brookhaven Reports (1973).

40) E.L. Berger and M. Jacob - Phys.Rev. D6, 1930 (1972) ;
E.L. Berger, M. Jacob and R. Slansky - Phys.Rev. D6, 2580 (1972).

41) Vanderbilt-Brookhaven Collaboration, W. Burdett et al. - Nuclear Phys. B48, 13 (1972) ;
Vanderbilt-Yale Collaboration, J. Hanlon et al.- Report Yale 3075-45 (July 1973).

42) D. Sivers and G.H. Thomas - Phys.Rev. D6, 1961 (1972).

43) C. Quigg, J.-M. Wang and C.N. Yang - Phys.Rev.Letters 28, 1290 (1972).

44) For a summary of data and possible theoretical interpretations, see :
E.L. Berger, D. Horn and G.H. Thomas - Phys.Rev. D7, 1412 (1973) ;
D. Horn and A. Schwimmer, Nuclear Phys. B52, 627 (1973).

45) For other theoretical discussions of correlations covering some material which I do not treat here, consult :
M. Jacob - Ref. 1) ;
C. Quigg - Ref. 38) ; and
M. Le Bellac, R. Peccei and L. Caneschi - in "Multiparticle Phenomena and Inclusive Reactions", Seventh Rencontre de Moriond (1972), Ed. by J. Tran Thanh Van.

46) The long history of the one and two fireball approach is hard to trace completely. Some references, prior to those in Ref. 3), include :
M. Good and W.D. Walker - Phys.Rev. 120, 1857 (1960) ;
G. Cocconi - Phys.Rev. 111, 1699 (1958) ;
P. Ciok et al. - Nuovo Cimento 10, 741 (1958).
See also :
E.L. Feinberg - Physics Reports 5C, 238 (1972).

47) M. Le Bellac and J.L. Meunier - Phys.Letters 43B, 127 (1973).

48) E.L. Berger - Argonne Report ANL/HEP 7239 (1972), submitted to 1972 Chicago-NAL Conference.

49) Michigan-Rochester-NAL Collaboration data at 103 GeV/c as presented in Fig. 5 of :

J. Whitmore - International Conference on High Energy Collisions, Vanderbilt (1973).

50) CERN-Holland-Lancaster-Manchester ISR Collaboration, M. Albrow et al. - Phys.Letters 44B, 207 and 518 (1973).

51) Pisa-Stony Brook ISR Collaboration, G. Bellettini - XVI International Conference on High Energy Physics, Chicago-Batavia, Vol. 1, 279 (1972).

52) This point has also been emphasized by :

M. Jacob - Ref. 1).

53) Preliminary data on this question have been obtained by :

Aachen-CERN-Harvard-Genova-Torino ISR Collaboration, G. Goldhaber - Contribution to the Chicago-NAL International Conference (1972).

54) F. Sannes et al. - Phys.Rev.Letters 30, 766 (1973).

55) Columbia-Stony Brook Collaboration, S. Childress et al. - Contribution to Vanderbilt Conference (1973) ;

S. Childress et al. - Report submitted to Phys.Rev.Letters (1973) ; and

R. Schamberger et al.

56) University of Rochester - University of Michigan 100 GeV Bubble Chamber Collaboration, C.M. Bromberg et al. - Report Nr. UMBC 72-14 and UR 416 (January 1973).

57) Argonne-NAL 205 GeV/c Bubble Chamber Collaboration, S.J. Barish et al. - Argonne Report ANL/HEP 7338 (1973) ; M. Derrick et al. - Argonne Report ANL/HEP 7332 (1973).

58) NAL-UCLA 303 GeV/c Bubble Chamber Collaboration, F.T. Dao et al. - Phys.Letters 45B, 399 and 402 (1973).

59) NAL-LBL 205 GeV/c Bubble Chamber Collaboration, F.C. Winkelman et al. - Report Nr. LBL-2113 (1973).

60) This observation has also been made by K. Kajantie, private communication.

61) J.C. Sens - Ref. 1).

62) A similar conclusion is reached upon comparing data on $< n(M_x^2) >$ from $\pi^- p \to pX$ at 205 GeV/c, with $< n(s) >$ from $\pi^- p \to X$. NAL-LBL Collaboration, Ref. 59).

63) As remarked by K. Gottfried, the relatively low multiplicity observed in collisions of hadrons with nuclei is also consistent with this suggestion.

64) Pisa-Stony Brook ISR Collaboration.

65) CERN-Holland-Lancaster-Manchester ISR Collaboration, M.G. Albrow et al. - CERN Report (July 1973), submitted to Nuclear Phys.

66) J. Finkelstein and K. Kajantie - Phys.Letters 26B, 305 (1968).

67) See, for example, the papers listed in Ref. 34) and other papers cited in those articles. A recent paper is that of :
J.L. Cardy and A.R. White - CERN Preprint TH. 1726 (1973).

68) A similar request has been made by C. Quigg, private communication.

69) The factor $(\frac{1}{2})$ has also been derived by :
D. Snider and W. Frazer - Phys.Letters 45B, 136 (1973).

70) A. Mueller - Phys.Rev. D4, 150 (1971).

71) The idea of two distinct components has received much attention especially in attempts to fit multiplicity distributions. See, for example :
E.L. Berger - Ref. 14) ;
C. Quigg and J.D. Jackson - NAL Report NAL-THY-93 (1972) ;
K. Fialkowski and H. Miettinen - Phys.Letters 43B, 61 (1973) ;
W. Frazer, R. Peccei, S. Pinsky and C.-I. Tan - San Diego Preprint (1972) ;
H. Harari and E. Rabinovici - Phys.Letters 43B, 49 (1973) ;
L. Van Hove - Phys.Letters 43B, 65 (1973) ; and
J. Lach and E. Malamud - Phys.Letters 44B, 474 (1973).

72) P. Pirilä and S. Pokorski - Phys.Letters 43B, 502 (1973).

73) The use of clusters in one form or another to interpret or to imitate positive inclusive correlations has recently become very popular. Clusters are discussed phenomenologically in my Refs. 4), 36) and 39). Recent articles which came to my attention after I gave these lectures at Erice are by :
F. Hayot and A. Morel - Saclay Preprint D.Ph.T/73/58 (1973).;
W. Schmidt-Parzefall - CERN Report (1973), submitted to Phys.Letters ;
P. Pirilä and S. Pokorski - CERN Preprint TH.1686 (1973) ;
A. Białas, K. Fialkowski and K. Zalewski - Phys.Letters B45, 337 (1973) ;
J. Kripfganz, G. Ranft and J. Ranft - Nuclear Phys. B56, 205 (1973).

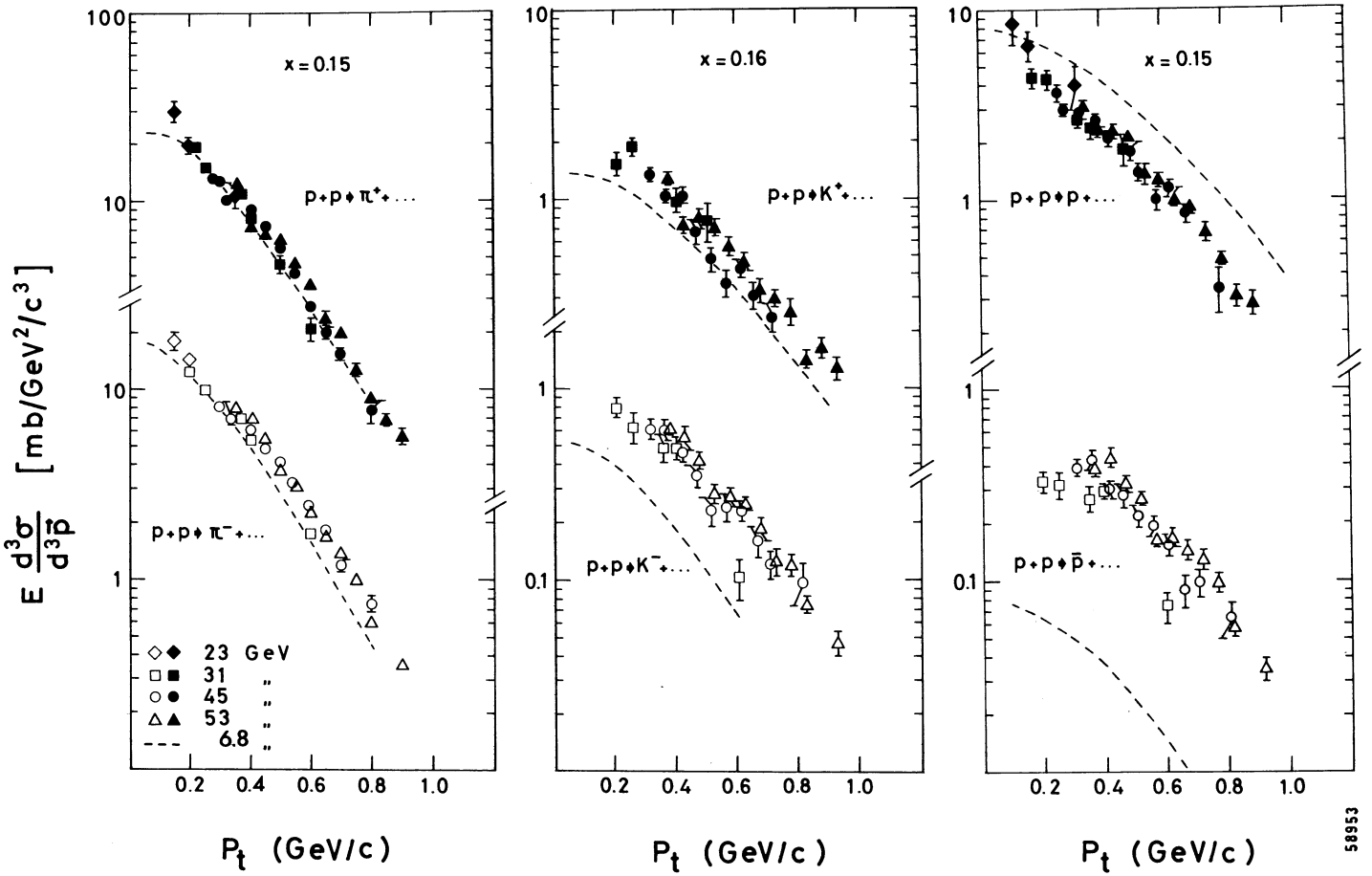


Fig. 1a The invariant inclusive cross-sections $Ed\sigma/d^3p$ are plotted versus $p_T$ at fixed x for the production of $\pi^{\pm}$, $K^{\pm}$, p and $\bar{p}$. ISR data from the Argonne-CERN-Bologna collaboration, Ref. 10). The dashed lines represent interpolations through data at $p_{lab}$ = 24 GeV/c and $x \approx 0.16$ [Ref. 27)].

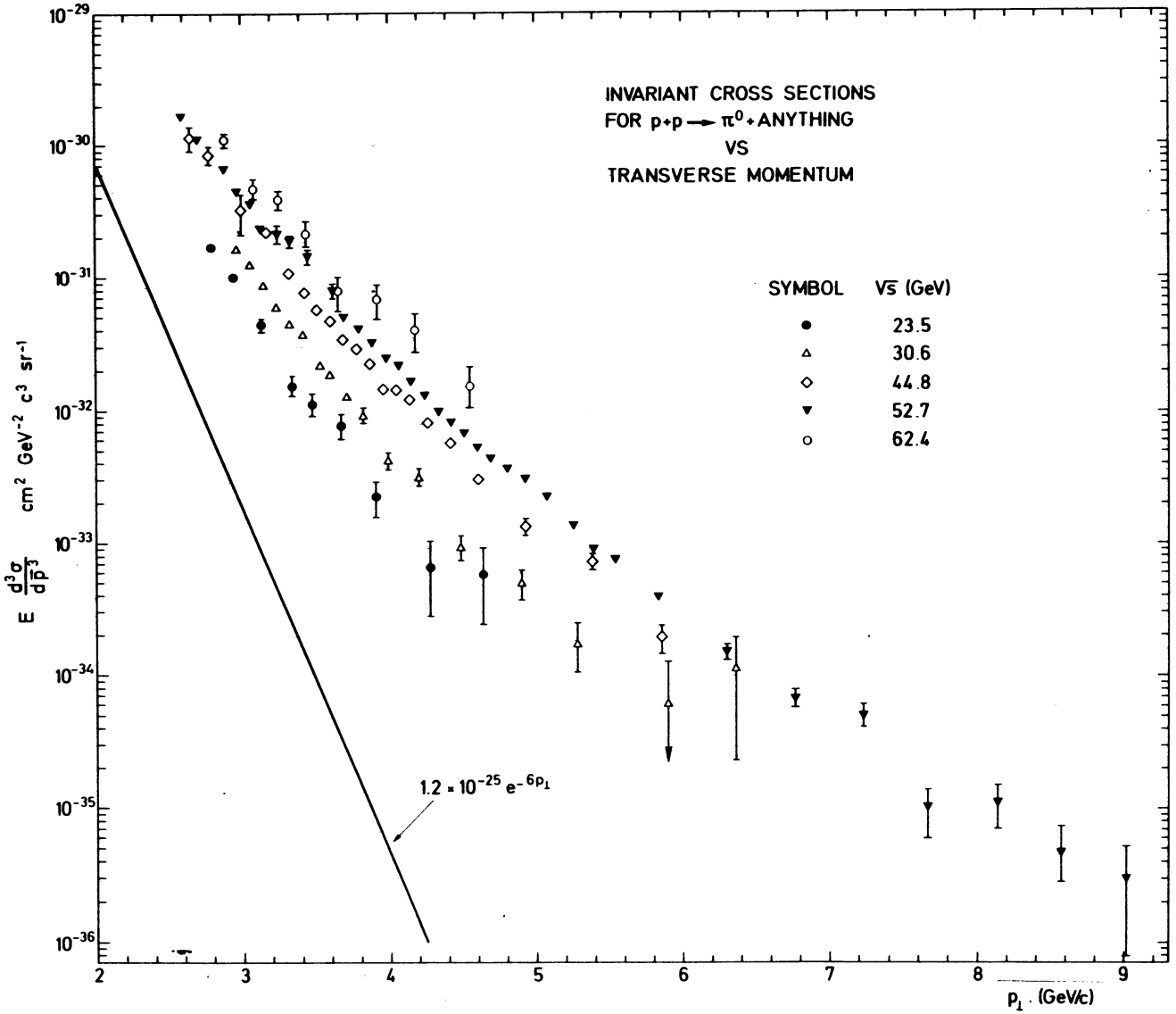


Fig. 1b The transverse momentum dependence at $x \approx 0$ of the invariant inclusive cross-section $Ed\sigma/d^3p$ at five centre-of-mass energies. Data of the CERN-Columbia-Rockefeller collaboration, Ref. 12). Shown for comparison is the extrapolation to large $p_T$ of a fit to data in the interval $p_T < 1$ GeV/c.

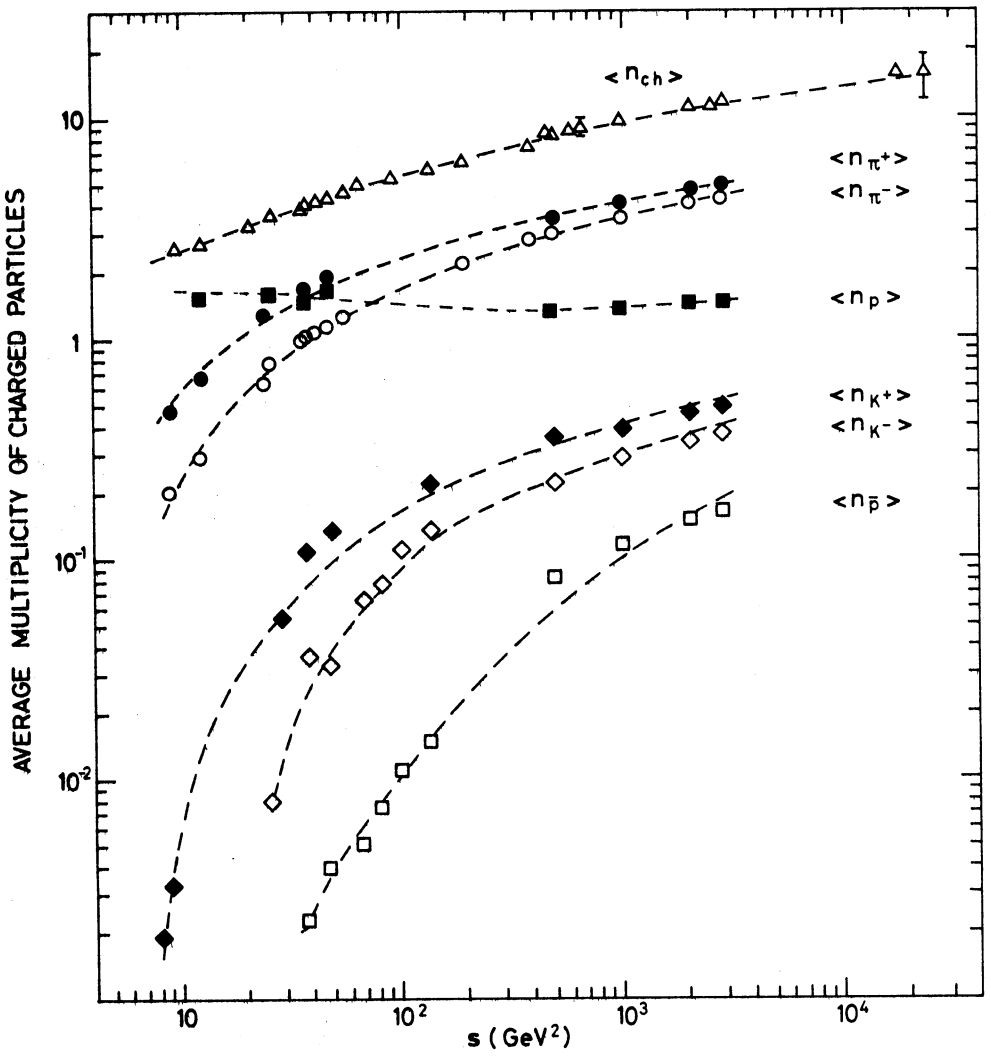


Fig. 2 The average multiplicities of $\pi^-$, $\pi^+$, $K^-$, $K^+$, $\bar{p}$ and p observed in pp interactions are plotted as a function of s. From Ref. 13).

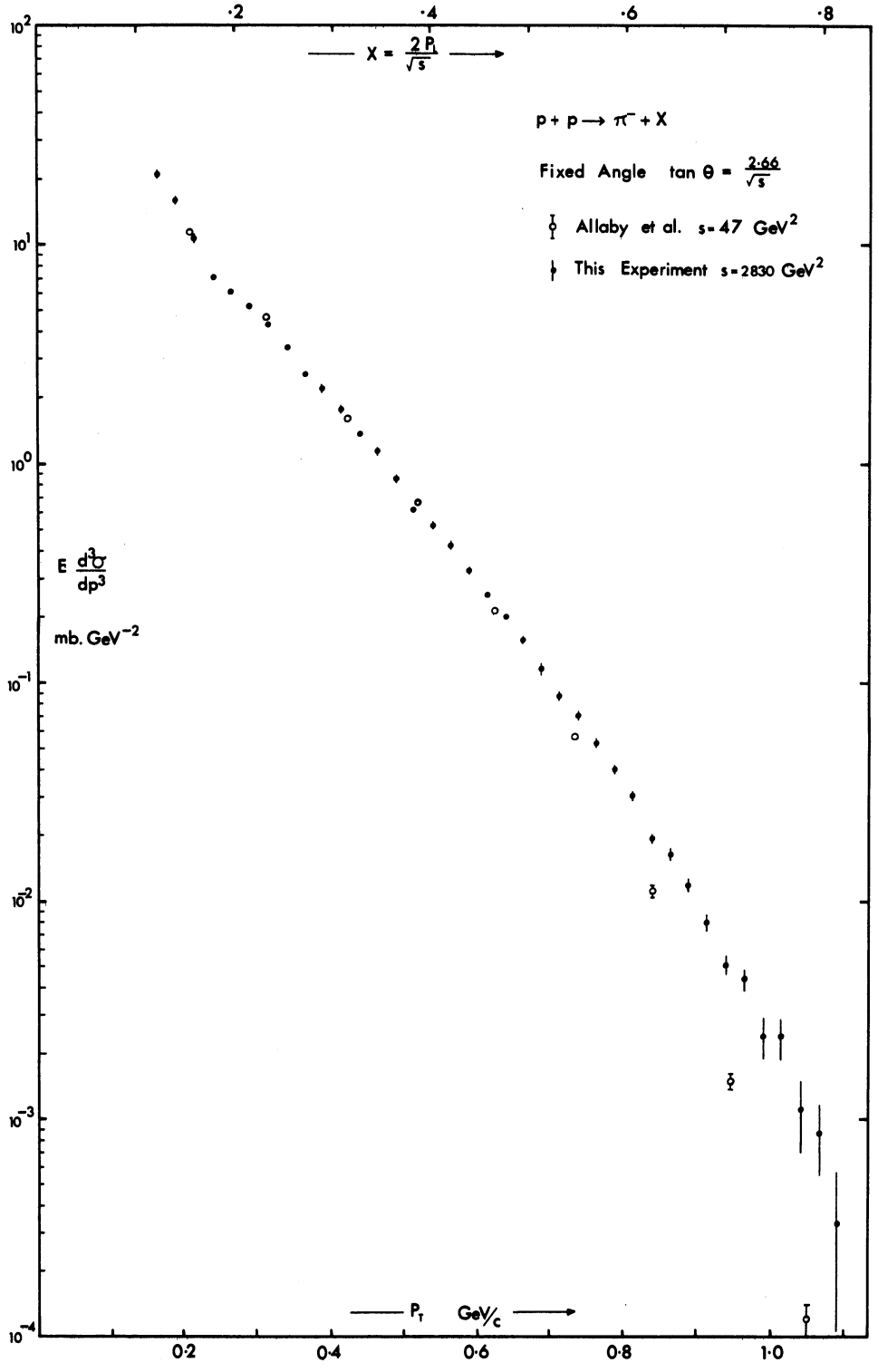


Fig. 3a Invariant cross-section $Ed\sigma/d^3p$ for $pp \to \pi^- X$ at fixed centre-of-mass angle $\tan\theta = 2.66/\sqrt{s}$ plotted versus $x = 2p_L/\sqrt{s}$ and $p_T = 1.33x$ GeV/c. Data from the CHLM experiment at $s = 2830$ GeV$^2$ [solid points, Ref. 25)] are compared with data at $s = 47$ GeV$^2$ [open circles, Ref. 27)].

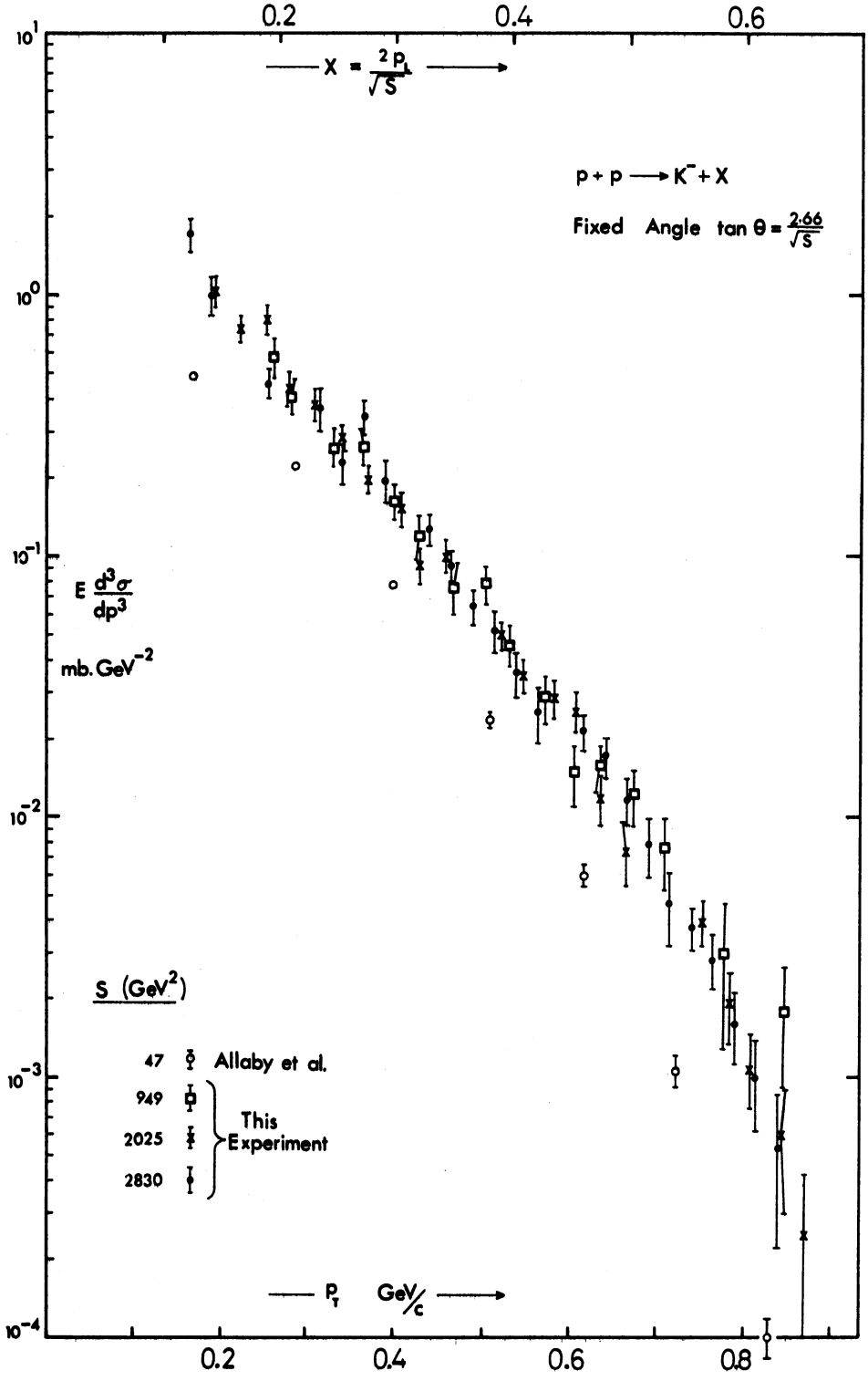


Fig. 3b As in Fig. 3a, for the reaction $pp \rightarrow K^- X$. CHLM data are shown at 3 centre-of-mass energies.

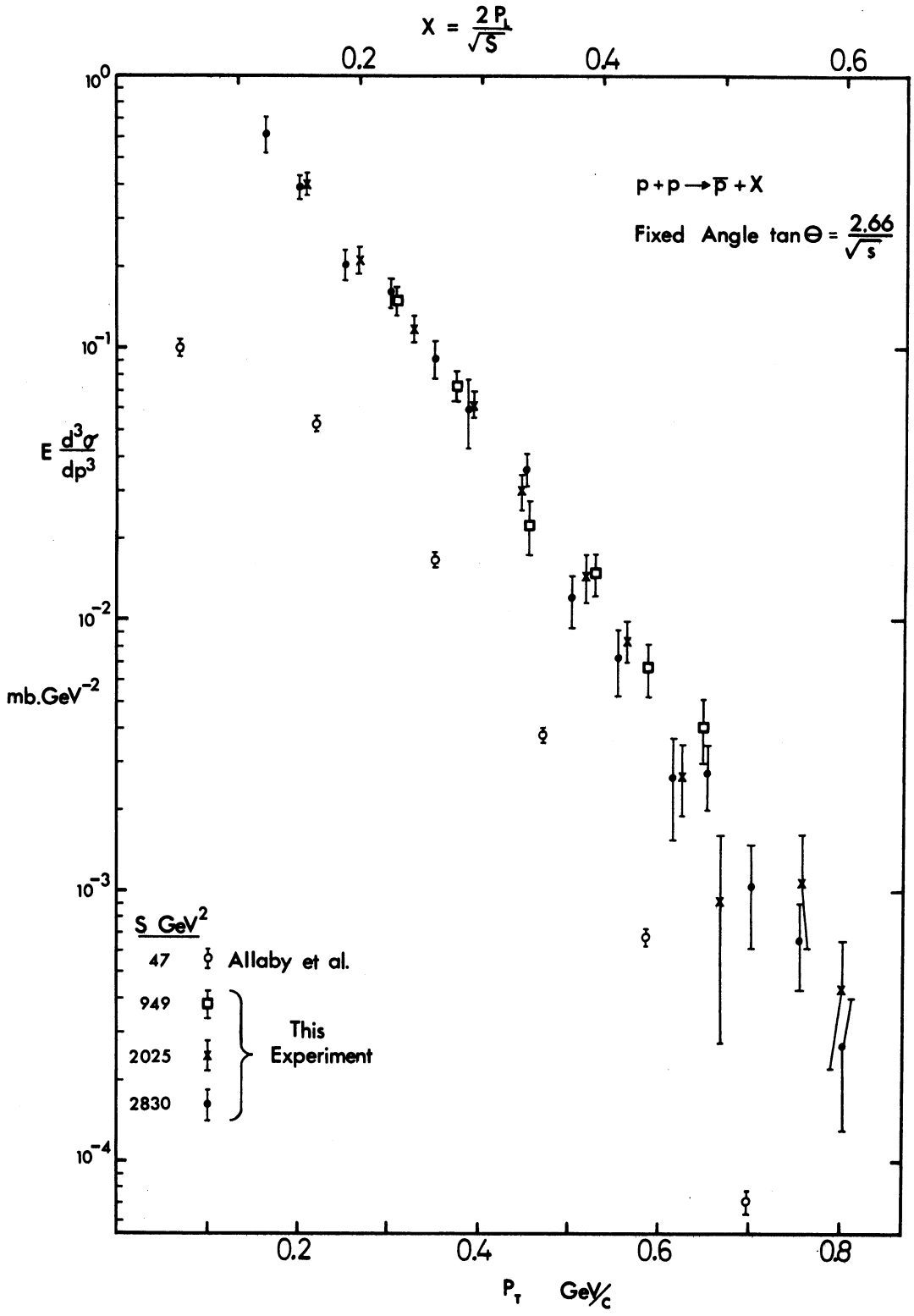


Fig. 3c As in Fig. 3b, for the reaction $pp \rightarrow \bar{p}X$.

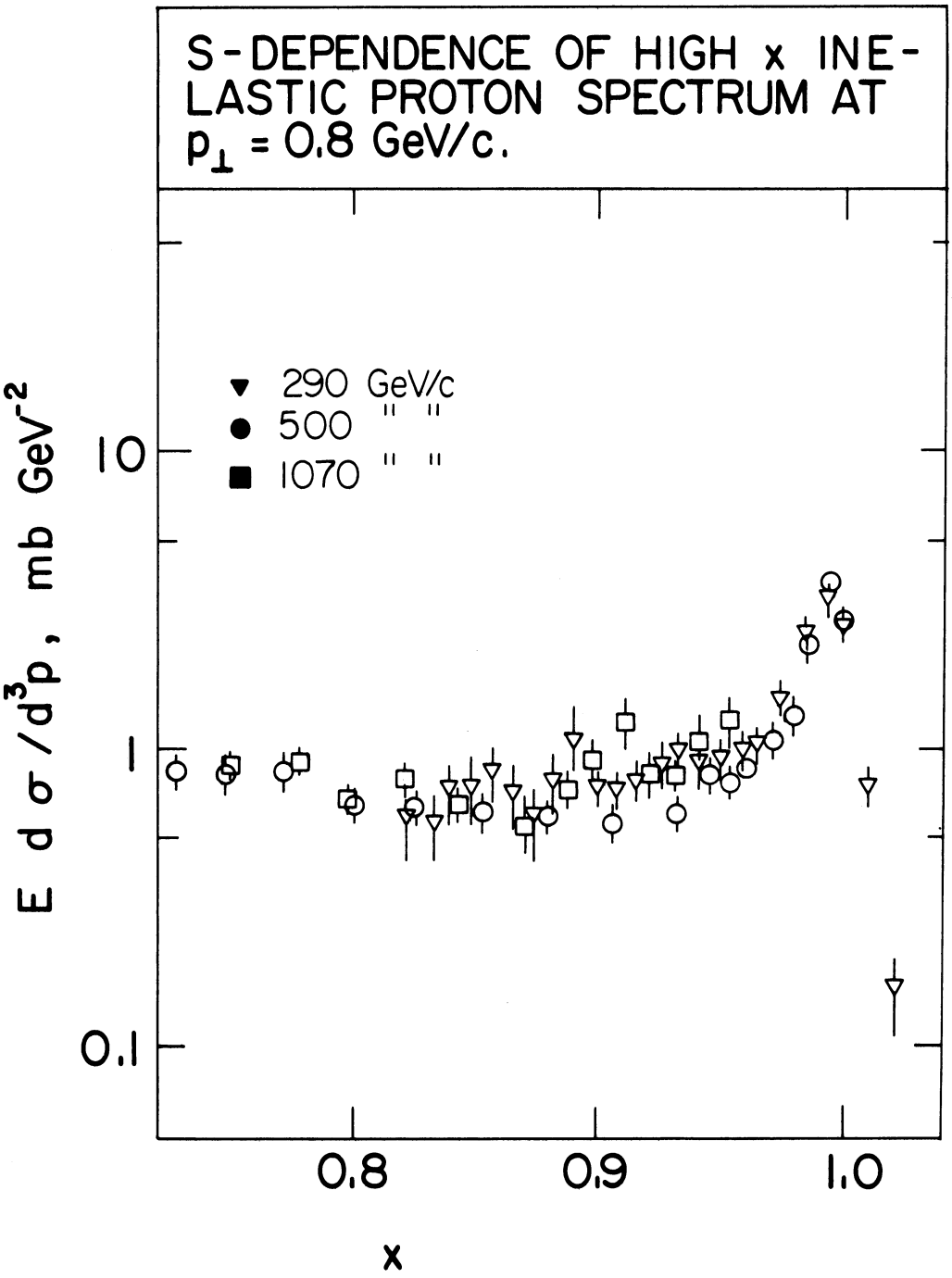


Fig. 4 Invariant inclusive distribution $Ed\sigma/d^3p$ for $pp \to pX$ at $p_T = 0.8$ GeV/c is plotted versus x. CHLM data [Ref. 5)] are given at 3 energies.

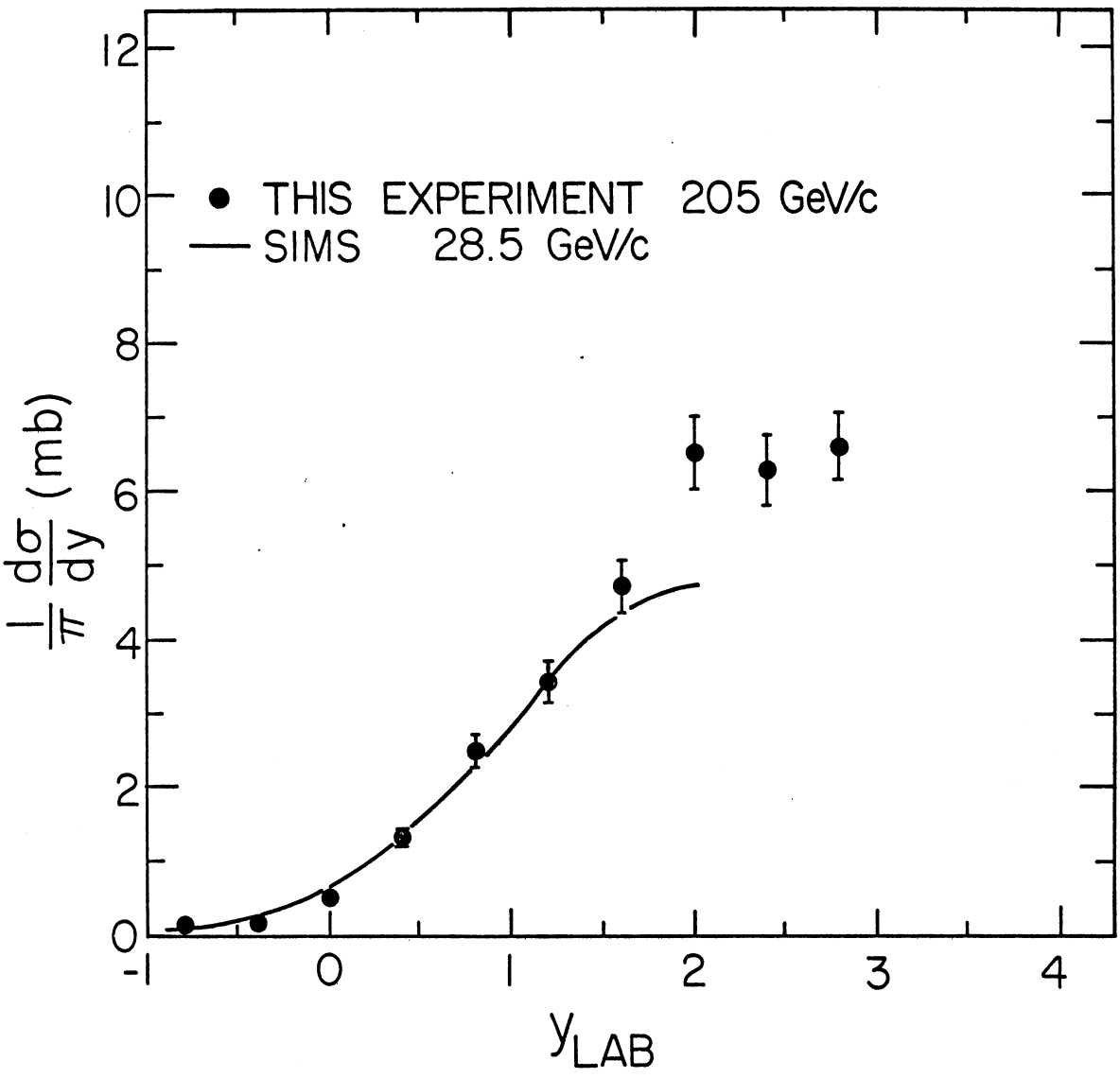


Fig. 5 The inclusive $\pi^-$ rapidity distribution from $pp \to \pi^- X$ at 205 GeV/c [Ref. 28)] is plotted versus rapidity in the lab. frame. Shown for comparison is a solid curve fitted to 28.5 GeV/c data [Ref. 29)].

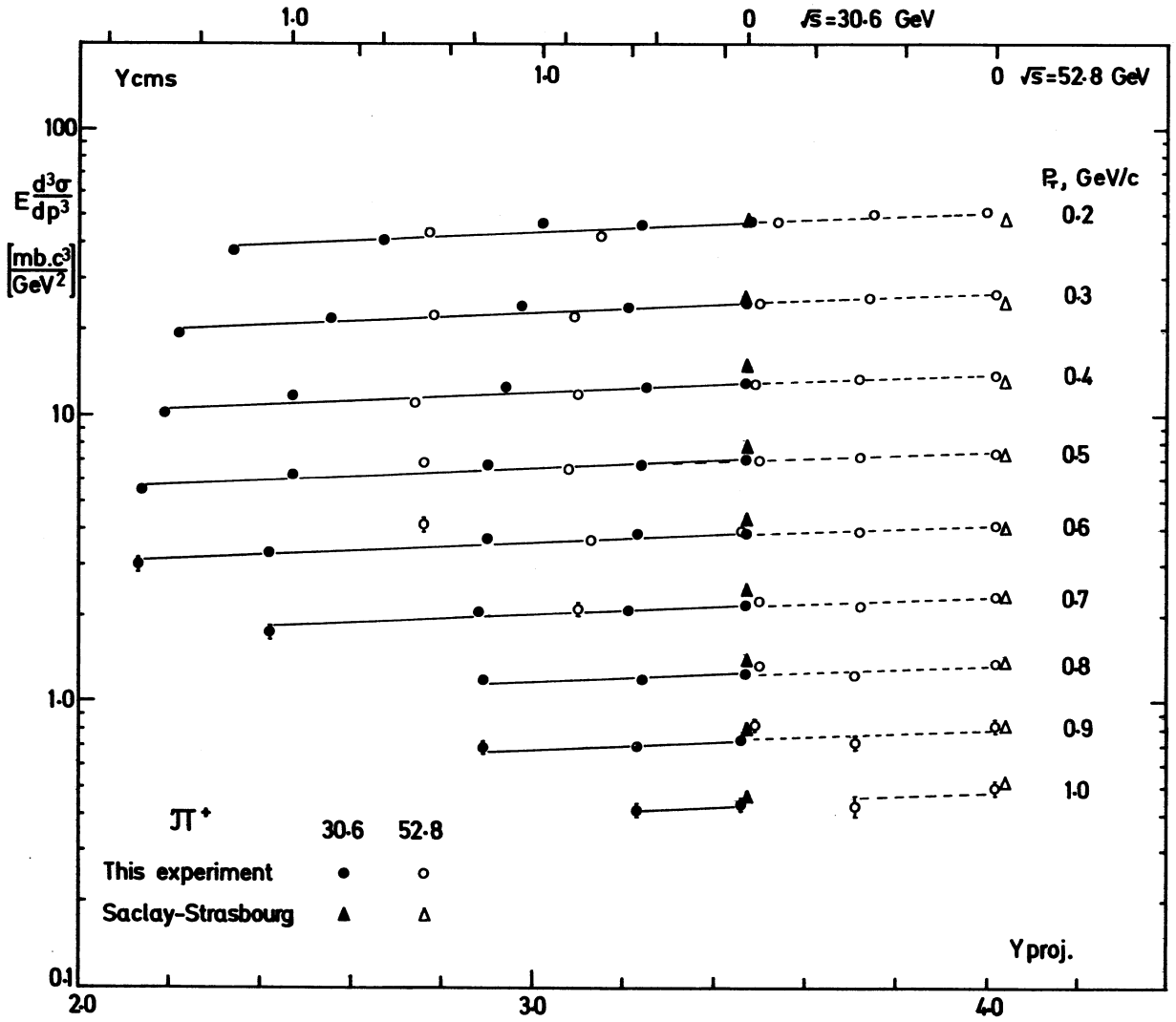


Fig. 6 Inclusive rapidity distribution for $pp \to \pi^+ X$ in the projectile frame of reference. British-Scandinavian data [Ref. 30)] at $\sqrt{s} = 30.6$ and 52.8 GeV are given for several fixed values of $p_T$. For comparison results of the Saclay-Strasbourg experiment at $90^0$ are given [Ref. 31)]. The data are fitted to the form

$$A(1+\alpha y_{cms}) \exp(b p_T + c p_T^2),$$

where $A \simeq 187$, $b \cong -6.9$, $c \cong 0.9$, and $\alpha \cong -0.14$.

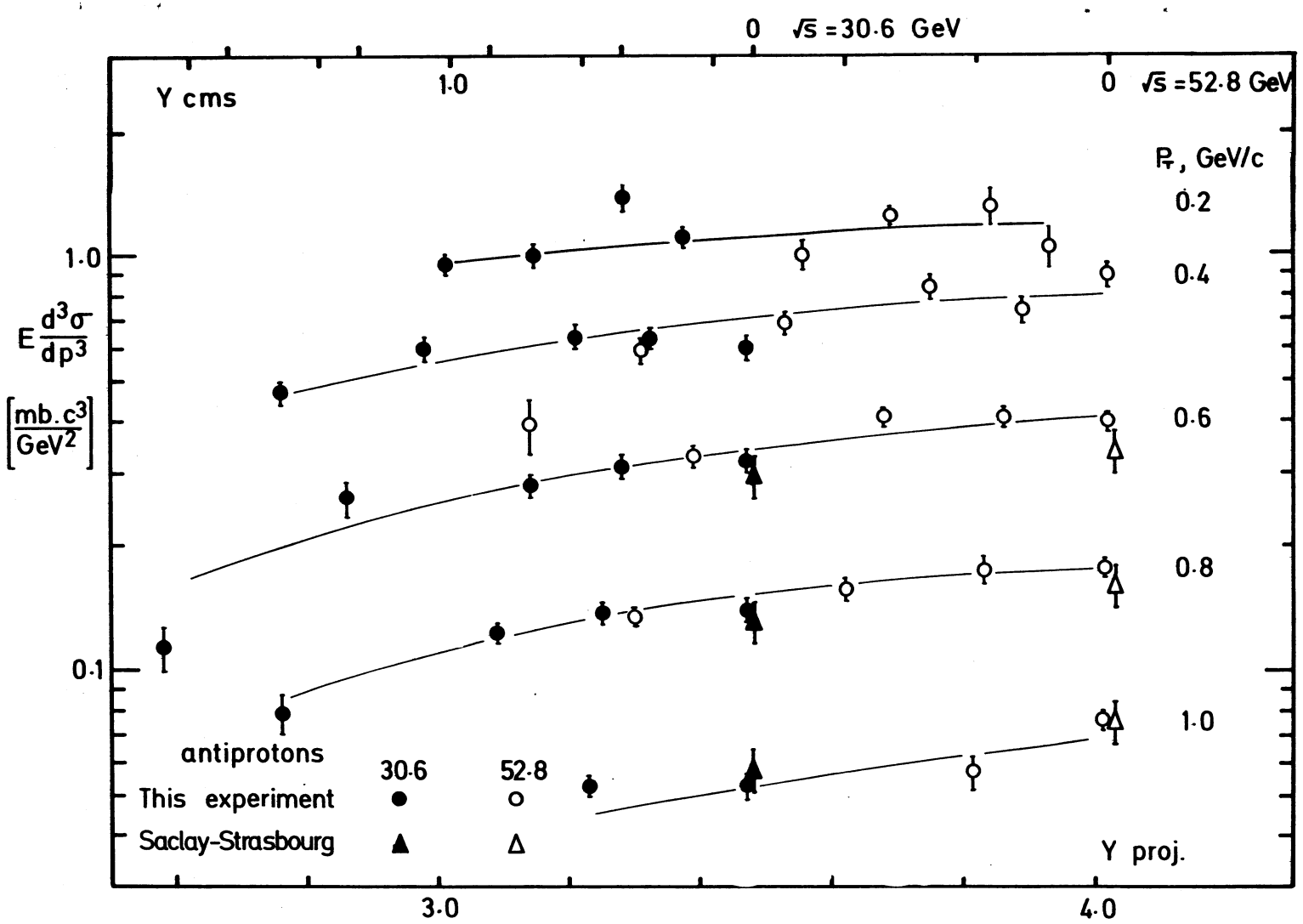


Fig. 7 Inclusive rapidity distribution for $pp \rightarrow \bar{p}X$ in the projectile frame of reference, as in Fig. 6. Here the lines are drawn to guide the eye.

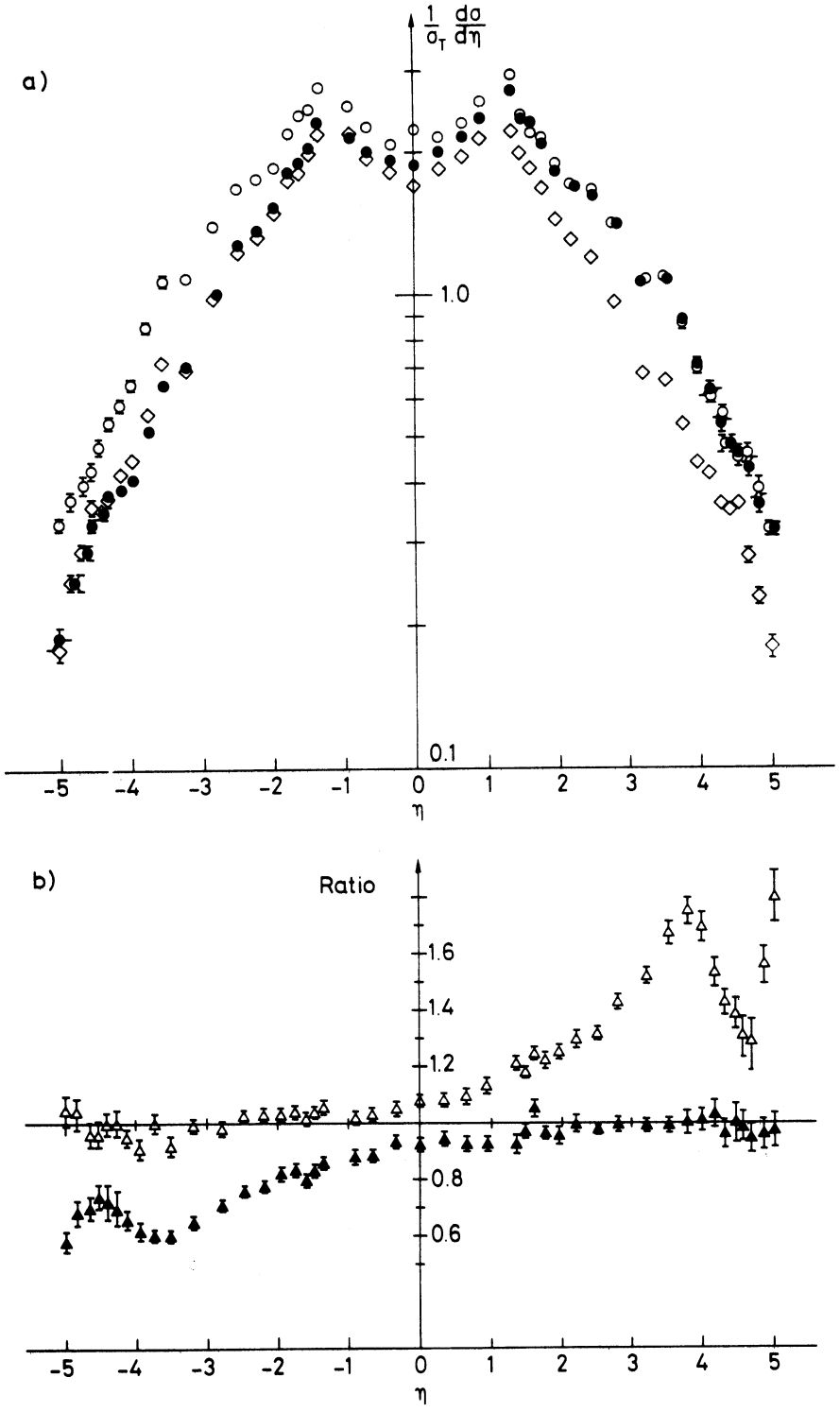


Fig. 8 Pisa-Stony Brook [Ref. 32)] single-particle inclusive density distributions $(1/\sigma_T)(d\sigma^{(1)}/d\eta)$.

a) Comparison of $(1/d\sigma_T)(d\sigma^{(1)}/d\eta)$ for three runs :
(A) $p_1=p_2=15.4$ GeV/c; ◇
(B) $p_1=p_2=26.6$ GeV/c; ○
(C) $p_1=15.4$ GeV/c, $p_2=26.6$ GeV/c; ●

b) Ratios of $(1/\sigma_T)(d\sigma^{(1)}/d\eta)$ for asymmetric energy to $(1/\sigma_T)(d\sigma^{(1)}/d\eta)$ same energies are plotted versus $\eta$.
△ : run (C)/run (A)
▲ : run (C)/run (B).

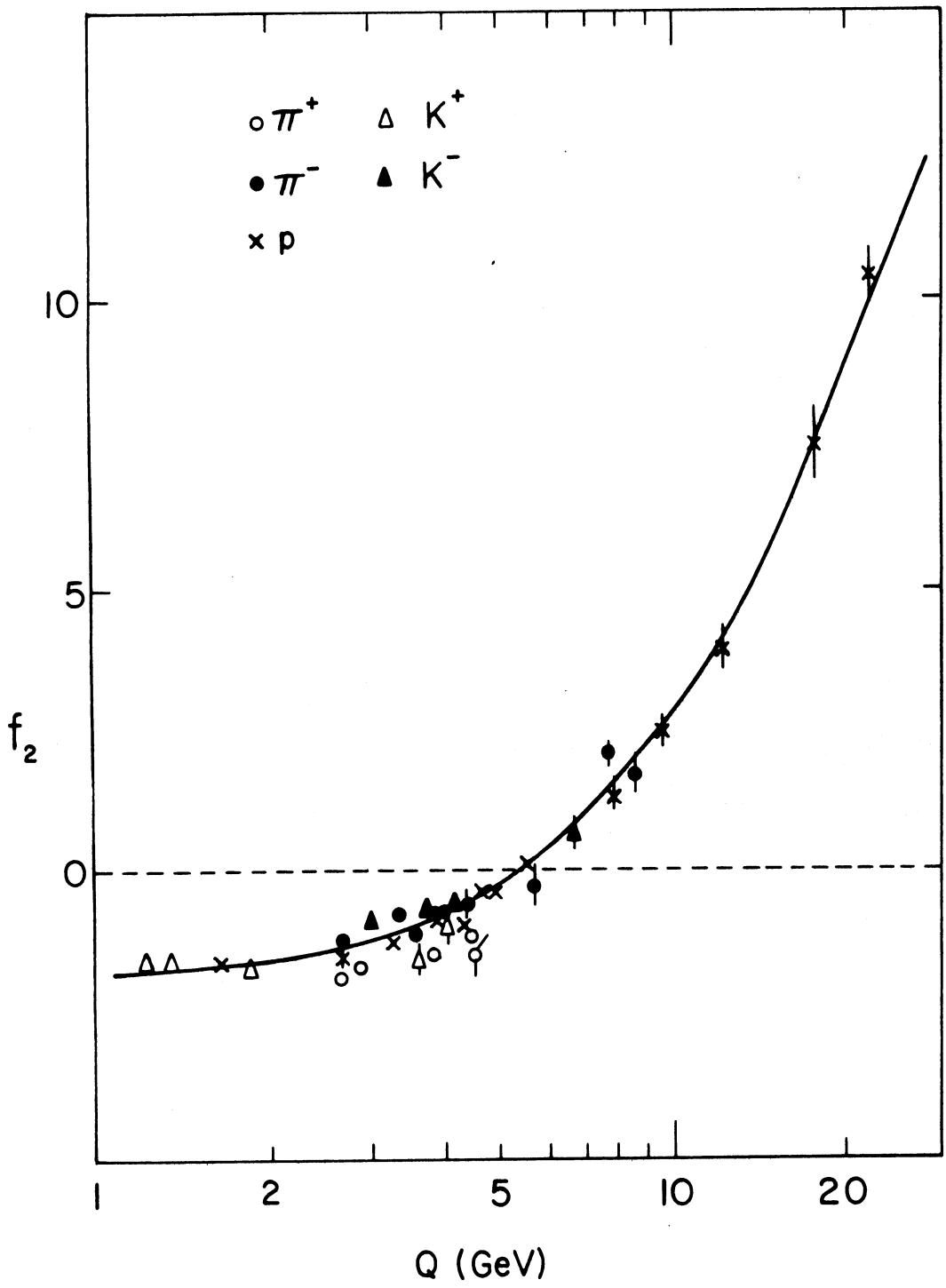


Fig. 9 The correlation moment $f_2 = \langle n_c(n_c-1)\rangle - \langle n_c\rangle^2$ is plotted versus $Q = [\sqrt{s}-(M_A+M_B)]$. Here $n_c$ denotes the number of charged particles of system X in the reaction $A+B\rightarrow X$. $M_A$ and $M_B$ are the masses of the incident particles. Data are shown for the indicated choices of particle A ($\pi^{\pm}$, $K^{\pm}$, and p); in all cases B = proton. This figure is taken from Ref. 15).

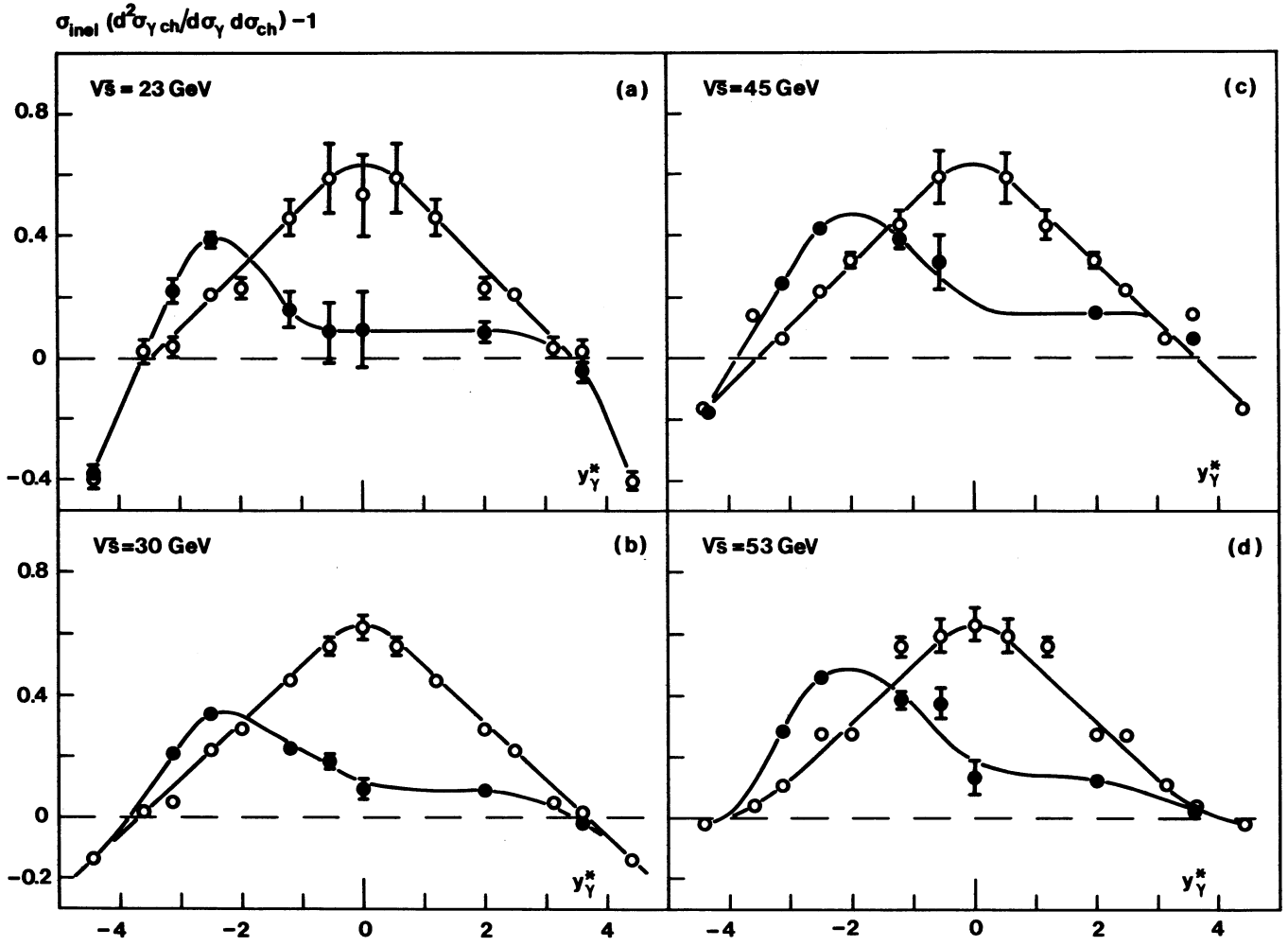


Fig. 10 For the reaction $pp \to \gamma hX$, the reduced correlation function $R(y_\gamma, y_{ch})$ is plotted versus centre-of-mass gamma rapidity $y_\gamma$ for two fixed values of approximate centre-of-mass rapidity $y_{ch}$ of charged hadron h. Open circles give CHV data [Ref. 17)] with $y_{ch} \approx 0$ and full circles for $y_{ch} \approx -2.5$. Results are presented at four energies, a) $\sqrt{s}$ = 23, b) $\sqrt{s}$ = 30, c) $\sqrt{s}$ = 45 and d) $\sqrt{s}$ = 53 GeV.

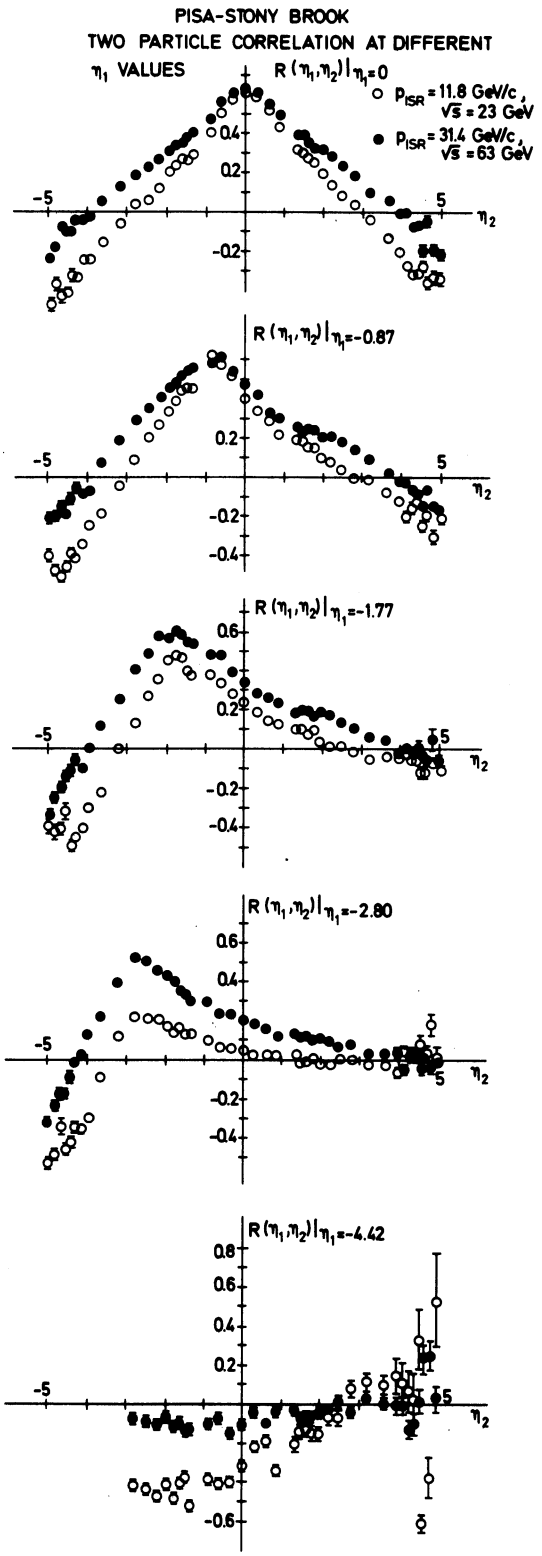


Fig. 11 Reduced charged particle correlation functions $R(\eta_1, \eta_2)$ for several fixed $\eta_1$ are plotted versus $\eta_2$. Open circles $\sqrt{s}$ = 23 GeV. Dark circles $\sqrt{s}$ = 62 GeV. Errors shown are statistical only; from Ref. 18).

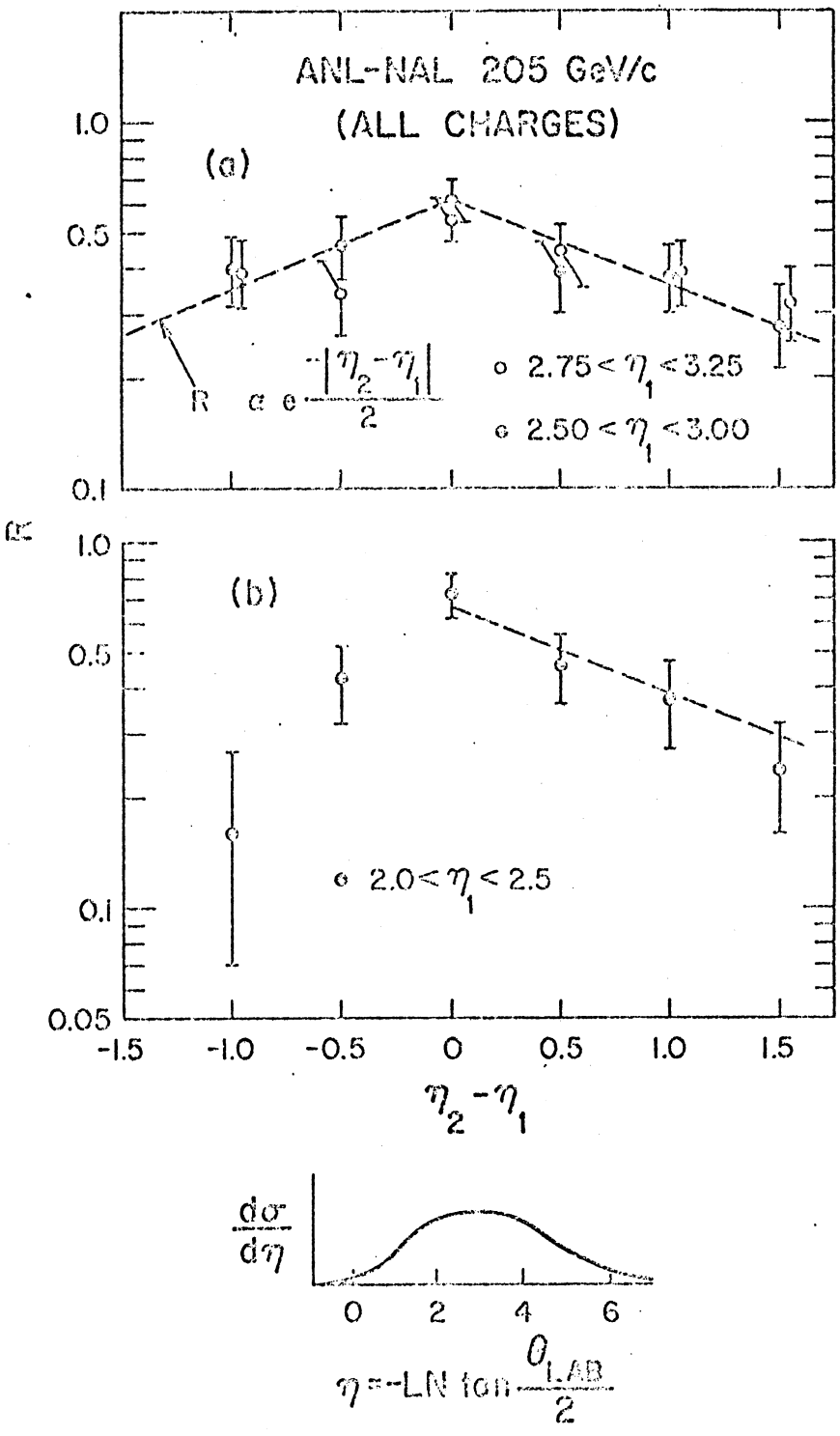


Fig. 12 The reduced charged particle correlation function $R(\eta_1, \eta_2)$ at 205 GeV/c is plotted versus $(\eta_1 - \eta_2)$ for three selections on $\eta_1$, defined in the lab. rest frame. The zero value of centre-of-mass longitudinal momentum corresponds to $\eta \approx 3$. In a), the two selections place $\eta_1$ in the central plateau interval. In b), $\eta_1$ is near the edge of the rapidity plateau. Data from Ref. 19).

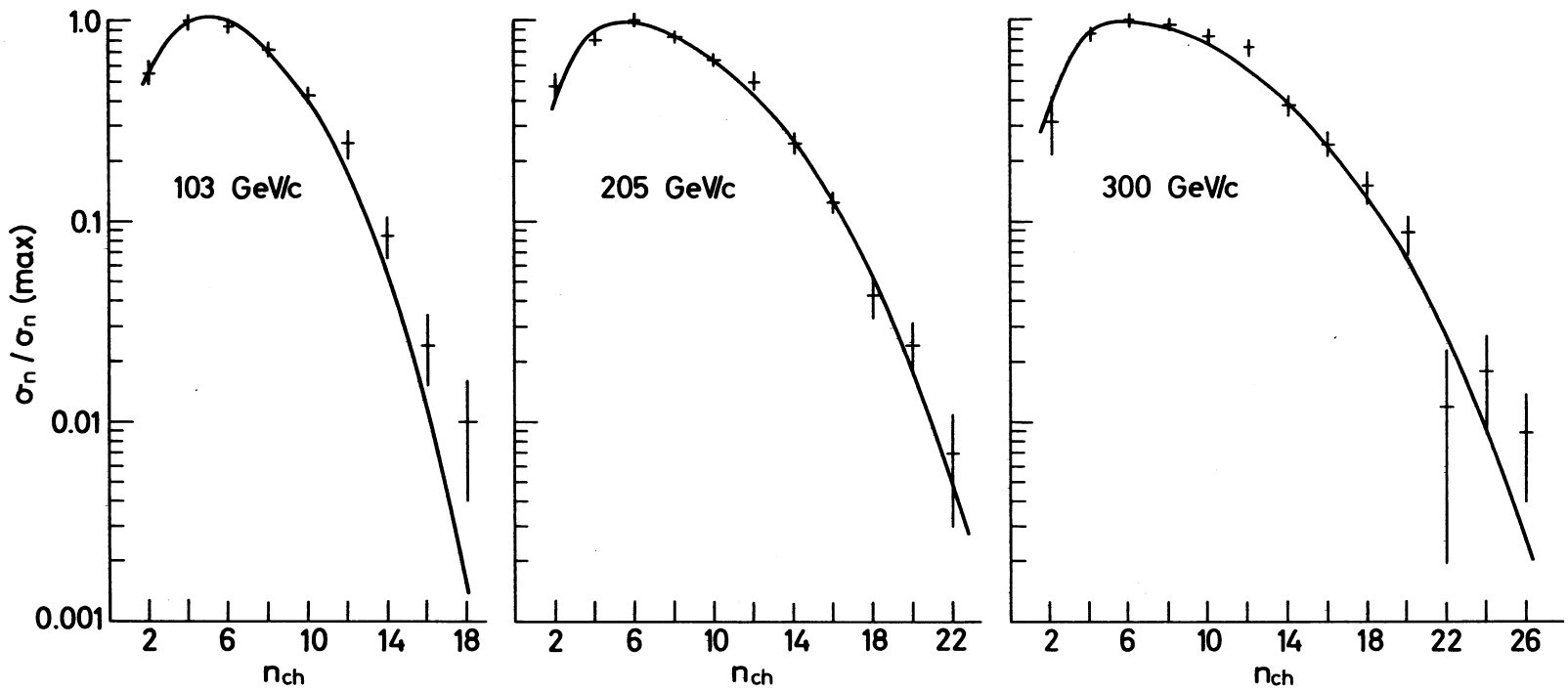


Fig. 13 Data on the charged particle multiplicity distributions at 103, 205, and 300 GeV/c [Ref. 20)] are compared with results observed in the multiperipheral cluster emission model of Ref. 4). Data are given as the ratio $\sigma_n/\sigma_n(\max)$, where $\sigma_n(\max)$ is the largest prong cross-section at a given energy.

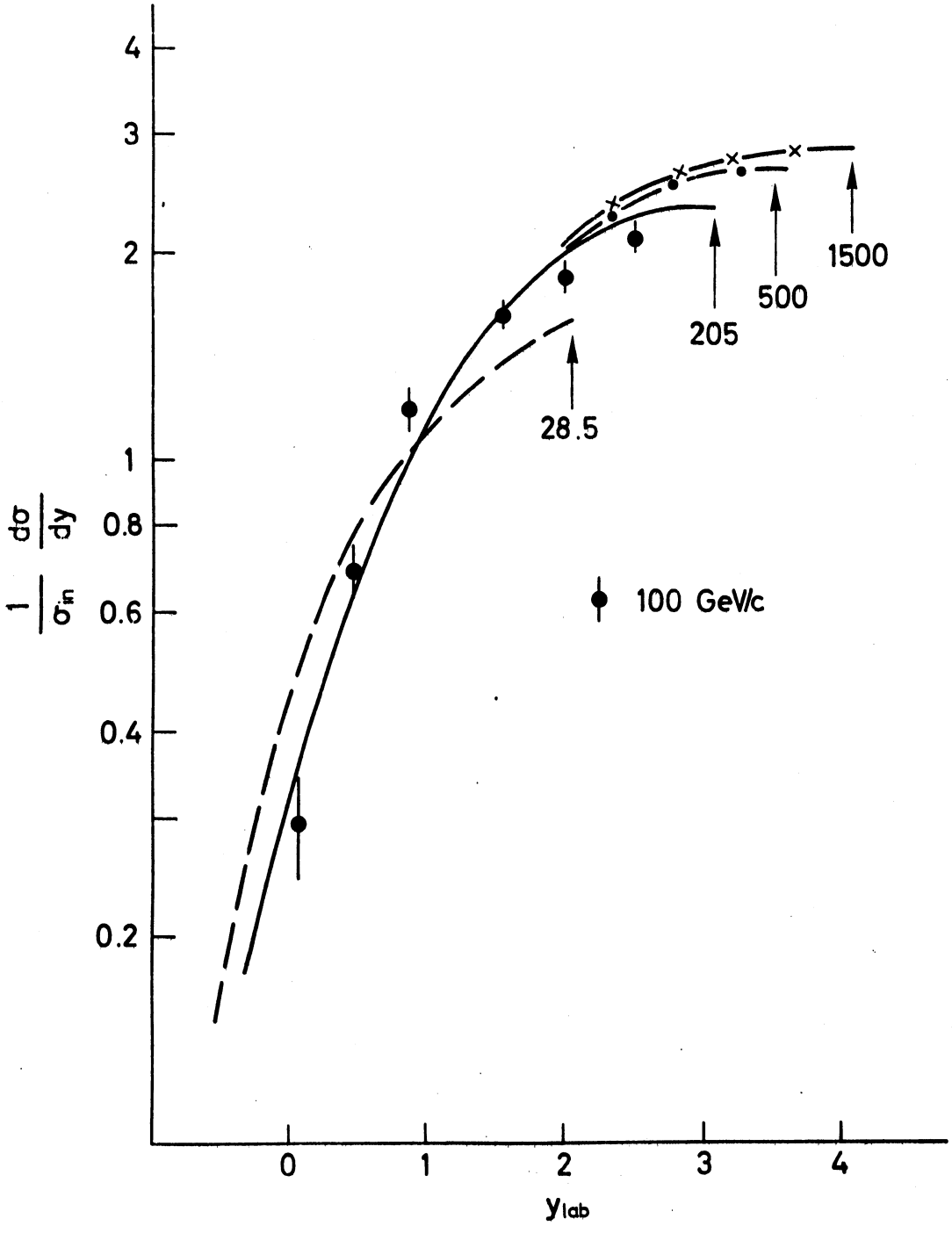


Fig. 14 Single pion inclusive rapidity distribution $\sigma_{inel}^{-1} d\sigma/dy$ versus $y_{lab}$ for 28.5, 205, 500 and 1500 GeV/c. Theoretical curves are normalized absolutely and summed over all charges. Data at 100 GeV/c [Ref. 49)] are $1.5 \times [d\sigma/dy(\pi^+) + d\sigma/dy(\pi^-)]/\sigma$. Theoretical curves are computed from a multiperipheral cluster emission model, Ref. 4).

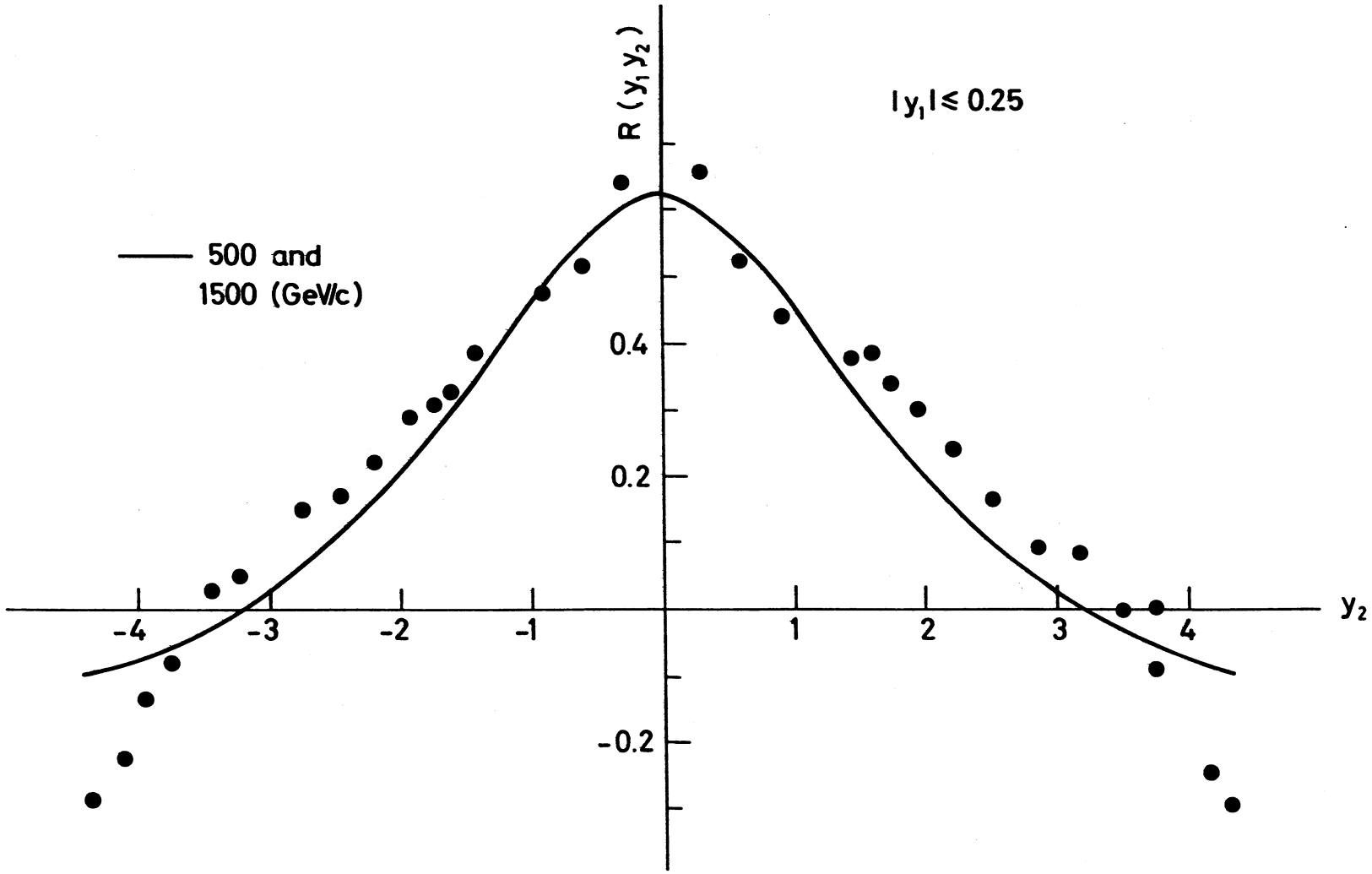


Fig. 15a Normalized inclusive charged particle correlations function $R(y_1,y_2)$, defined in the text [Eqs. (3.23) and (4.3)] is calculated from the multiperipheral cluster emission model [Ref. 4)] and plotted versus $y_2$ for selection $|y_1| \leq 0.25$. Preliminary data are from Ref. 18) at 500 GeV/c while predictions are given at 500 and 1500 GeV/c. In the data the approximation $y \approx \log(\tan\theta/2)$ is used but the Monte Carlo program indicates this has little effect on distributions.

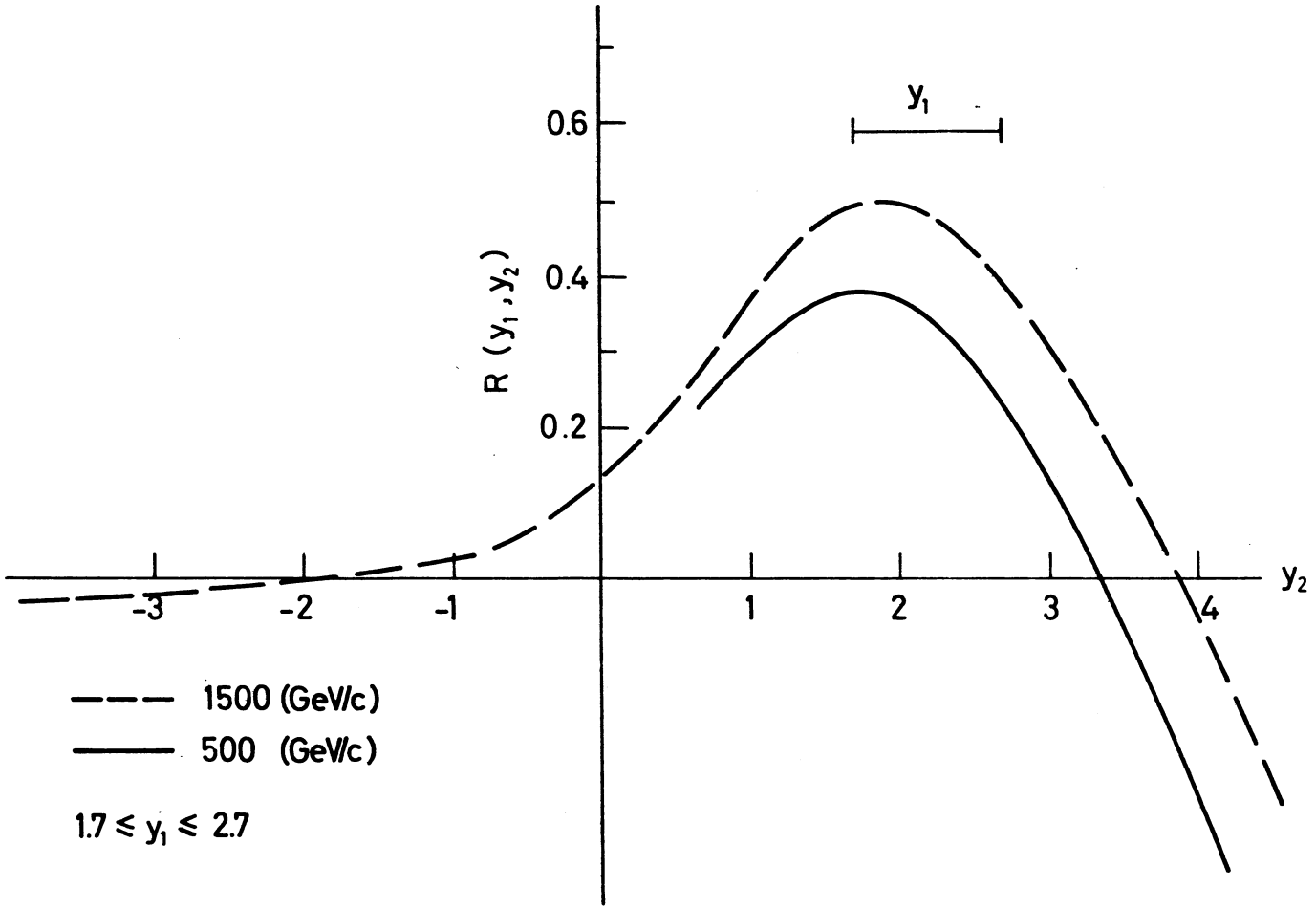


Fig. 15b As in Fig. 15a, but for the selection $1.7 \leq |y_1| \leq 2.7$.

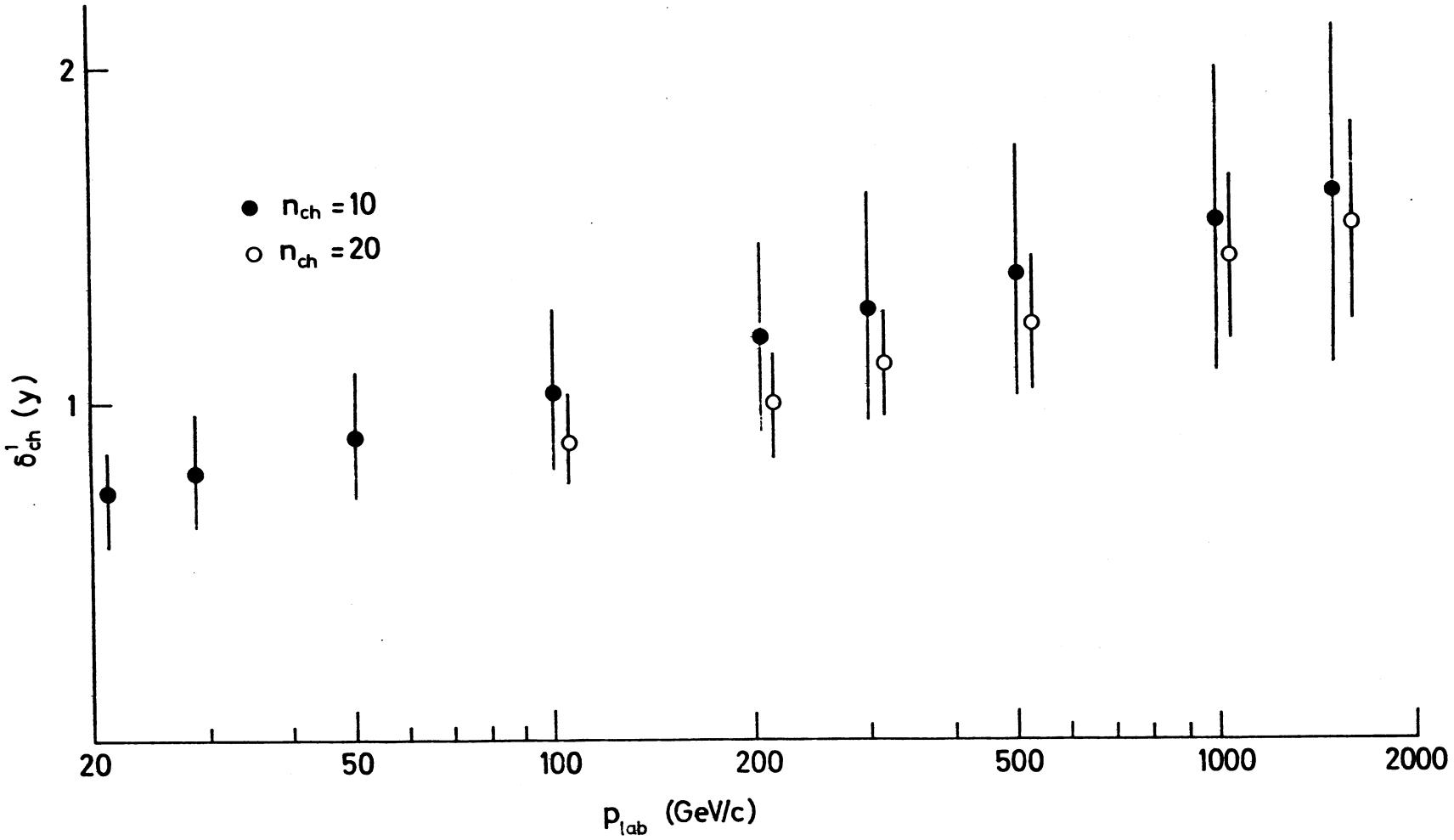


Fig. 16 Central value and standard deviation of dispersion $\delta^1$ of individual events in rapidity. Dispersion is defined in Eq. (4.9) of the text. Theoretical results are obtained from the model of Ref. 4), with an average of four hadrons per cluster. Values as a function of $p_{lab}$ are given for charged multiplicity $n_{ch}$ = 10 and 20.

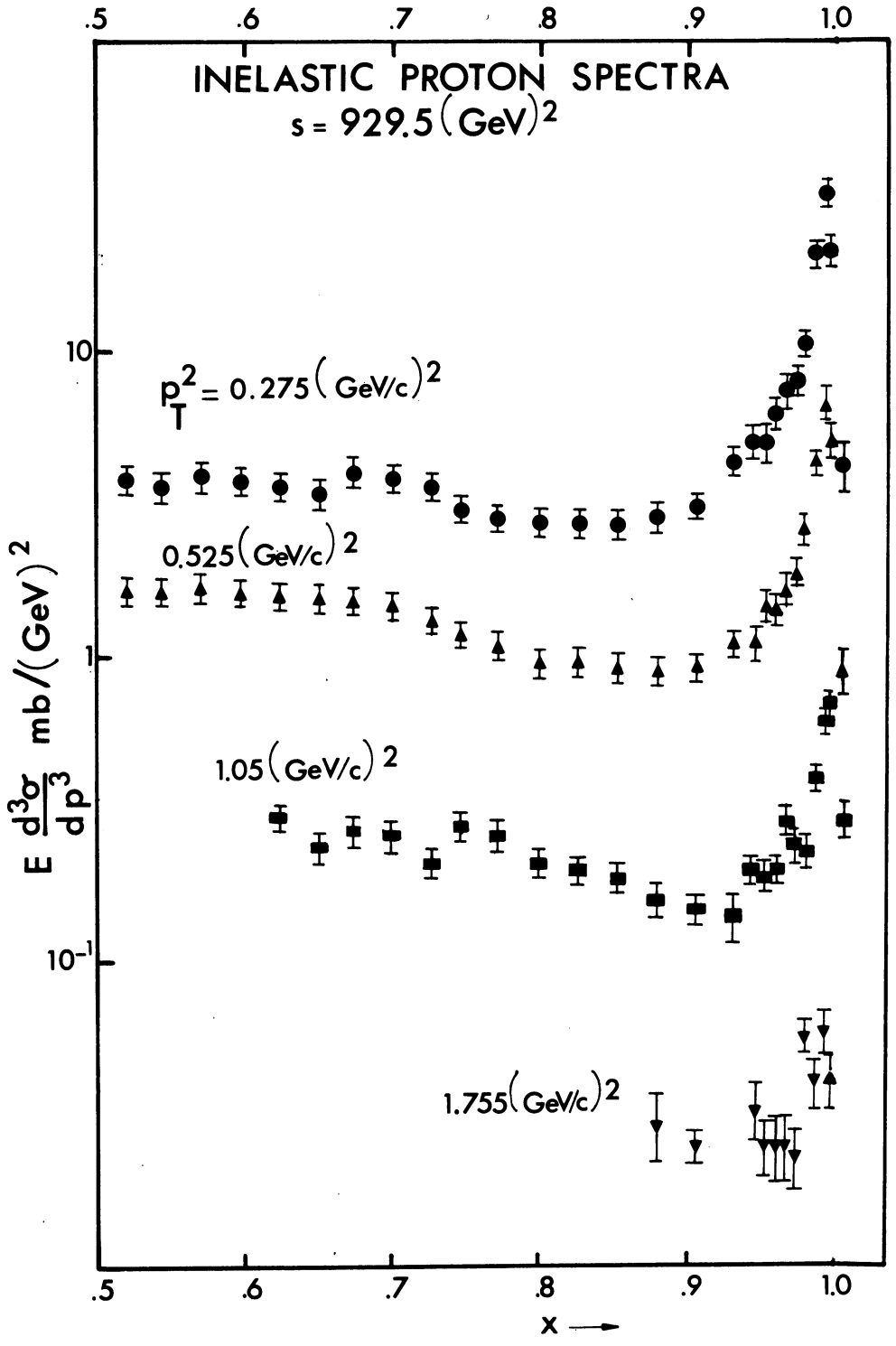


Fig. 17 The CHLM invariant inclusive spectrum $Ed\sigma/d^3p$ for $pp \to pX$ at $s = 929.5\ (GeV)^2$ is plotted as a function of $x$ for four different fixed values of $p_T$. Ref. 5).

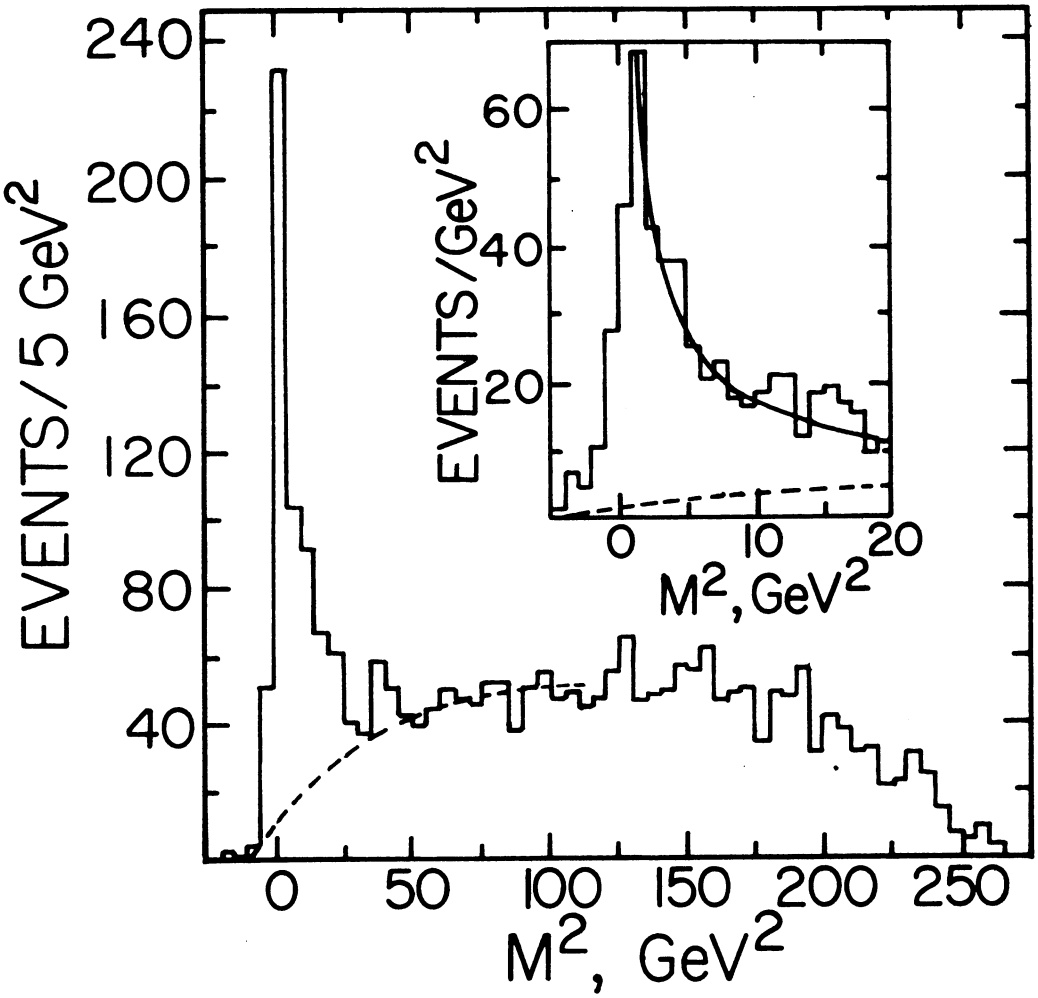


Fig. 18 The distribution in missing squared, $M^2$, for inelastic events of the type $pp \rightarrow$ slow $p + X$ at 205 GeV/c. The insert shows the low $M^2$ region in in 1 $GeV^2$ bins. The dashed lines represent a hand-drawn background used to estimate the number of events in the peak. The solid line on the insert shows background plus a $1/M^2$ dependence for the tail of the peak. From Barish et al., Ref. 57).

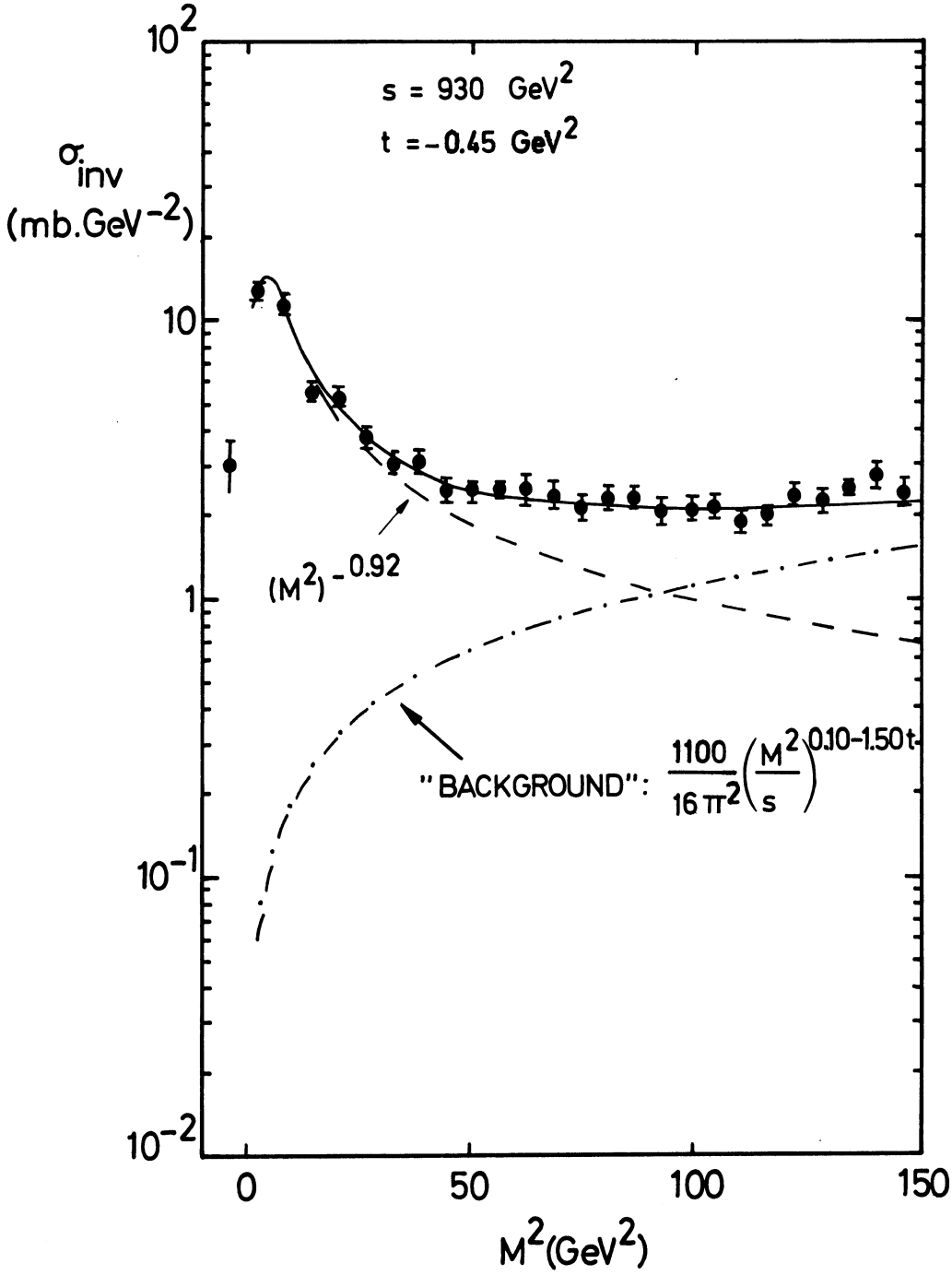


Fig. 19 The invariant inclusive cross-section $(s/\pi)d^2\sigma/dt\,dM^2$ measured by the CHLM group, Ref. 65), for the reaction $pp \to pX$ at $s = 930$ GeV$^2$ and $t = -0.45$ GeV$^2$ is plotted versus $M^2$, where $M$ is the mass of system $X$ and $t$ is the square of the momentum transfer to the final proton. The solid curve results from a triple-Regge fit to the data, as discussed in Ref. 65).

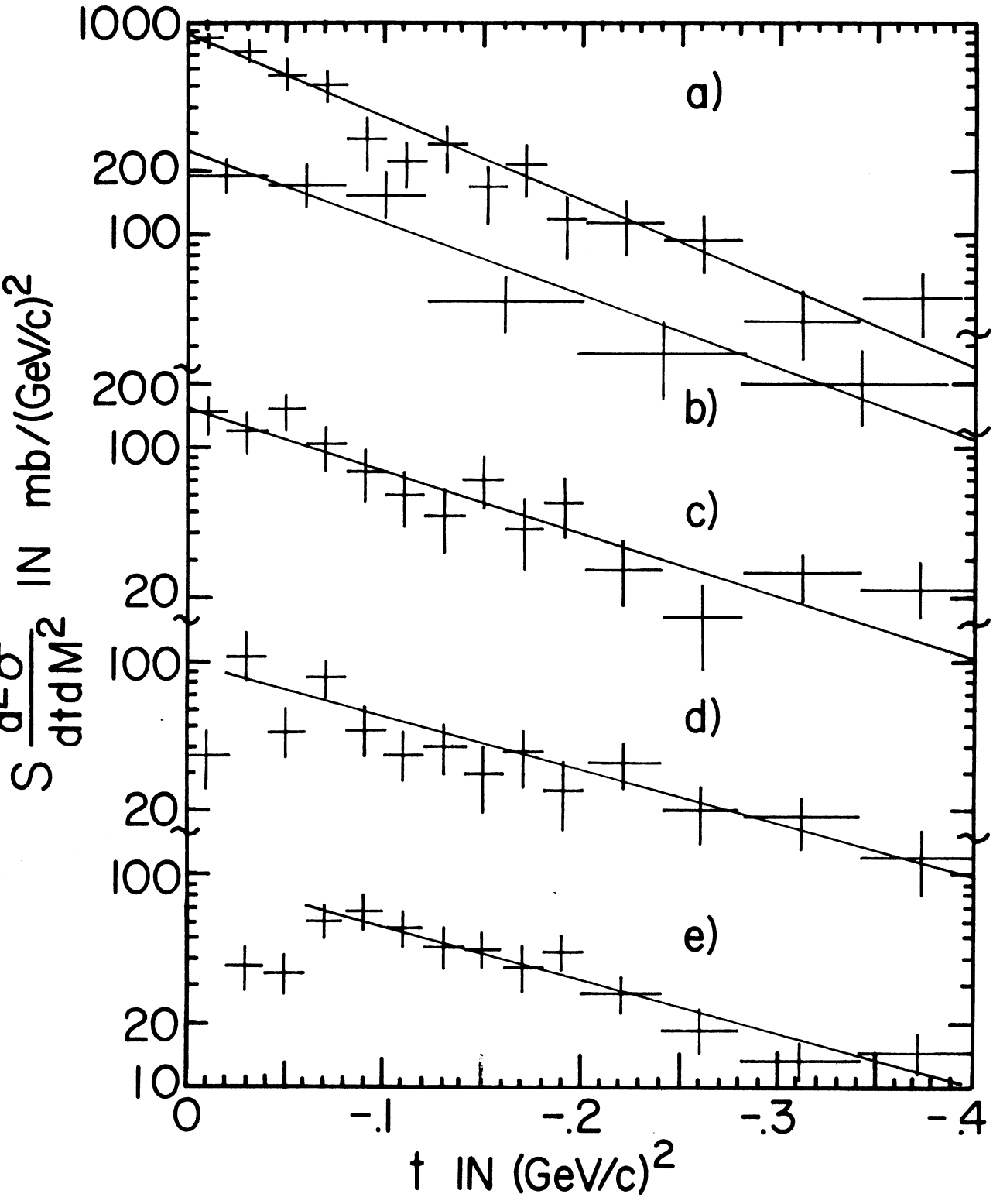


Fig. 20 Invariant cross-section $s(d^2\sigma/dt\ dM^2)$ versus four-momentum transfer squared t for all events from $pp \rightarrow pX$ at 205 GeV/c. a) for $M^2 < 5$ GeV$^2$, b) $5 \leq M^2 < 10$ GeV$^2$, c) $10 \leq M^2 < 25$ GeV$^2$, d) $25 \leq M^2 < 50$ GeV$^2$ and e) $50 \leq M^2 < 100$ GeV$^2$. The lines drawn show fits of the form $Ae^{Bt}$ to the data (see Table in Section 5.2.4.) [Ref. 57].

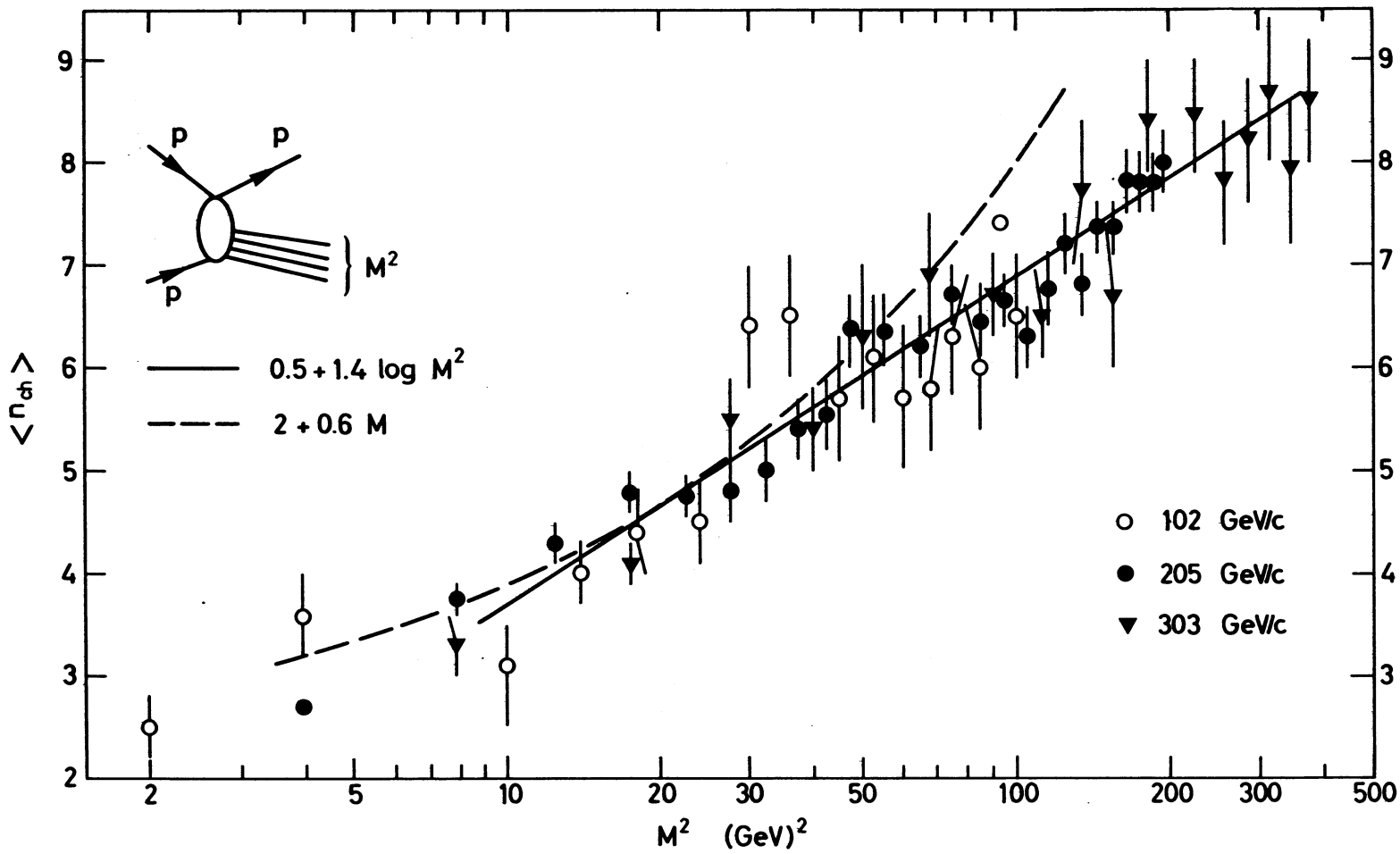


Fig. 21 The total mean charged multiplicity observed in the reaction $pp \rightarrow pX$ is plotted as a function of mass squared of system X. The figure includes data from the 100, 200 and 300 GeV/c NAL 30 inch bubble chamber exposures, Refs. 56), 57) and 58). Two curves are drawn for comparison. Neither is a "best-fit".

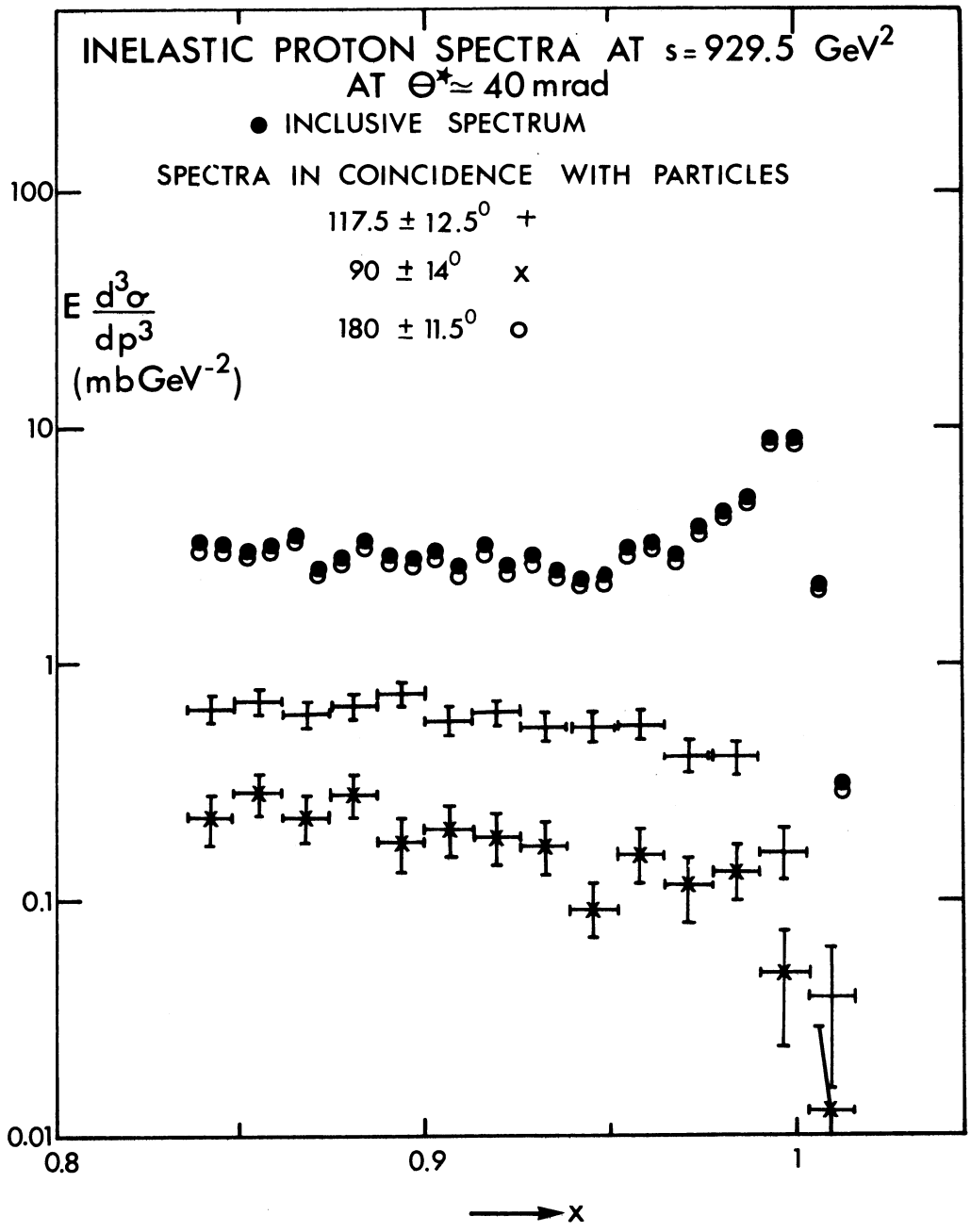


Fig. 22 The invariant cross-section for the production of inelastic protons at $s = 929.5\ \text{GeV}^2$ as a function of x. Data from the CHLM Collaboration, Ref. 50). The upper curve shows the fully inclusive spectrum. The points marked x, +, 0 show the spectrum in coincidence with one or more charged particles registered in telescopes placed at the indicated angular positions.

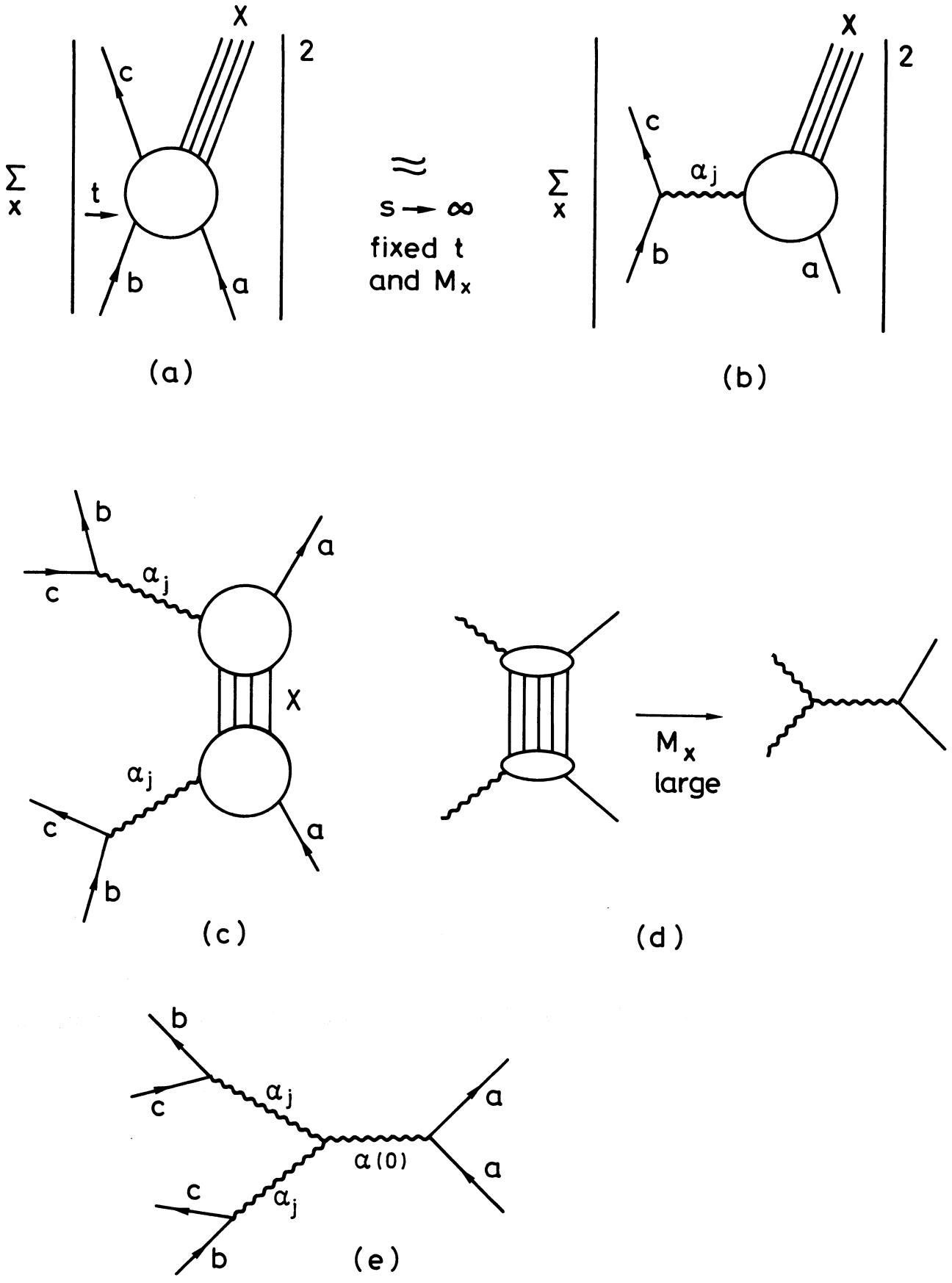


Fig. 23 Sequence of diagrams illustrating various Regge expansions made in passing to the triple-Regge graph shown in (e). The corresponding equations are found in Section 5.4.

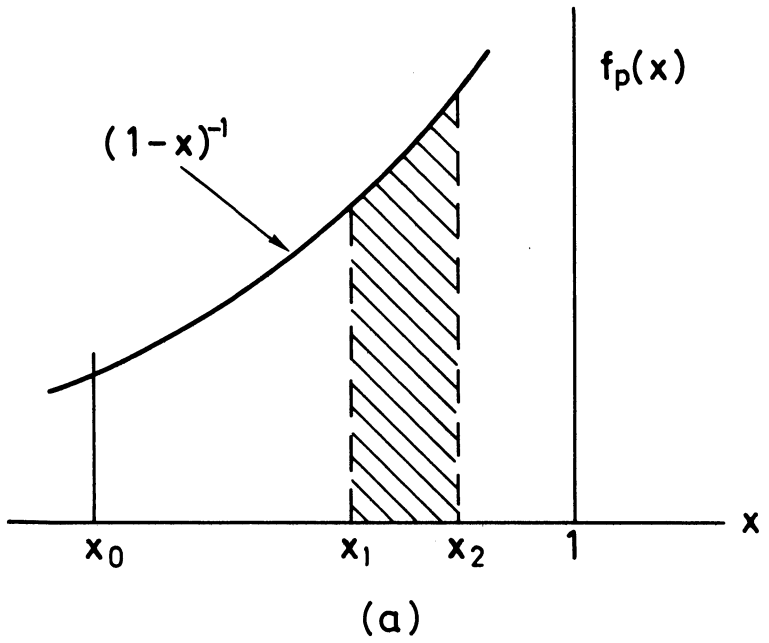


(a)

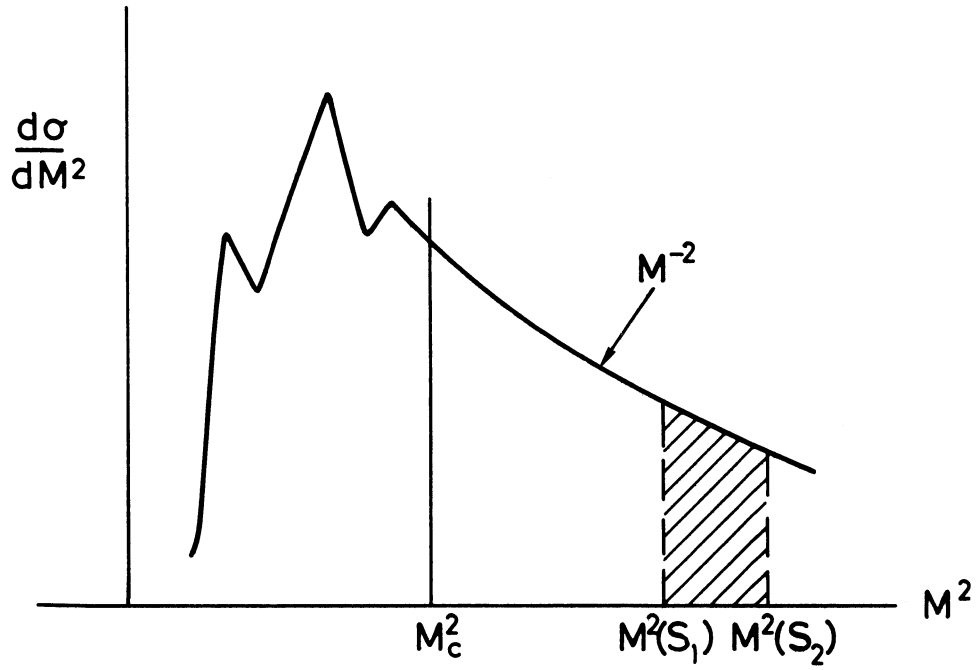


(b)

Fig. 24 Fanciful portrayal of the same invariant inclusive distribution $f_p(x) = Ed\sigma/d^3p$ at small fixed $p_T$ plotted versus : (a) x, and (b) $M^2$ at two different energies : $s_1$ and $s_2$. The shaded portion shows the increase of diffractive cross-section $\sigma_D$ from $s_1$ to $s_2$. In (a) [(b)], $x_0$ [$M_c^2$] denotes a lower limit of integration, below which the triple-Pomeron expression may be inapplicable.